POLITECNICO
MILANO 1863

SCUOLA DI INGEGNERIA INDUSTRIALE
E DELL'INFORMAZIONE

Executive Summary of the Thesis

Intermolecular Nuclear Overhauser Effect in Ionic Liquids: Beyond the State of Art

Laurea Magistrale in Chemical Engineering - Ingegneria Chimica

Author: Chiara Vaccarini

Advisor: Prof. Andrea Mele

Co-advisor: Dr. Maria Enrica Di Pietro, Prof. Franca Castiglone

Academic year: 2020-2021

1. Introduction

Ionic liquids (ILs) are defined as molten salts that are at liquid phase below 100° [1]. They are made of an organic and highly asymmetric cation usually consisting in a polar ring with some alkyl chains attached to it and a counter anion. The steric hindrance of the ions and the scarce symmetry of the cation hampers the formation of a crystal lattice, thus leading to salts easily found in the liquid state at room temperature.

Nowadays ILs are widely used as solvent for synthesis, catalysis or extraction due to their peculiar properties and because they are considered *greener* than the traditional solvents, mainly because their negligible vapour pressure avoids the release of VOCs. The properties of ionic liquids can be modulated by the selection and coupling of cation and anion, properties such as hydrophilicity/hydrophobicity, the coordination capability of the solvent or the moisture sensitivity can be tuned by proper choice of the cation-anion pairs. Also the polarity of ionic liquids may change according to the ions selection but, generally speaking, since the cation is made of polar head and non polar chains, they are suitable solvent both for polar and non polar substances. Further remarkable properties are the thermal and chemical stability, low volatility and high ionic conductivity which made ionic liquids also good electrolytes [1].

From the structural viewpoint, the most intriguing feature of the ILs is the nanostructuration due to the formation of polar and apolar domain at the nanometric length-scale. A pictorial sketch is reported in Figure 1, taken from the milestone paper by Canongia-Lopes and Padua[2]. How can the existence and structure

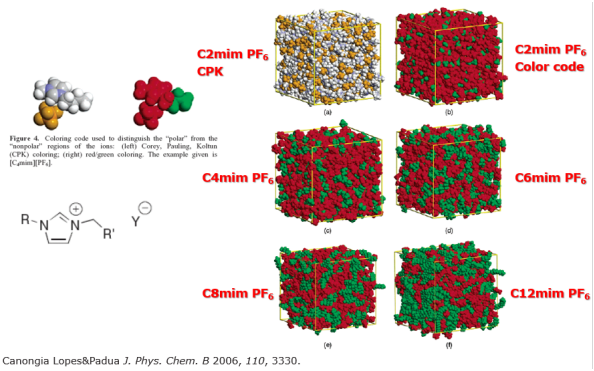

Figure 1: Polar (red) and non polar (green) domains formation according to the alkyl chain selected in imidazolium ionic liquids . From ref.[2]

of nanometric domains in ILs be investigated?

Along with the traditional approaches based on molecular dynamics, X-ray and neutron scattering, NMR spectroscopy is a useful approach to get insights at molecular level on the intermolecular interactions leading to aggregation phenomena in ILs. In particular the Nuclear Overhauser Effect (NOE), that is one of the most powerful tool of the NMR spectroscopy repertoire of experiments for the elucidation of the molecular structure and molecular interactions. The intermolecular NOE was applied to ionic liquids for the first time in 1995 [3], when the author distinguished intra- and intermolecular interactions in a qualitative work leading to the first evidence at atomic level of the ions organization in ILs. In the following year the heteronuclear NOE was applied to ionic liquids by other authors [4], [5] that have interpreted their results according to the hypothesis that the observed intermolecular NOE could be processed as intramolecular NOE in stable aggregates, thus undergoing the rapid decrease of intensity with increasing distance r of the interacting nuclei, the so-called r^{-6} rule. The observed intermeolecular NOE would give details of the structure at short distances, thus spotting basically on the structure of the first coordination shell.
In 2013 the study [6] introduced a great novelty in the heteronuclear NOE's world, in fact they have calculated the contribution of the ion diffusion to the cross-relaxation - i.e to the NOE - concluding that the heteronuclear NOE in ionic liquids does not only detect the spins that are closer in space, i.e. the first solvation shell, but also the long-range effects linked to the solvation shells beyond the closest neighbours. The influence of the long range effects is strictly dependent on the Larmor frequency of the interacting nuclei: it is dominant in ^{1}H - ^{1}H or ^{1}H - ^{19}F NOE due to the similar Larmor frequencies, it is expected to be negligible in ^{1}H - ^{7}Li NOE (for example), due to the large difference of the Larmor frequencies between proton and ^{7}Li. Strictly speaking, the long range and short range structure detectable via intermolecular NOE depends on the type of nuclei we are observing. Frequency matters...
This thesis work is part of a wider project [7] in collaboration with the Vienna university in which NMR and molecular dynamics (MD) are used to prove the theory proposed in 2013. Specifically, this work is focused on the experimental side of the project performing all the NOE experiments necessary to validate the already cited theory.

2. Materials and Methods

The NOE experiments have been performed on the pure 1-ethyl-3 -methylmidazolium - trifluoromethanesulphonate (EMImTfO) ionic liquid and its mixture with Lithium-trifluoromethanesulphonate (EMImTfO + LiTfO) in order to measure the cross relaxations rate and evaluate the local proximity among the nuclei. In particular the dynamics parameters, like T_1 (time constant of the longitudinal relaxation) and D (diffusion coefficient), have been measured, then the correlation experiments (Hoesy, both 1D and 2D) have been performed on both sample at different temperatures. All the experiments have been done using the Brucker's ultra-shielded magnet operating at 11.74 T, and each time the spectrometer has been properly set.

2.1. Hoesy experiments

2D Hoesy (Heteronuclear Overhauser Effect Spectroscopy) experiments are the traditional methodology used for the measurement of the cross relaxations and they actually consist in a series of experiments at a certain temperature when a parameter, called *Mixing time* (the time interval in which the mutual relaxation of nuclei takes place, thus allowing the NOE to grow), is varying. In particular ^{1}H - ^{19}F Hoesy have been performed on both samples at 288 K and 298 K while ^{7}Li -^{1}H Hoesy on the blended sample only at 288 K, 298 K and 318 K to investigate the interactions between protons and fluorine and protons and lithium respectively. The TopSpin software allows processing the data and taking out the intensities of the already mentioned interactions that are then normalized and plotted to draw the so called *Build up curves* (Fig.2). These curves are supposed to be properly fitted to get the values of the cross relaxation, i.e. the NOE.
For what concerns the 1D Hoesy, they are intended as trails to verify whether these experiments are a reliable tools for the measurement of the cross relaxations because they require much less time than the standard methodology. The

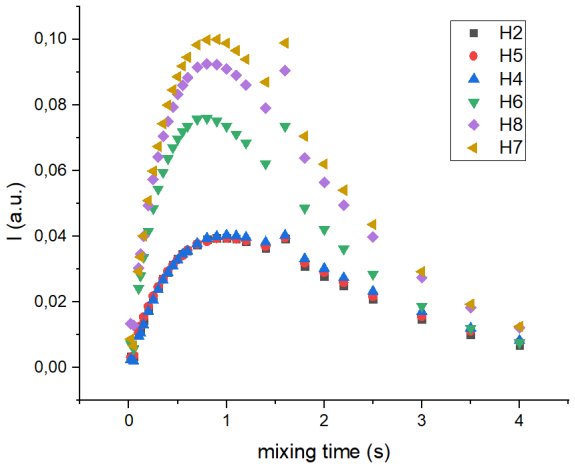

Figure 2: Example of build up curves, ^{1}H - ^{19}F 2D Hoesy, EMimTfO + LiTfO, 298 K

processing is the same of the 2D hoesy.

2.1.1 Fitting of the build up curves

First of all the Solomon equation [8], [9] has been tried both considering the relaxation rate as constant, its value coming from T_1 inversion recovery experiment, or a fitt-able parameter.

$$NOE = \frac{1}{2}\exp(-(R-\sigma)\tau)(1-\exp(-2\sigma\tau)) \quad (1)$$

In the equation 1, R is the averaged relaxation rate between the ones of protons and fluorine or lithium, τ is the variable and in our case is the mixing time and σ is the cross relaxation.

$$NOE = M_0\sigma\frac{2\sinh\Delta\tau}{\Delta}\exp(\frac{R_I+R_S}{2}\tau) \quad (2)$$

$$\Delta = \frac{\sqrt{R_I^2 - 2R_IR_S + R_S^2 + 4\sigma^2}}{2} \quad (3)$$

2 and 3 are the modified Solom's equation where it not considered the averaged cross relaxation anymore, but "I" refers to the proton while "S" to fluorine or lithium, and a normalization factor M_0 is introduced. After several attempts and a careful analysis the equation 1 has been chosen as the best option for the fitting considering the averaged relaxation rates as parameters.

3. Results and discussion

3.1. 2D Hoesy

The most relevant results of this work are the relative cross relaxations, σ, taken out for both 2D and 1D Hoesy experiments. Figure 3 and

σ relative	*Blended*	*Neat*
H2	0.346±0.008	0.350±0.006
H5	0.344±0.008	0.359±0.009
H4	0.333±0.008	0.283±0.009
H6	0.817±0.032	1.00±0.012
H8	0.953±0.029	0.959±0.017
H7	1.00±0.013	1.983±0.012

Table 1: Relative cross relaxation, ^{1}H - ^{19}F hoesy, both samples, 298 K

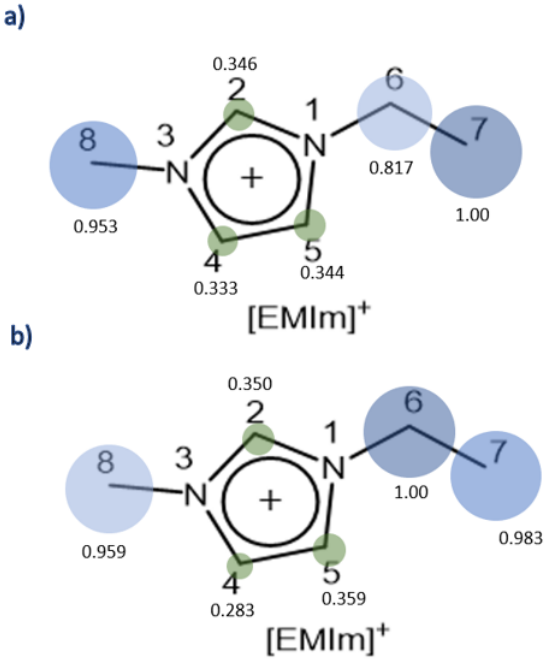

Figure 3: Relative cross relaxation of the blended sample (a) and of the neat sample b), ^{1}H - ^{19}F 2D Hoesy at 298 K

Table 1 report the comparison between the relative cross relaxation measured in both samples for the ^{1}H - ^{19}F 2D Hoesy at 298 K. The presence of the lithium salt does not significantly affect the interactions between ^{1}H and ^{19}F that are comparable and very similar. Figure 3 shows a clear trend of ^{19}F that preferentially interacts with the protons located on the alkyl chain, positions 6, 7 and 8, and much less with the ones on the ring.

In figure 4 there are the relative cross relaxations of the 2D ^{7}Li - ^{1}H Hoesy series on the blended sample at 298 K. The trend shown in this figure, compared with the ones in figure 3, is very different since the interaction between ^{7}Li and^{1}H are mainly focused on the protons in position 8. All the others interactions located on different

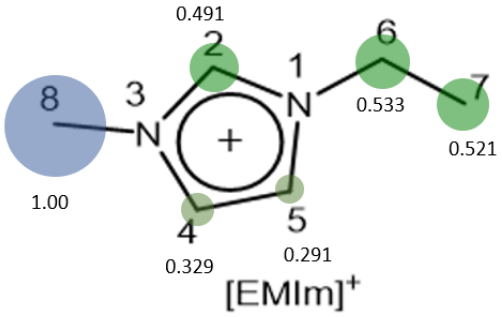

Figure 4: Relative cross relaxation, ^{7}Li - ^{1}H 2D Hoesy for the sample EMImTfO + LiTfO at 298 K

positions are significantly lower.
According to the theory proposed in 2013 by [6], the ^{1}H - ^{19}F pair generates long-range effects that are not negligible because of they have similar gyromagnetic ratios, thus similar resonance frequencies. Thereby the cross relaxations reported in figure 3 represent also the interactions between isotopes located beyond the first solvation shell as sum of both long- and short-range effects. Conversely, ^{7}Li and ^{1}H have significantly different resonance frequencies, thus the interactions reported in figure 4 refer to the isotopes placed in the first solvation shell only and only short-range effect are relevant in this case.
The result found in this work matches with the theoretical computations performed by our colleagues working in the University of Vienna as reported in this study [7] and in figure 5.
The correspondence between the experimental data collected in this work and those from the simulations done by our colleagues validates the theory proposed in 2013.

3.2. 1D Hoesy

For what concerns the 1D Hoesy, they gave good results only for the ^{1}H - ^{19}F while ^{7}Li - ^{1}H series didn't work at all. In figure 5 there is and example of HOESY 1 fitted build for the ^{1}H - ^{19}F, it curves are comparable and well fitted and lead

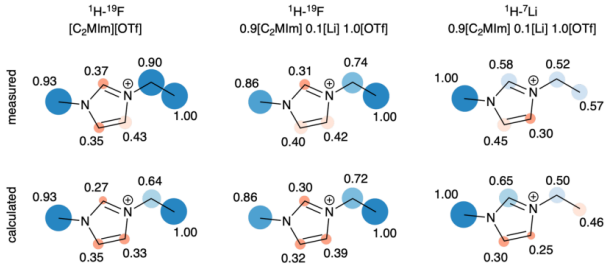

Figure 5: Relative cross relaxation comparison between experimental and simulated data, c and ^{7}Li - ^{1}H 2D Hoesy, EMImTfO + LiTfO, 298 K, [7]

to the relative cross relaxations reported in figure 7 (For sake of simplicity in this picture the position of protons are omitted). The resulting

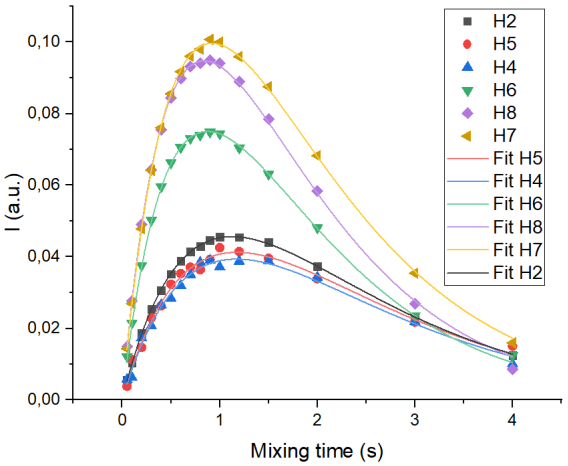

Figure 6: Build up curves with relative final fitting, ^{1}H - ^{19}F 1D hoesy, non selective sequence, EMImTfO + LiTfO, 298K

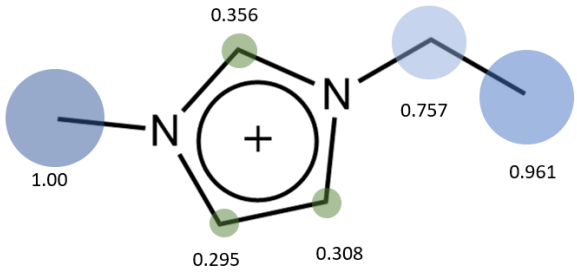

Figure 7: Relative cross relaxations on [EMIm]$^{+}$ cation, ^{1}H - ^{19}F 1D hoesy, non selective sequence for the sample EMImTfO + LiTfO at 298K

cross relaxations are comparable to the ones in figure 2 and seem reliable. It's clear again the trend according to which the fluorine isotopes interact preferentially with the protons located

on the alkyl chains.

4. Conclusion

The 2D Hoesy well behaved giving reliable and meaningful results and their extremely high matching with the simulation done by our colleagues allows completing the picture of the closest neighbours via ^{7}Li - ^{1}H hoesy and the solvation beyond the first shell via ^{1}H - ^{19}F hoesy. This is a remarkable results that validates the theory proposed by [6], but some critical points have arisen during the processing especially regarding the fitting which gave satisfying results only with HOESY 1 and strictly considering the averaged relaxation rate as a parameter. It would be nice understanding why the other fitting equation did not work and why the relaxation rate must be considered a parameter.
The 1D hoesy represent a good and faster alternative to the classical 2D only for the ^{1}H - ^{19}F series giving comparable and very similar result to those obtained following the classical 2D methodology. Conversely, 1D technique failed when dealing with lithium because the acquired spectra were pretty bad and the build up curves could not be drawn.
By now it is not clear why the ^{7}Li - ^{1}H 1D hoesy present this issue but it might be related the sample itself, thus further experiments on different samples and with difference isotopes pair should be performed.

References

[1] Jason P. Hallett and Tom Welton. Room-temperature ionic liquids: Solvents for synthesis and catalysis. 2. *Chemical Reviews*, 111(5):3508–3576, 2011.

[2] José N. A. Canongia Lopes and Agilio A. H. Padua. Nanostructural Organization in Ionic Liquids. *J. Phys. Chem. B*, 110:3330–3335, 2006.

[3] Robert A. Mantz, Paul C. Trulove, Richard T. Carlin, and Robert A. Osteryoung. ROESY NMR of basic ambient-temperature chloroaluminate ionic liquids. *Inorganic Chemistry*, 34(14):3846–3847, 1995.

[4] Andrea Mele, Chieu D. Tran, and Silvia H. De Paoli Lacerda. The structure of a room-temperature ionic liquid with and without trace amounts of water: The role of C-HO and C-HF interactions in 1-n-butyl-3-methylimidazolium tetrafluoroborate. *Angewandte Chemie - International Edition*, 42(36):4364–4366, 2003.

[5] Andrea Mele, Greta Romanò, Matteo Giannone, Enzio Ragg, Giovanni Fronza, Guido Raos, and Valentina Marcon. The local structure of ionic liquids: Cation-cation NOE interactions and internuclear distances in neat [BMIM][BF4] and [BDMIM]-[BF 4]. *Angewandte Chemie - International Edition*, 45(7):1123–1126, 2006.

[6] Sonja Gabl, Othmar Steinhauser, and Hermann Weingärtner. From short-range to long-range intermolecular NOEs in ionic liquids: Frequency does matter. *Angewandte Chemie - International Edition*, 52(35):9242–9246, 2013.

[7] Philipp Honegger, Maria Enrica Di Pietro, Franca Castiglione, Chiara Vaccarini, Alea Quant, Othmar Steinhauser, Christian Schröder, and Andrea Mele. The Intermolecular NOE Depends on Isotope Selection: Short Range vs Long Range Behavior. *The Journal of Physical Chemistry Letters*, pages 8658–8663, 2021.

[8] Yves Lingscheid, Sven Arenz, and Ralf Giernoth. Heteronuclear NOE spectroscopy of ionic liquids. *ChemPhysChem*, 13(1):261–266, 2012.

[9] Yves Lingscheid, Mathias Paul, Andreas Bröhl, Jörg Martin Neudörfl, and Ralf Giernoth. Determination of inter-ionic and intra-ionic interactions in a monofluorinated imidazolium ionic liquid by a combination of X-ray crystallography and NOE NMR spectroscopy. *Magnetic Resonance in Chemistry*, 56(2):80–85, 2018.

POLITECNICO DI MILANO

School of Industrial and Information Engineering

Master of Science in Chemical Engineering

INTERMOLECULAR NUCLEAR OVERHAUSER EFFECT IN IONIC LIQUIDS: BEYOND THE STATE OF ART

Advisor:
Prof. Andrea Mele
Co-advisors:
Dr. Maria Enrica di Pietro
Prof. Franca Castiglione

Master Thesis of:
Chiara Vaccarini
945154

Academic Year 2020-2021

Ringraziamenti

In questa sezione vorrei dedicare qualche parola alle tante persone che mi sono state accanto durante questi anni di studi universitari e a cui vorrei esprimere tutta la mia gratitudine.
In primo luogo, il Professor Andrea Mele che mi ha accompagnata e guidata nel mio lavoro di tesi. Per me è stato un piacere lavorare con lui che si è dimostrato sempre estremamente disponibile e gentile nei miei confronti, fin dal primo giorno. Allo stesso modo voglio esprimere un profondo e sentito ringraziamento alla Dott.ssa Maria Enrica Di Pietro che ha lavorato accanto a me sempre con estrema disponibilità e pazienza, seguendomi in ogni fase di questo lavoro, sia in presenza che a distanza ed istaurando un bellissimo rapporto professionale. Grazie anche alla Prof.ssa Franca Castiglione che ha seguito questo progetto mettendo a disposizione la sua competenza ed esperienza e con lei ringrazio tutto il gruppo di ricerca NMR del Politecnico di Milano.
Dopo di che voglio ringraziare con tutto il cuore mamma e papà che mi sono sempre stati accanto dandomi la calma, la sicurezza e i mezzi per portare avanti gli studi nel migliore dei modi supportandomi in ogni momento. Con loro ci tengo a ringraziare anche mio fratello Davide che è un fantastico esempio di come si può portare avanti e concludere brillantemente questo lungo percorso di ingegneria, lo ringrazio per aver condiviso con me lunghe giornate di studio, soprattutto durante i miei primi anni d'università, e per avermi "fatto forza" ad ogni esame. Un pensiero e un grazie va anche a Sofia che non si è mai risparmiata nel darmi consigli ed informazioni soprattutto relativi alla vita al Politecnico.
Voglio dedicare un grande abbraccio ai miei nonni che mi sono sempre stati accanto informandosi riguardo ai miei studi, consigliandomi e pregando per me ad ogni esame e allo stesso modo ringrazio anche mio zio e mia zia.
Un grazie speciale va a tutti i miei amici, a partire da coloro che conosco da tutta la vita: Sabry, Giorgia, Chiara e Fabry con cui condivido quotidianamente

risate, bellissime serate e so che ci sono sempre per me quando ho bisogno. Grazie anche a tutti i miei altri amici come Carla, Riccardo, Sofi e Teo che non mi hanno mai fatto mancare il loro appoggio e la loro vicinanza. Tra gli amici non posso non ricordare i ragazzi e le ragazze che ho conosciuto in università e in particolare ci tengo a ringraziare Ilaria con cui ho condiviso tutto il percorso di ingegneria chimica, dal primo all'ultimo giorno frequentando insieme lezioni e preparando esami. Grazie anche a Lucia che ha frequentato con me la laurea triennale e con cui, nonostante abbiamo scelto indirizzi diversi per la magistrale, mi sento ancora quotidianamente.
Inoltre, voglio ringraziare tutte le mie amiche e compagne di squadra con cui gioco o ho giocato a pallavolo in questi anni: per me è fondamentale venire in palestra con voi, divertirmi, scaricare un po' di tensione e ridere, ridere tanto e mi è mancato tantissimo quando non abbiamo potuto allenarci a causa della pandemia. In particolare, ci tengo a ringraziare Sofi, Ele, Manu ed Ele che mi sono state accanto e mi hanno consigliata quando ce n'è stato bisogno riguardo cose non legate alla pallavolo. Un grazie particolare va anche a Bea che da anni ci allena e ci sopporta.
Per concludere, vorrei ringraziare don Roberto, che oltre ad essere sacerdote, per me è un amico sempre pronto ad ascoltare (sia cose belle che problemi), consigliare e, se serve, a darmi conforto.

Con affetto
Chiara

Contents

List of Figures

List of Tables

Sommario

Il NOE (Nuclear Overhauser effect) è uno strumento molto potente della spettroscopia a Risonanza Magnetica Nucleare (NMR) attraverso il quale è possibile far luce sulla nanostruttura e sulle proprietà dei liquidi ionici. Questo è ancora più vero per il NOE eteronucleare poiché fornisce informazioni riguardo la vicinanza e le interazioni tra le diverse specie ioniche. Nell'ultimo decennio c'è stata una rivoluzione riguardante il NOE eteronucleare applicato ai liquidi ionici con l'introduzione di una nuova teoria secondo cui degli effetti long-range possono insorgere a seconda delle frequenze di risonanza degli isotopi selezionati per svolgere gli esperimenti. In questo lavoro di tesi, per la prima volta, degli esperimenti NOE sono stati effettuati sullo stesso campione considerando isotopi sia con frequenza di risonanza molto simile come la coppia ^{1}H -^{19}F che significativamente diversa come ^{1}H e ^{7}Li. I dati sperimentali raccolti sono stati analizzati anche tramite simulazioni di dinamica molecolare svolte dai nostri colleghi dell'università di Vienna. Questo approccio combinato ha dimostrato che gli effetti long-range hanno un ruolo determinante solo quando si lavora con isotopi con frequenza di risonanza molto simile come nel caso di ^{1}H -^{19}F, altrimenti il comportamento short-range è dominante come nel caso della coppia ^{1}H-^{7}Li.

Parole chiave: NMR, NOE, liquidi ionici, long-range vs short-range

Abstract

The Nuclear Overhauser effect (NOE) is a powerful tool of the NMR spectroscopy by means of which is possible to enlighten the nanostructure and the properties of ionic liquids. This holds even more true for the heteronuclear NOE that gives access to information about proximity and interactions between the different ionic species. In the last decade there has been a revolution in the interpretation of the heteronuclear NOE in ionic liquids with the introduction of a new theory according to which some long-range effects may arise depending on the resonance frequencies of the isotopes selected for the experiments. In this thesis work, for the first time, NOE experiments have been performed on the same sample considering isotopes both with very similar and significantly different resonance frequencies, ^{1}H -^{19}F and ^{1}H-^{7}Li respectively. The experimental collected data have been analyzed jointly with the molecular dynamics (MD) simulations run at the University of Vienna. The combined approach demonstrated that the long-range effects play a crucial role only when dealing with isotopes with similar resonance frequencies as^{1}H -^{19}F, otherwise short-range behavior is ruling like in case of ^{1}H-^{7}Li .

Keywords: NMR, NOE, ionic liquids, long-range vs short-range

Chapter 1

Introduction

1.1 Ionic liquids, main features

Ionic liquids (ILs) are basically salts showing extremely low melting points. In some cases, the melting point (mp) is below room temperature [1]. In a more realistic way, those salts with mp below the ordinary boiling point of water (100°C) are classified as ILs. The liquid state at $T<T_{eb}$ (H_2O) is mainly due to the lack of symmetry typical of the cation they are made of and to the largely delocalized charge in the cation and, often, in the anion too [2].
These ingredients provide the system with "packing frustration" leading to lattice enthalpy values much lower than those commonly observed in "conventional" salts, where spherical symmetry of anions and cations is very often encountered and drive the system towards close packing of the ions with formation of strong lattices. For clarity, the meting point of NaCl is reported as 801 °C, while 1-methyl-3-ethylimidazolium chloride melts at 86 °C.
Usually the organic cation selected consists of a polar ring such as imidazolium or pyridinium and some alkyl chains attached to it. Such particular arrangement does not allow creating neither a long-range order nor a space lattice, thus these substances have melting point around 20°-30° C, but since the beginning of the 21^{st} century, the definition of ionic liquids has included all the salts found at liquid state below 100°C [3], [4], [5].
In that years, ionic liquids became easily available and deeply investigated in chemical laboratories because it was thought that, in principles, cation and anion could be coupled in a million different ways giving rise to compounds with particular properties that make the ionic liquid suitable for any specific appli-

cation [3]. In truth, it is actually a great challenge to predict the real melting point of a new ionic liquid just selecting a different combination of cation-anion and designing it ad hoc for an application [6].
Nowadays ionic liquids are widely applied in chemistry as solvents for synthesis, catalysis and extraction due to their peculiar properties that, in most of the cases, depend on the cation and anion selection and because they are considered a *green option* with respect to traditional molecular solvents.[2]
One of the most important features of ionic liquids is the tunability of their polarity and their behavior with water. ILs can be either hydrophilic or hydrophobic as reported in this study [6], some ionic liquids sharing the cation and differing just for the anion, are mixable or not in water (also the concentration of water added plays a role) and, for what concerns the cation selection, the hydrophobicity intuitively increases with the length of the alkyl chains.
A simple sketch of the modulation of the physicochemical properties of some important class of ILs is reported in Figure 1.1, taken from [7]. As just intro-

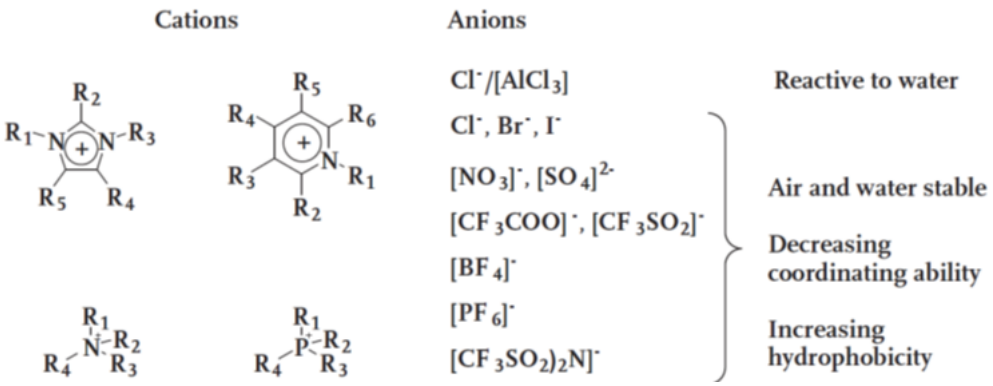

Figure 1.1: *Examples of common cation and anion pairs used in the formation of ionic liquids and general progression of changes in Il properties with anion type*

duced, ionic liquids have a polar head consisting of the ring of the cation plus the anion and non-polar tails made of the alkyl. These parts of ILs components drive the polarity of these compound as discussed in many studies as [6], [2]. Generally speaking, ionic liquids are suitable solvent for organic and inorganic compound, polar or non-polar because of their double nature: non-polar compounds interacts with the chains while the polar ones with the ring and the anion.
Other remarkable properties of ionic liquids are the chemical and thermal stability and low volatility that hinder their crystallization or evaporation respec-

tively at room temperature, moreover they are not flammable and show high ionic conductivity and that's why they are suitable also as electrolytes [1], [2], [5], [8].

1.2 Alkylimidazolium ionic liquids

The 1-alkyl-3-methylimidazolium ions are one of the most famous family of cation used in ionic liquid [2], [3], [9]. They have all similar structure, reported in figure 1.2, but for the length of the alkyl chain in position 1. As stated in [9], this kind of molecules arrange themselves in the volume forming polar and non-polar domains interacting one another but with no phase separation. In other words, they exhibit heterogeneity on nanometric scale (nanostructural organization) but they are isotropic on a macroscopic scale. The formation of the

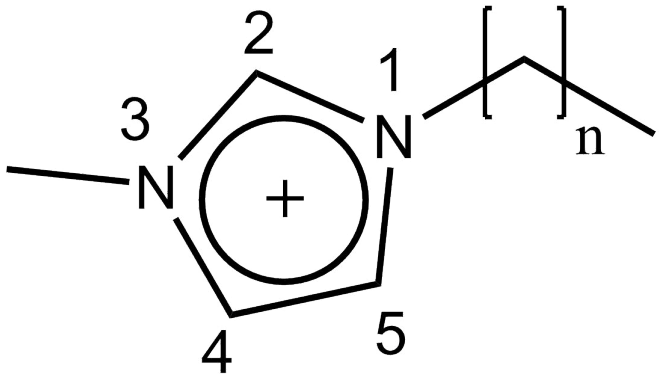

Figure 1.2: *1-alkyl-3-methylmidazolium cation, general structure with counter anion*

domains in the volume of the sample depends on which is the particular cation selected for the composition of the ionic liquid that means how long is the alkyl chain attached in position 1.
Following the seminal paper by Canongia-Lopes and Padua [9], a graphic representation of the domain formation, extension and interaction can be observed in Figure 1.3, where the color code (red=polar, green=non-polar) is a guide for eye in recognizing the formation of the domains in the bulk of imidazolium based ILs.
As presented by [9], the size of the polar and non-polar domains is enlarged by increasing the length of such chain. Indeed, in figure 1.3 it is possible to note how passing from the shorter 1-alkyl-3-methylmidazolium cation that presents

an ethyl radical in position 1 (which is the one selected for this thesis work) to C4, C6, C8 or C12 the size of the domains increases making this kind of aggregation stronger. These authors in their work have chosen the hexafluorophosphates $[PF_6]^-$ as counter anion, but generally speaking this behavior can be extended to different anions.

In section 1.1 it was stated that also the anion may affect the ionic liquid properties, besides that the anion may influence also the nanostructural organization and the formations of polar and non polar domains [5]. In the just cited work by Di Pietro, Castiglione and Mele two different kind of anions $[BF_4]^-$ and the bis(trifluoromethane)sulfonimide (TFSI), have been coupled with the same cations by analyzing how the nanostructure of the sample changes. $[BF_4]^-$ which is small, symmetric and with localized charge while TFSI the is large, asymmetric with diffused-charge and with conformational flexibility. For sake of simplicity, the anion can be defined as hard and soft, respectively. That study claims that hard anions are clearly located close to the polar ring of 1-alkyl-3-methylmidazolium cation while the soft ones are polarized enough to explore the apolar domain made of the alkyl chains.

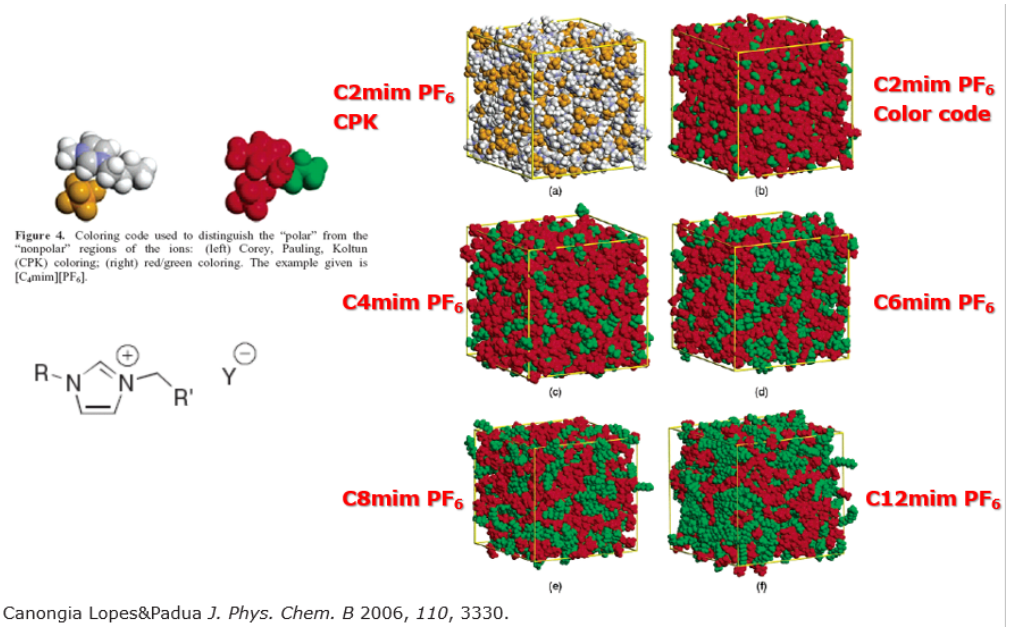

Figure 1.3: *Polar and non polar domains formation according to the alkyl chain selected in ionic liquids [9]*

1.3 Intermolecular NOE in ionic liquids

Since the discovery of the nanostructural organization of ILs, e.g. the formation of nanosized polar an non-polar domains in the bulk of the isotropic liquid and with no observable phase separation, many groups made efforts to give experimental evidence of what was postulated on the basis of moleculer dynamics simulations only [9]. The first experimental validation of the microheterogeneity in imidazolium ILs came from and Italian team [10] by using small angle X.ray diffraction. This methodology is extensively used to figure out the structure of liquids and it is extremely powerful, especially if associated to synchrotron X-ray sources. Nevertheless, it suffers from the absence of a clear cut interpretation of the intermolecular interactions at atomic level.
From this standpoint, NMR spectroscopy can be considered an powerful and complementary approach. In particular, the Nuclear Overhauser Enhancement (or Effect), commonly abbreviated as NOE, is one of the most informative tool in the toolcase of the NMR experiments. [11]
Broadly speaking, the Nuclear Overhauser Effect (NOE) is one of the outcome of the through space dipole-dipole interaction between nuclei close in space. In the very much popular approach of the "stationary NOE" a significant change of a given signal intensity is observed when a close in space spin is selectively perturbed. The enhancement is the result of the so-called cross-relaxation σ, i.e. the mutual relaxation of the nuclei due to dipolar coupling. As the signal enhancement (NOE) is detectable only if the interacting nuclei are close in space, this approach has been massively used to assess the stereochemistry of organic molecules and inorganic complexes.[12]
From a quantitative viewpoint, the kinetic of NOE - the so called "NOE build up rate" - allows for the measurement of internuclear distances provided an intramolecular calibration distance, is known (for example from MO calculations of X-ray diffraction data), thus allowing a detailed 3D picture of the molecule [12], [13].
Indeed, the change in intensity depends on two main factors: the distance r between the interacting nuclei and the molecular tumbling which is providing the fluctuating, local magnetic fields promoting the mutual cross relaxation σ, i.e. the NOE.
The time correlation function G(T) here reported describes both effects and it

is basically the temporal evolution (randomization rate) of the NOE:

$$G(t) = \frac{1}{\vec{r}(0)^3}\frac{1}{\vec{r}(t)^3}(\frac{3}{2}cos^2(\theta(t)) - \frac{1}{2}) \tag{1.1}$$

with $\vec{r}$ as the vector connecting the two interacting nuclei I and S at time t, and $\theta(t)$ is the angle swept by this vector during timespan t. In the frequency domain, the Fourier transform of G(T) gives the spectral density function (SDF) or J(ω_{IS}).

$$J(\omega) = Re[\int_0^\infty e^{-i2\pi\omega t}G(t)dt] = \int_0^\infty cos(-2\pi\omega t)G(t)dt \tag{1.2}$$

Overall, the NOE (=σ_{IS}) can be described in terms of suitable spectral density functions:

$$\sigma_L(\omega) = 0.6J(\omega_I + \omega_S) - 0.1J(|\omega_I - \omega_S|) \tag{1.3}$$

This equation is a general conclusion and it states the important fact that NOE is considered at two different frequencies, i.e. the sum and the difference of the Larmor frequency of the interacting nuclei.
In the case of intramolecular NOE, it can be assumed that:

1. The $\vec{r}$ vector connecting the two interacting nuclei is constant. This correspond to a fixed interaction distance of the nuclei
2. The random tumbling of the vector r is described by a single parameter, the rotational correlation time τ_{C}.

Under these assumptions, a popular expression of the J(ω) can be derived:

$$J(\omega) = K_I S\frac{1}{r^6}\frac{\tau_C}{1 + (\omega\tau_C)^2} \tag{1.4}$$

$\mathrm{K_{IS}}$=[($\mu_0/4\pi\mathrm{h}\gamma_{\mathrm{I}}\gamma_{\mathrm{S}}$]^{2}is the dipolar coupling constant, where γ_{I} and γ_{S} are the gyromagnetic ratios of the spins, and μ_0 is the permeability of the vacuum.
In the following we will examine the consequence of these equation in the case of intra- and intermolecular NOE.
Concerning the distance dependence of the NOE with the $\vec{r}$ of the interacting spins, it globally goes as $1/\vec{r}^{\,6}$. This is a pivotal point, as the rapidly decreasing NOE intensity with increasing internuclear distance leads to the commonly accepted threshold of 4 Å distance of the interacting nuclei for detection of NOE. This statement is strictly true for intramolecular NOE. As we will see in the

following, the "4 Å rule" cannot be applied to intermolecular NOE in the generality of cases.
The present thesis develops this concept and will provide experimental and theoretical clues for the correct applicability and interpretation of intermolecular NOE.

The main question, at this point, is how can NOE be used to study the nanostructural features of ILs?
The first example of application of intermolecular NOE dates back to 1995 when it was used for the first time in ionic liquids for the analysis of the intermolecular distances [14]. This author have proposed a qualitative work where the interactions related to intra- and intermolecular NOE have been distinguished for the first time and the intermolecular 1-ethyl-3-methylmidazolium (EMIm) cation has been detected and recognized.
The experiment is summarized in figure 1.4. The left panel shows the 2D NOE

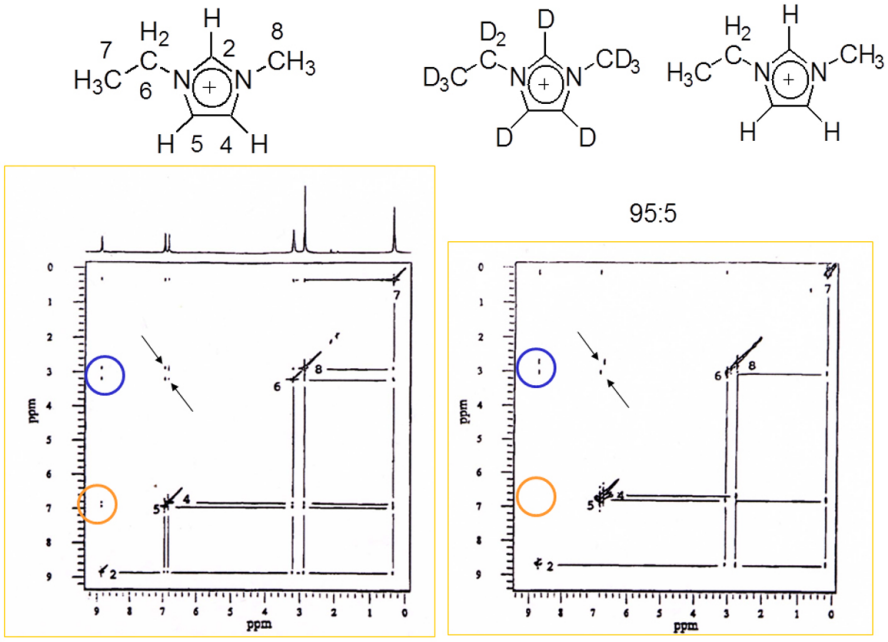

Figure 1.4: *1995 experiments scheme [14]*

correlation experiment carried out on the pure EMIm $AlCl_4$. The off-diagonal peaks (cross-peaks) are indicative of NOE contact between the nuclei assigned as diagonal peaks at the same coordinates. The orange circled cross-peaks con-

nect H2 and H4/H5. As the internuclear distance is < 4 Å, these signals have been assigned to intramolecular NOE, thus they have a structural meaning but say nothing on the nanostructural organization. Conversely, the blue circled peaks correlate H2 with H6 and H8. The calculated distances are > 4 Å, thus these contribution cannot be originated intramolecularly, but rather are the result of cation-cation organization within a structured liquid. This hypothesis was elegantly confirmed by the second experiment, reported in the right panel. Here the authors run the same 2D NOE correlation on a sample made of 95% deuterated cations and 5% protium cations. The rationale is to solvate the protium with deuterated analogue, in order to quench the intermolecular NOE. The result showed the disappearance of the blue circled NOEs, which were thus confirmed to be intermolecular and, consequently, a fingerprint of the nanostructuration of the liquid.

A decade later, the group of my thesis supervisor proposed in two different studies [15], [16] the application of homo- and heteronuclear NOE experiments to investigate the local structure of ionic liquids and their mixtures with water. The results were, once again, interpreted according to the assumption that the observed intermolecular NOE could be approximated as a intramolecular NOE within a long lived, structured aggregate. This allowed the authors to use the r^{-6} approximation to access the intermolecular interactions and local proximity in the system.

In 2013 a a milestone study from the group of Weingärtner [17] proposed a careful calculation of $J(\omega)$ for model ILs and the dynamic description of intermolecular NOE. The authors demonstrated, via molecular dynamics simulations, that the long-lived approximation was questionable and that the long-range contribution to NOE dominated over the short range one. The discriminating parameter was the Larmor frequency difference of the interacting nuclei. This fact prompted the author to state: "Frequency matters".
It is necessary, at this stage, to summarize the main difference between the theoretical development of intramolecular and intermolecular NOE. In the intramolecular case, the interacting nuclei are on the same molecular frame, thus the intermolecular distance is constant. On the contrary, in the case of the intermolecular NOE, the following points should be kept in mind:

1. A reference spin interacts with many surrounding spins due to the trans-

lational motion (diffusion). Instead of one internuclear distance, there is a distribution of distances, known as the radial distribution function (RDF). The most important structural information came from the first contact shell surrounding a reference molecule. The molecules beyond the first shell form the bulk. The number of partner spins increases by an order of r^2 with increasing distance.

2. The greater the distance between two interacting spins, the more time the spin-joining vector needs to randomize its length and orientation. The randomization time also increases by order of r^2.

3. Summing up over all spherical distance shells r adds an order of r. Thus, the power law of scaling NOE shifts from r^{-6} (intramolecular case, accounting short range interactions only) to r^{-1} (limiting case for intermolecular NOE, accounting especially long range interactions, thus beyond the first solvation shell). In general:

    - Distance dependence of intramolecular NOE: r^{-6}. Only short range contacts ($r \leq 4$).
    - Distance dependence of intermolecular NOE: r^{-n}, $1<n<6$. The length scale of the NOE very much depends on the Larmor frequency of the interacting nuclei. In many cases, n=1, thus giving only long-range NOE.

These concepts are summarized in figure 1.5 Let's now examine now the case study of 1-butyl-3-methylimidazolium (bmim) tetrafluoroborate developed in ref [5]. Figure 1.6 contains the key concepts of [17]. For the model system 1-butyl-3-methylimidazolium (bmim) tetrafluoroborate, the homonuclear ^{1}H-^{1}H NOE and heteronuclear ^{1}H-^{19}F NOE may give information on the cation-cation and cation-anion organization in the liquid, respectively. The authors calculated the spectral densities and expressed the observable NOE (reported as cross-relaxation parameter σ , see figure 1.6, left part) in terms of long range and short range interactions. The equation clearly shows that the two contributions are function of the difference (ω_2) and the sum (ω_4) of the Larmor frequencies of the interacting nuclei I and S, respectively. This fact introduces an important aspect of the intermolecular NOE: the intensity very much depends on the type of nuclei which are observed. In particular, for homonuclear NOE, the difference ω_2 of the Larmor frequency is basically 0, for heteronuclear ^{1}H-^{19}F the

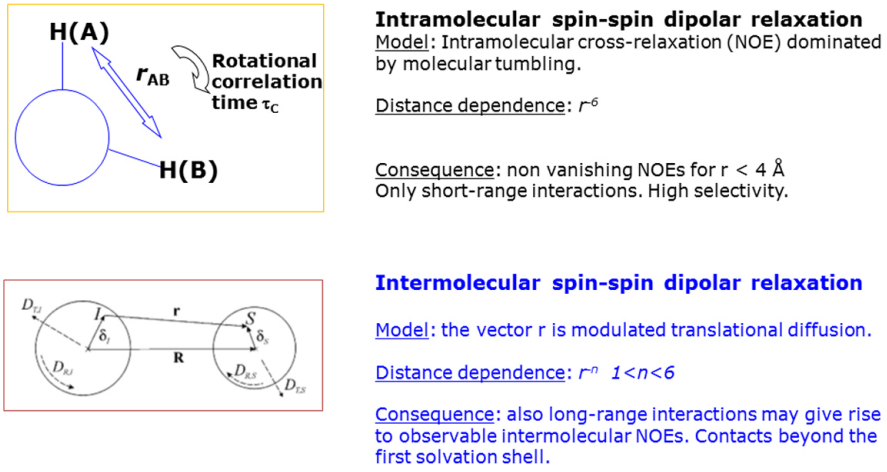

Figure 1.5: *Intramolecular vs intermolecular spin-spin dipolar relaxation*

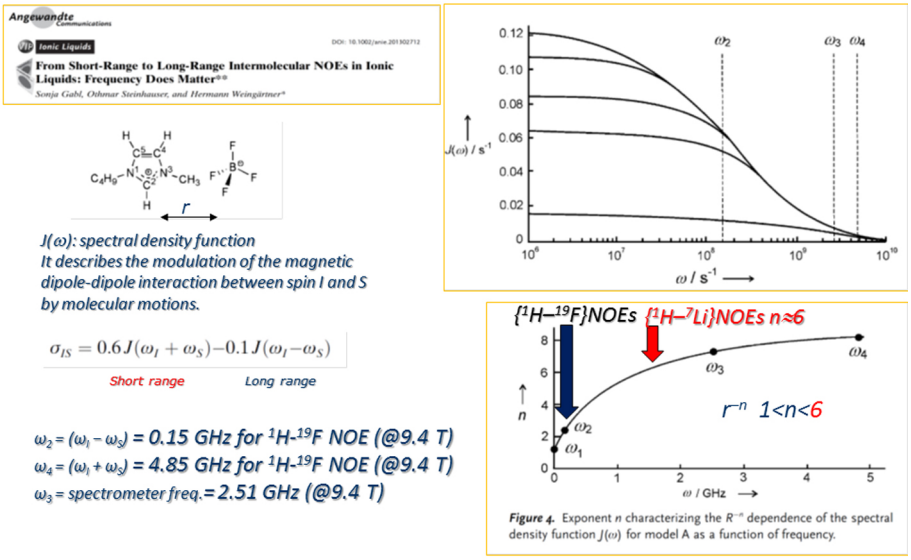

Figure 1.6: *Scheme of spectral density function computation [17]*

difference is very small. In general, the difference depends on the Larmor frequency of the nuclei, which is an intrinsic property. For example, if we consider an NMR instrument with a magnet giving a Larmor frequency of 400 MHz (in angular frequency it is 2.51 GHz) the ω_2 values are 0.16 GHz for ^{1}H-^{19}F NOE and 1.53 GHz for ^{1}H-^{7}Li NOE. The consequence of this calculation is shown in the graph placed on top right of figure 1.6. The largest contribution to NOE

is given by J(ω_2) for both homonuclear ^{1}H-^{1}H NOE and heteronuclear ^{1}H-^{19}F NOE. This means that the structural picture emerging from these experiments basically extend beyond the first solvation shell, thus making NOE less effectinve to figure out the first neighbours contacts. However, the distance dependence for vanishing NOE, r^{-n}, was also found to depend dramatically on the difference of the Larmor frequencies of the interacting nuclei. The larger the difference, the larger the exponent n in the power law, thus the higher the short range contribution to the intermolecular NOE. This key concept is described by the curve of the right bottom graph of figure 1.6. The y axis reports the n exponent of the r^{-n} dependence of NOE on the internuclear distance vs the Larmor frequency. Accordingly, ^{1}H-^{19}F NOE is expected to be dominated by long range interactions, ^{1}H-^{7}Li NOE by short range ones.

In 2015 Castiglione and her collaborators [18] proposed an experimental work for the validation of this theory.
The authors demonstrated that the molecular distances estimated by the ^{1}H-^{7}Li HOESY (heteronuclear NOE spectroscopy) were in excellent agreement with the distribution of contacts previously reported for the same system after crystallization of the IL-Li salt system and single crystal X-ray diffraction analysis. [19]
The main result of [18] was a first experimental evidence (although indirect as it compared liquid state NMR data with solid state distances in the crystal) of the short-range character of HOESY experiment involving nuclei with very different gyromagnetic ratios such as ^{1}H and ^{7}Li. Thus, frequency matters...

The previous paragraphs outlined the scientific background that originated this project and my thesis. In 2019 the research group of my supervisor agreed in a joint experimental and theoretical study on model systems based on 1-ethyl-3-methylmidazolium-triflourosulfonate IL added of Li triflate salt. The main purpose was measuring, on the one side, the heteronuclear HOESY build-up curves in the two cases of similar and different gyromagnetic ratios of the I and S spins, and on the other the analytical calculation of the spectral density in both the cases. The matching of the experimental and calculated data would represent the first direct validation of the Weingärtner's theory. The research involved Politecnico di Milano and the former Weingärtner's group at University of Wien and at Harvard Medical School. Such a validation is expected to

contribute to a new chapter of the NMR theory. This thesis work is part of such a wider project.
My personal contribution was in carrying out the of ^{1}H-^{19}F and ^{1}H-^{7}Li HOESY at variable contact time, fitting the data, extracting the cross-relaxation values and discuss them in terms of long- vs short-range contacts in collaboration with the Austrian partners. They did a massive work of computing the spectral density function and highlighting its dependence on the Larmor frequencies, pointing out the role of the frequency difference in enhancing the short-range or the long-range behavior.

It was an extremely rewarding sensation realizing that the main results of my thesis showed a perfect matching of theory and experiments. Part of my thesis has already been published – including myself as co-author – in the prestigious Journal of Physical Chemistry Letters of the American Chemical Society.[13]

Chapter 2

Materials and methods

In this chapter, after a brief description of the samples preparation, all the NMR experiments performed are introduced.
The analysis was carried out on two samples of ionic liquids: the pure liquid 1-ethyl-3 -methylmidazolium - trifluoromethanesulphonate (EMImTfO) and its mixture with Lithium-triflouromethanesulphonate (EMImTfO + LiTfO) at different temperatures aiming to describe the interaction of ^{1}H both with ^{19}F and ^{7}Li isotopes.

2.1 Sample preparation

EMImTfO (purity of 99%) and LiTfO (purity of 96%) are commercial products purchased from IoLiTec and Sigma Aldric, respectively.
The ionic liquid EMImTfO is constituted by a positively and negativity charged ion free to move separately in volume of the sample.
The cation shows a polar head made by the ring and two short substituent attached in its positions 1 and 3, as reported in figure 2.1. A mixture of the

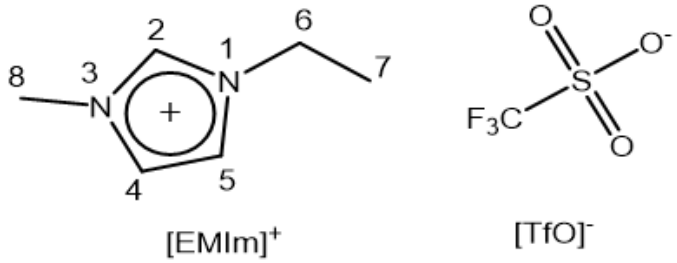

Figure 2.1: *1-ethyl-3- methylmidazolium trifluoromethanesulphonate*

ionic liquid and the salt was obtained by adding 0.0613 g of LiTfO to 0.99139 g of EMImTfO under magnetic stirring (Fig. 2.2) which translates into a molar fraction of lithium salt equal to 0.1.

$$\frac{n(LiTfO)}{n(EMImTfO) + n(LiTfO)} = 0.1M \tag{2.1}$$

As previously done [18], the mole fraction of LiTFSI e.g., 0.1 was chosen because it usually gives electrolytes with good to high Li^+ conduction values and, at the same time, is far from too viscous, quasi-solid, compositions.
The pure EMImTfO and the mixture with LiTfO were transferred into 5 mm diameter NMR tube adding also a close-end capillary tube filled with deuterated dimethylsulfoxide (DMSO-d_6). DMSO is required to guarantee a uniform magnetic field during the NMR experiment: by locking such field at the its frequency, oscillations in time are reduced improving the quality of measurements. The samples were then placed under vacuum for approximately one day to get rid of possible traces of water, finally the samples were flamed-sealed (Fig. 2.3).

Figure 2.2: *Stirring process*

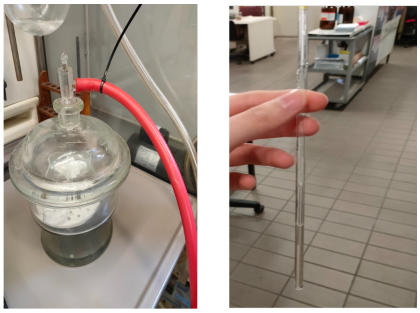

Figure 2.3: *Vacuum pump and final sample*

2.2 NMR experiments

The NMR investigation of the samples consists in several experiments including the measurement of the dynamic parameters like T_1 (time constant of the longitudinal relaxation) and D (diffusion coefficient) as well as the correlation experiments (Hoesy, both 1D and 2D) aiming to evaluate how close are the nuclei in the volume of the sample .
All the experiments reported in this work were performed using Brucker's ultrashielded magnet operating at 11.74 T, which corresponds to ^{1}H and ^{19}F Larmor frequencies of 500.13 MHz and 470.59 MHz, respectively. The instrument was carefully tuned, shimmed and the 90° pulses calibrated each time.
The processing has been done using Brucker's TopSpin 4.1.1. software and Origin 2901b version was used for all the numerical analysis.

Figure 2.4: *Bruker ultra-shielded magnet*

2.2.1 T_1 experiment

T_1 is the time constant related to the longitudinal relaxation of the spins and it is important for the correct setup of the NMR experiments that will be introduced later on.
In simple vector model, before starting any NMR experiment, the equilibrium magnetization, M_0, is aligned on z axis and parallel to the static magnetic field, but in this conditions it is not observable. When a radiofrequency pulse is applied to the equilibrium magnetization, the z-magnetization is rotated towards the transverse plane (x,y) until such pulse is switched off. At this point the

equilibrium conditions are going to be re-established. This process is called *longitudinal relaxation or spin-lattice relaxation* and consists in the recovery of the magnetization along z axis by losing some energy since at the equilibrium we are at the lowest energy level (energy is not actually lost, but released as heat even if there are not appreciable changing in temperature).
The equation governing the longitudinal relaxation phenomenon is the one proposed by Bloch.

$$\frac{dM_z}{dt} = \frac{(M_0 - M_z)}{T_1} \tag{2.2}$$

It describes an exponential behaviour where M_0 is the magnetization at equilibrium and T_1 is the spin-lattice relaxation time constant. Solving the (2.2) with the initial condition of M_z, magnetization at t=0 s, equal to zero.

$$M_z = M_0(1 - \exp(-\frac{t}{T_1})) \tag{2.3}$$

T_1 pulse sequence and measurement

T_1 is experimentally measured using the so called *inversion recovery pulse sequence*, reported in Fig 2.5. It is a pulse sequence where the magnetization is first inverted from the equilibrium position by a 180° pulse till it reaches the -z axis. After the pulse, the magnetization is allowed to relax for a time τ, and moves back to z axis passing though transverse plane x,y.
After a suitable time τ, a 90°pulse pushes back the magnetization toward the transverse plane. The resulting FID is observed and then Fourier transformed to give the spectrum.
If τ is very short, magnetization is still on -z axis at the end of the delay. The 90° pulse will rotate the magnetization onto the -y axis giving the highest negative signal (Fig 2.6a). The experiment is then repeated increasing τ. As τ gets longer more relaxation takes place and the magnetization shrinks towards zero: the result is a negative line in the spectrum, but with decreasing intensity. Eventually the magnetization goes through zero and then starts to increase along +z axis, giving a positive line in the spectrum. Very long delays ($\tau = \tau^*$) will allow the full recovery of the magnetization. In this conditions the 90° pulse rotates it to +y axis giving the highest positive signal (Fig 2.6b). Thus, by recording spectra with different values of the delay it is possible to map out the recovery of the z-magnetization from the intensity of the observed lines.

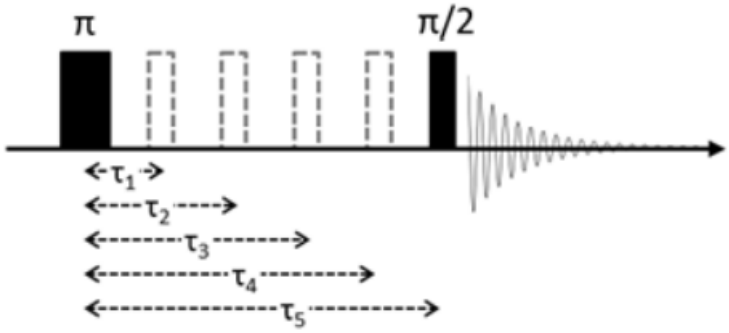

Figure 2.5: *The pulse sequence for the inversion recovery experiment used to measure longitudinal relaxation*

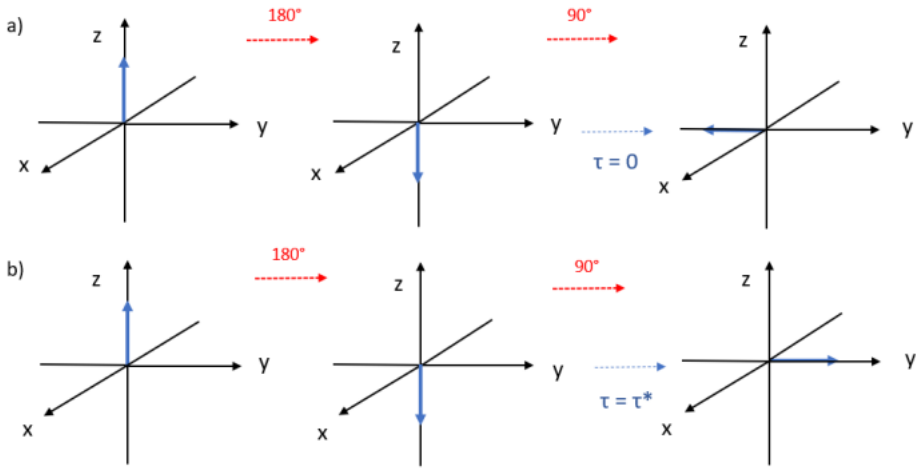

Figure 2.6: *vector model describing the T^1 sequence for (a) a very short delay time τ=0, and (b) a very long delay time, $\tau = \tau*$*

2.2.2 Dosy experiment

Molecular diffusion is the transitional movement of molecules due to the Brownian motion of particles above absolute zero and is often simply called diffusion or self-diffusion. It depends on may different parameters like size and shape of the molecule, temperature and viscosity. Assuming a spherical shape of the molecule, the self-diffusion coefficient D is described by the Stokes-Einstein equation relating to Boltzmann constant (k), viscosity (μ), temperature and the hydrodynamic radius.

$$D = \frac{kT}{6\pi\mu r_s} \tag{2.4}$$

Unlike the T_1 relaxation time, all the nuclei present on a given species, i.e. cation, have the same diffusion coefficient D.
Diffusion of molecules can be evaluated by pulsed field gradient (PFG) NMR via dosy experiment. The dosy experiments run in this thesis provided us with the D values of different species in the ionic liquid samples, that is protons in the $[EMIm]^+$ cation as well as fluorine in the $[TfO]^+$ anion and lithium Li^+ in case of the mixture.

Diffusion pulse sequence and measurement

PFG NMR can be used to evaluate the position of a specific molecule inside of the ionic liquid volume. Gradients are used to spatially label the molecule, i.e. mark them according to their position in the sample tube. Broadly speaking, after a 90° pulse, spins in the y-axis are de-phased by a gradient characterized by a certain duration δ, length of the gradient. After the gradient, the molecule is free to diffuse. After a suitable diffusion time, Δ, an opposite gradient re-phases the spins.
If the molecule does not move during Δ (sketched din blue in figure 2.7), the signal is perfectly refocused with no loss in intensity. Otherwise, in case of diffusion (sketched in red in figure 2.7), the intensity of the signal is attenuated according to the Stejskal–Tanner equation [20]

$$I = I_0 \exp\left(-D\gamma^2 g^2 \delta^2 (\Delta - \frac{\delta}{3})\right) \tag{2.5}$$

where g is the strength of the gradient, γ is the gyromagnetic ratio of the nucleus involved and I_0 is the intensity of unattenuated signal. Several pulse sequences have been introduced to mitigate some artefacts and improve the experiments.

Here we used the bipolar pulse longitudinal eddy current delay (BBB-LED) pulse sequence. Before starting the experiment Δ and δ need to be optimized

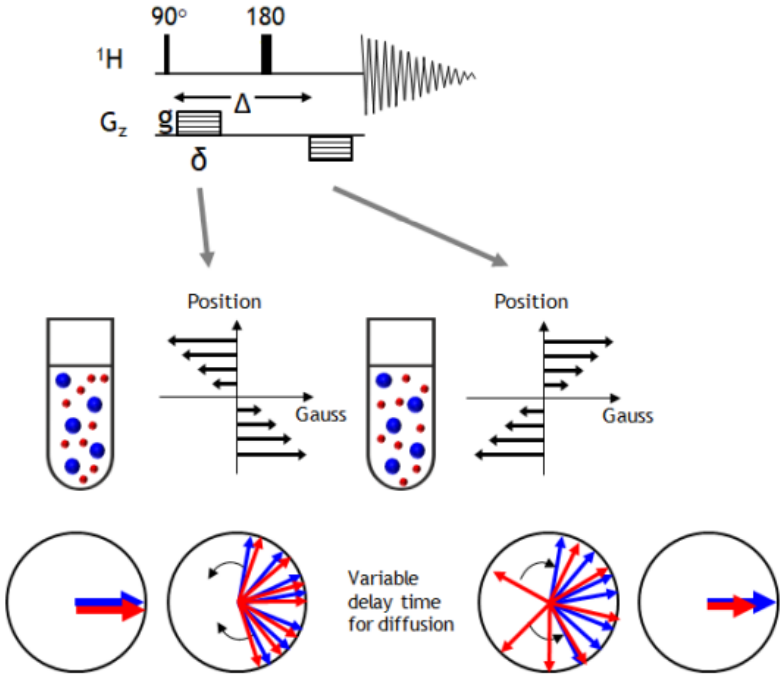

Figure 2.7: *Basics of a gradient echo*

to obtain reliable and precise D values.
The optimization is carried out by 1D experiments making a comparison between a reference spectrum recorded with 2% of the gradient strength (g) and some trail values of Δ and δ and a second spectrum where g is increased till 95%. An attenuation of roughly 5% has to be achieved, otherwise the procedure is repeated adjusting the values of Δ and δ until matching this condition and then the 2D diffusion experiment can be performed.

2.2.3 2D ^{1}H-^{19}F and ^{1}H-^{7}Li Hoesy experiments

In this section the main part of the experiments performed in this work are presented: the aim was to understand the interaction between the protons of the IL cation and both the fluorine of the IL anion and lithium cations present in the samples using the heteronuclear NOE spectroscopy (Hoesy).
The Nuclear Overahauser effect (NOE) is a tool used in NMR spectroscopy to evaluate mutual interactions among nuclei.

During the NOE experiment a family nuclei changes its resonance intensity when another family of nuclei is perturbed [12]. This technique gives a relative measurement of the distances among nuclei in the sample, which can be of the same (homonuclear case) or different type (heteronuclear case). In this project, hoesy spectra were used to understand which proton is closer to the fluorine or lithium atoms.
From the pratical standpoint, the heteronuclear NOE is a 2D experiment, so the pulse sequence is characterized by pulses on two different channels, one for the proton, and one for the heteronucleus (^{19}F or ^{7}Li). Figure 2.8 shows the pulse sequence used in this thesis. This kind of sequence is particularly interesting for ionic liquids and their mixtures as different nuclei (^{1}H, ^{19}F, ^{7}Li) are located on different ions: the hoesy spectra will then give access to the relative proximity between the different species in the system.
In this thesis, ^{1}H-^{19}F hoesy experiments were performed with proton in the 1st channel and fluorine on the 2nd channel, on both EMImTfO and EMImTfO + LiTfO at 288K and 298K. Similarly to ^{1}H-^{19}F hoesy, ^{7}Li-^{1}H hoesy experiments were carried out to investigate the interactions between lithium and protons in sample EMImTfO + LiTfO being the only one containing Lithium. The temperature selected were 288 K, 298 K and 318 K. Due to technical reasons, in these series of Hoesy an inverse detection has been used, with lithium on the 1st channel and proton in the 2nd channel. This inverse-detected sequence works as well as the direct one, but it takes a little bit longer in order to achieve an acceptable resolution in the indirect dimension.

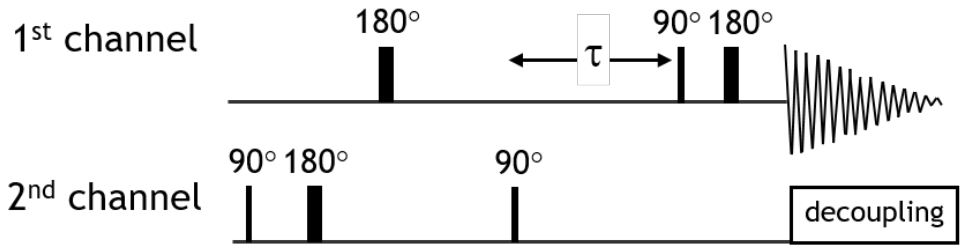

Figure 2.8: *Hoesy pulse sequence*

In this work a series of Hoesy experiments was performed for each nuclear pair in the two samples at each temperature varying the mixing time parameter, indicated as τ in figure 2.8. Such parameter is the time between the two consecutive 90° pulses in the two channels when the nuclei are free to interact one another and allows the NOE to build up. By integrating the cross preaks in

the 2D hoesy spectra measured at increasing τ and plotting them against the mixign time, it is possible to draw the NOE build up curves for each interacting ^{1}H-^{19}F or ^{1}H-$_7$Li nuclear pair. For a semiquantitative analysis of Hoesy cross peas, the absolutes integrated need to be corrected by a factor that takes into account the number of nuclei contributing to the NOE signal. The correction factor is calculated as follows:

$$\frac{N_I * N_S}{N_I + N_s} \tag{2.6}$$

with N_I the number of ^{1}H and N_S the number of ^{19}F or^{7}Li nuclei contributing to the observed NOE signal The proper fit of such build up curves gives the cross relaxation parameter, σ, that gives hints on "how close" are the nuclei.
Taking out the cross relaxation from the experiment is not so straightforward, but some steps in the data analysis procedure are necessary, as it will be deeply explained in chapter 3. By now, only the equations used to fit the build up curve are introduced.
Firstly the fitting with the *Solomon equation* [21], [22] was performed.

$$NOE = \frac{1}{2}\exp(-(R-\sigma)\tau)(1-\exp(-2\sigma\tau)) \tag{2.7}$$

In this equation, now called HOESY 1, τ is the variable representing the mixing time, σ is the cross relaxation to be calculated while R is the *relaxation rate*, which is defined as the reciprocal of the relaxation time.
In HOESY 1, the relaxation rate is an averaged value between the R of a single proton (R_I) and the one of the heteronucleus, fluorine or lithium, (R_S). Under this condition the fitting was tried both considering R as a constant and as a parameter whose value is an output of the fitting itself. In case of R considered as a constant its value is calculated from T_1, in particular it is the average between R_I=1/T_1(^{1}H) and R_S=1/T_1(^{19}F or ^{7}Li).
A modified version of the Solomon equation, now called HOESY 2, takes account of the differences in the relaxation rate between protons and fluorine [22] [21].

$$NOE = M_0\sigma\frac{2\sinh K\tau}{K}\exp(\frac{R_I+R_S}{2}\tau) \tag{2.8}$$

$$K = \frac{\sqrt{R_I^2 - 2R_IR_S + R_S^2 + 4\sigma^2}}{2} \tag{2.9}$$

Where M0 is a normalization factor that is necessary otherwise this kind of equation is unable to fit values of the order of magnitude as 1e9 or 1e10.
Also in this case the fitting was performed both considering R_I and R_S as constants and parameters. To reduce the numbers of unknown, the raw data obtained from the build up curve were already normalized, then the normalization factor was set to 1 during the iterations.
As the signal attenuation due to diffusion may affect the cross relaxation values, data were also fitted using a modified equation taking into account a Stejskal-Tanner term, as reported in [20]. We refer to this equation as HOESY 3.

$$NOE = M_0\sigma\frac{2\sinh K\tau}{K}\exp(\frac{R_I + R_S}{2}\tau)\exp\left(-D\gamma^2g^2\delta^2(\Delta - \frac{\delta}{3})\right) \qquad (2.10)$$

Basically, HOESY 3 corresponds to the modified Solom equation 2.7 multiplied by the signal attenuation already introduced in equation 2.5.
In this work the constants present in the equation 2.10 has the following values when Δ and δ have already been properly optimized:

- g=4574.3 G/m
- γ_H=4257.75 s^{-1} G^{-1}
- γ_F= 4004.71 s^{-1} G^{-1}
- γ_{Li}= 1654.60 s^{-1} G^{-1}
- Δ = as optimized in the corresponding diffusion experiment
- δ = as optimized in the corresponding diffusion experiment

In equation 2.10 R_I and R_S were treated both as constants and parameters as done with HOESY 2.
As in the initial part of the build-up curve, the signal intensities increase only due the magnetization transfer between nuclei, a linear fit of the beginning of the build-up curve is also possible to get rid of the relaxation effects and extract a measure of the interaction strength from the slope [18].
In this thesis all the proposed fitting equations have been tried on the ^{1}H-^{19}F on the EMImTfO + LiTfO sample at 298 K dataset and compared one another, as reported in chapter 3. After this comparison, the HOESY 1 (considering R as a parameter) has been chosen as the best option, thus all the other datasets have been fitted with this equation.

The 2D hoesy experiments are relatively time-consuming, since each single experiment lasts from 2 h to 4 h, according to its mixing time. All in all, performing an entire series of Hoesy at variable mixing times has taken more or less three days and this could be considered a drawback related to this technique.

2.2.4 1D Hoesy

2D Hoesy is the standard methodology to extract cross relaxation rates, but the experimental time may be an issue. Alternatively, 1D Hoesy experiments can be in principle carried out as they are so much faster than classical 2D Hoesy requiring only few minutes for each experiments (from 2 to 10 minutes). To verify if they are reliable tools to measure the cross relaxation of the investigated system, they were performed on the EMImTfO + LiTfO sample at a temperature of 298 K and analyzed to extract the cross relaxation σ as done in 2D Hoesy experiments.
Figure 2.9 shows the pulse sequence used in this thesis. Broadly speaking, the proton is detected (1^{st} channel) while pulsing on the heteronucleus (^{19}F or ^{7}Li, 2nd channel). The first 180° pulse on the heteronucleus can be a standard non-selective hard pulse, or a shaped selective soft pulse. The latter is needed when the molecule presents more than one ^{19}F atom, by means of the selective sequence we can choose which one to pulse making it interact with the protons. In our case, a selective pulse is actually not needed since EMImTfO shows only one peak of Fluorine atoms, since they are chemically and magnetically equivalent. However, both selective and non selective sequences have been tried to evaluate whether the use of a selective pulse affect somehow the quality of the spectrum. The analysis was carried out following the same procedure of classical Hoesy constructing the build up curve and fitting it to compute the cross relaxation σ. Fitting was performed using HOESY 1 only (equation 2.7) considering R as a parameter.

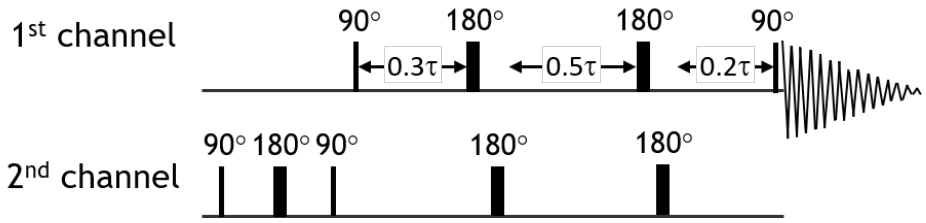

Figure 2.9: *1D Hoesy pulse sequence*

Chapter 3

Results and discussion

In this chapter all the results are reported including the processing steps from the raw NMR to the values of interest taken out from them. Finally the results are interpreted and discussed.

3.1 T_1 experiment

The T_1 relaxation time have been calculated for all nuclei of interest in this work, ^{1}H, ^{19}F and ^{7}Li following the same general procedure using TopSpin 4.1.1. software, here described only for ^{1}H in EMImTfO + LiTfO at 318 K.
The raw inversion-recovery experiment is reported in figure 3.1. The spectrum was manually phased, and different peaks integrated, as in figure 3.2. TopSpin 4.1.1 automatically exports the integrals taking out the T_1 value for each proton of the molecule (figure 3.3) using eq. (2.3) for the fit.
Now all the computed values are here reported in tables divided by sample, temperature and nucleus observed starting from ^{1}H. The error estimated to be within 2.5%.

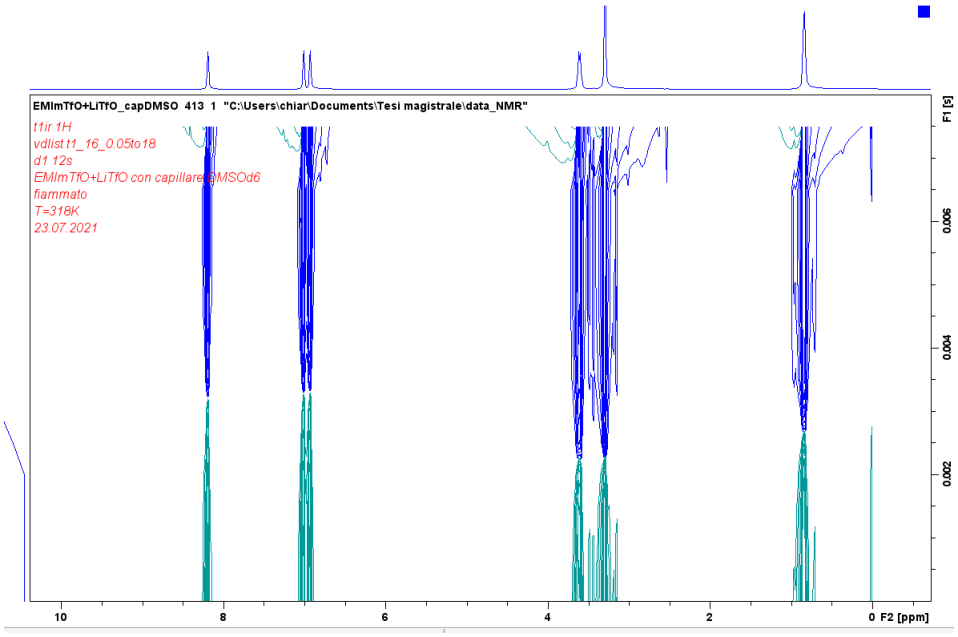

Figure 3.1: *^1H inversion recovery experiment for the T_1 measurement of the sample EMImTfO + LiTfO at 318 K.*

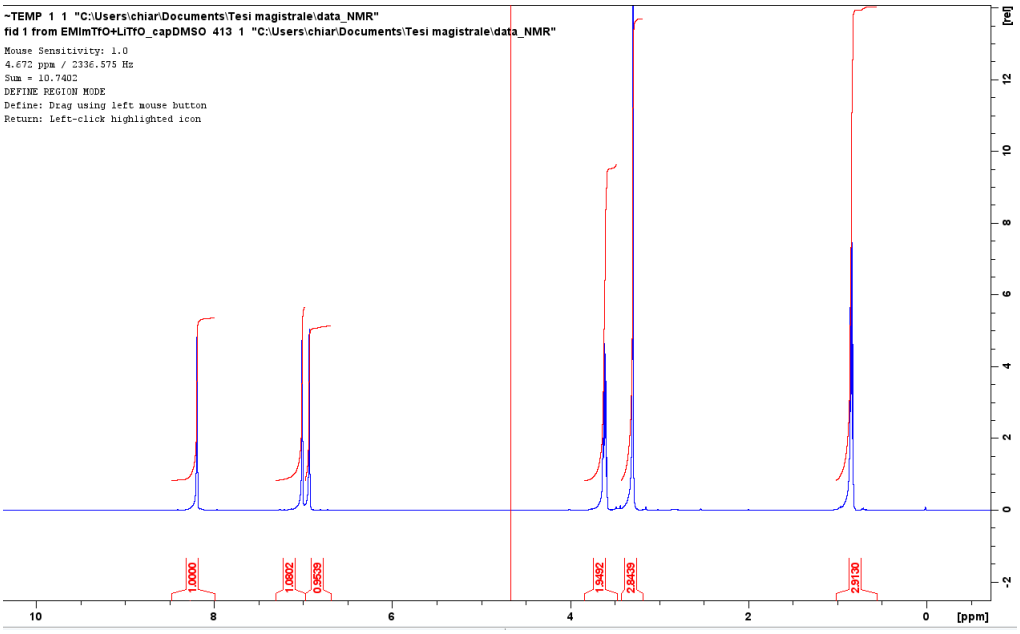

Figure 3.2: *Integration step during the analysis of ^1H inversion-recovery spectrum of the sample EMImTfO + LiTfO at 318 K.*

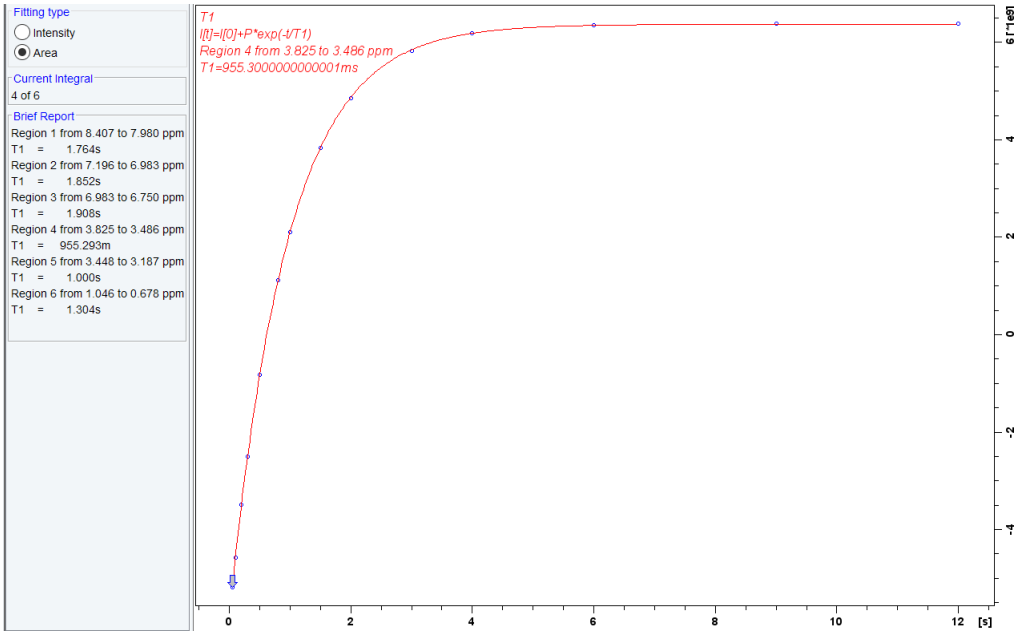

Figure 3.3: *Fit to T_1 decay corresponding to proton H4, ^1H, EMImTfO + LiTfO at 318 K*

3.1.1 ^{1}H T_1 results

The following tables report all the T_1 results relative to ^{1}H nuclei.

Table 3.1: *^1H T_1 values of , EMImTfO + LiTfO, , estimated error 2.5%*

$T_1[s]$	$318K$	$298K$	$288K$
H2	1.30	1.63	1.48
H5	1.00	1.73	1.57
H4	0.96	1.78	1.45
H6	1.90	0.94	0.94
H8	1.86	1.03	1.075
H7	1.77	1.08	0.95

Table 3.2: *^{1}H T_1 values of , EMImTfO, estimated error 2.5%*

$T1[s]$	$298K$	$288K$
H2	1.15	1.26
H5	1.57	1.47
H4	1.60	1.25
H6	0.81	0.80
H8	0.83	0.89
H7	0.99	0.89

3.1.2 ^{19}F and ^{7}Li T_1 results

EMImTfO shows only one fluorine peak, so just a single T_1 has been calculated per each experiment following the same procedure reported at the beginning of section 3, I report as an example a single inversion recovery spectrum relative to ^{19}F on EMImTfO + LiTfO at 298 K. All ^{19}F and ^{7}Li results are tabulated in the following tables.For what concerns ^{7}Li, there are not changes nor critical points to be underlined.

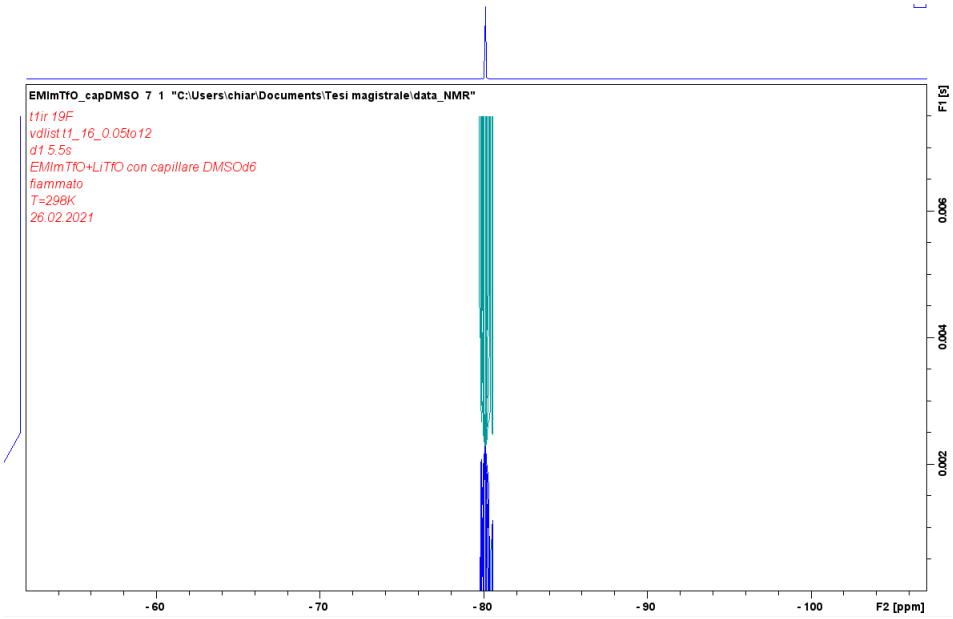

Figure 3.4: *^{19}F inversion recovery experiments for the T_1 measurement of sample EMImTfO + LiTfO at 298 K*

Table 3.3: *^{19}F T_1 values, estimated error 2.5%*

$^{19}F\ T_1[s]$	$298K$	$288K$
EMImTfO + LiTfO	0.99593	0.85771
EMImTfO	1.147	1.023

Table 3.4: *^{7}Li T_1 values, estimated error 2.5%*

$^{7}Li\ T_1[s]$	$318K$	$298K$	$288K$
EMImTfO + LiTfO	0.91226	1.154	1.270

Relaxation rates

As introduced in section 2.2.4 the relaxation rate can be directly computed from T_1 . Here Ravg, RI and RS are reported per each series of experiments since these values will be used to fit the build up curves.

Table 3.5: *Relaxation rates for, all protons (R_I) and for fluorine (R_S) of sample EMImTfO + LiTfO at 298K*

	$Ravg$	R_{I}	R_{S}
H2	0.81	0.61	1.00
H5	0.79	0.58	1.00
H4	0.78	0.56	1.00
H6	1.03	1.07	1.004
H8	0.99	0.97	1.00
H7	0.96	0.93	1.00

Table 3.6: *Relaxation rates for, all protons (R_I) and for fluorine (R_S) of sample EMImTfO + LiTfO at 288K*

	$Ravg$	R_{I}	R_{S}
H2	0.92	0.67	1.17
H5	0.90	0.64	1.17
H4	0.93	0.69	1.17
H6	1.11	1.06	1.17
H8	1.05	0.93	1.17
H7	1.11	1.05	1.17

Table 3.7: *Relaxation rates for, all protons (R_I) and for fluorine (R_S) of sample EMImTfO at 298K*

	$Ravg$	R_{I}	R_{S}
H2	0.82	0.77	0.87
H5	0.75	0.64	0.87
H4	0.75	0.63	0.87
H6	1.05	1.23	0.87
H8	1.00	1.20	0.87
H7	0.94	1.01	0.87

Table 3.8: *Relaxation rates for, all protons (R_I) and for fluorine (R_S) of sample EMImTfO at 288K*

	$Ravg$	R_{I}	R_{S}
H2	0.89	0.80	0.98
H5	0.83	0.68	0.98
H4	0.89	0.80	0.98
H6	1.12	1.26	0.98
H8	1.05	1.12	0.98
H7	1.05	1.12	0.98

Table 3.9: *Relaxation rates for, all protons (R_I) and for lithium (R_S) of sample EMImTfO + LiTfO at 298K*

	$Ravg$	R_{I}	R_{S}
H2	0.74	0.61	0.87
H5	0.72	0.58	0.87
H4	0.71	0.56	0.87
H6	0.97	1.07	0.87
H8	0.92	0.97	0.87
H7	0.90	0.93	0.87

Table 3.10: *Relaxation rates for, all protons (R_I) and for lithium (R_S) of sample EMImTfO + LiTfO at 288K*

	$Ravg$	R_{I}	R_{S}
H2	0.73	0.67	0.79
H5	0.71	0.64	0.79
H4	0.74	0.69	0.79
H6	0.92	1.06	0.79
H8	0.86	0.93	0.79
H7	0.92	1.05	0.79

Table 3.11: *Relaxation rates for, all protons (R_I) and for lithium (R_S) of sample EMImTfO + LiTfO at 318K*

	$Ravg$	R_{I}	R_{S}
H2	0.83	0.57	1.10
H5	0.82	0.54	1.10
H4	0.81	0.53	1.10
H6	1.07	1.05	1.10
H8	1.05	0.99	1.10
H7	0.93	0.77	1.10

3.2 Dosy experiment

As introduced in chapter 2, dosy is a pseudo-2D experiment requiring some preliminary 1D tests to properly set the diffusion parameters Δ and δ.
In this section the result of the preliminary part is reported followed by the processing of the 2D dosy and its results.

3.2.1 Preliminary Dosy experiments

In the optimization procedure two 1D spectra are recorded using 2% and 95% respectively, of the gradient strength (g) and some guess value of Δ and δ. The goal is to achieve an attenuation of roughly 95%. Δ and δ are considered properly set if the signal is attenuated to roughly the 5% of its initial value, otherwise the preliminary experiment must be repeated changing the diffusion parameters.

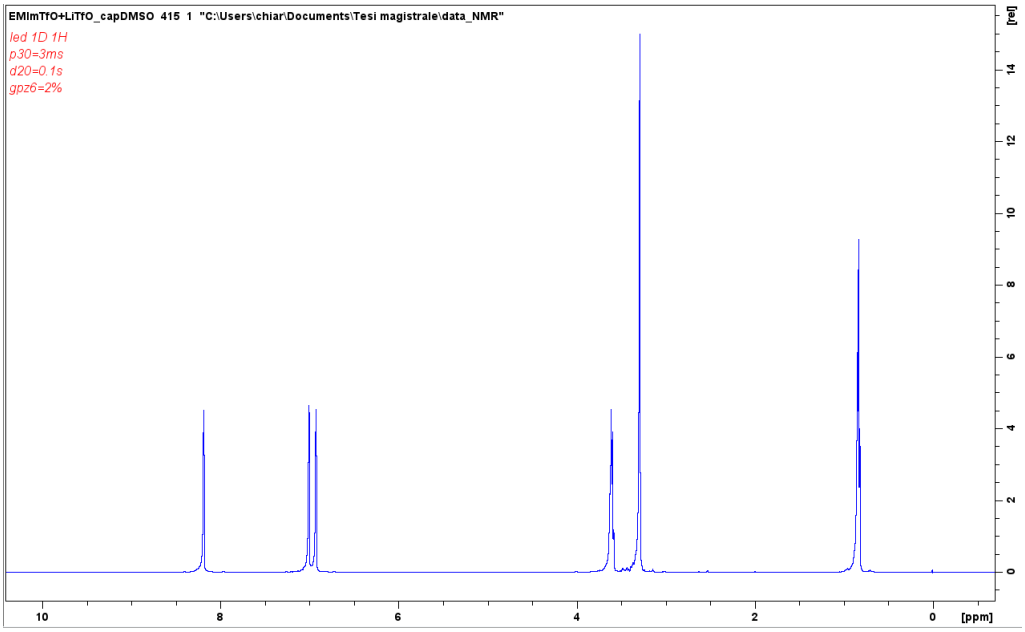

Figure 3.5: *^1H 1D dosy optimization spectrum 2% of gradient stregth for sample EMImTfO + LiTfO*

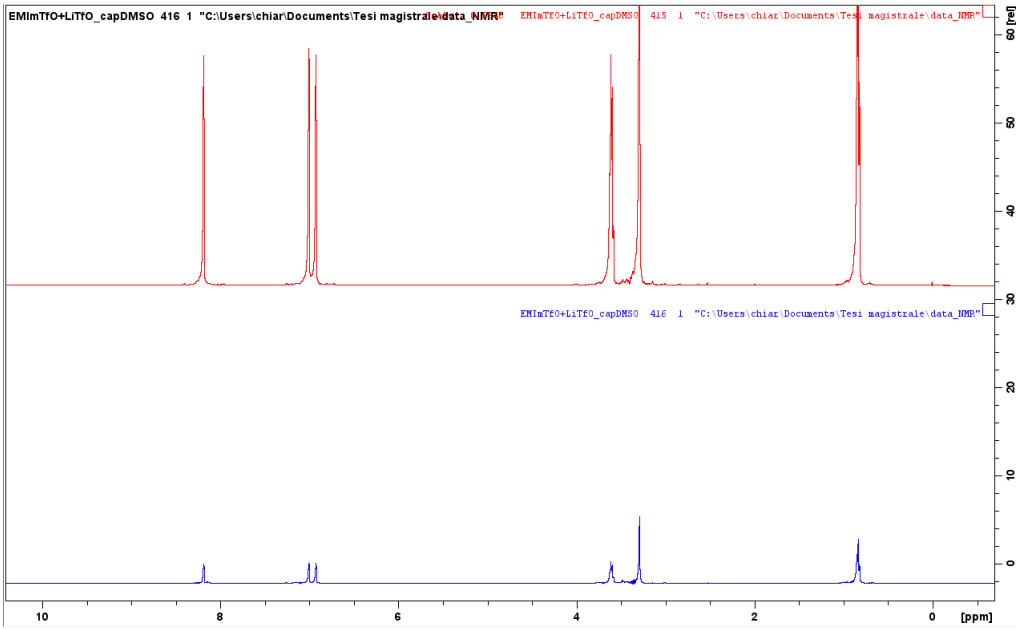

Figure 3.6: *Comparison of ^{1}H 1D dosy optimization spectra using2% (in red) and 95% (in blue) of the gradient strength for sample EMImTfO + LiTfO*

3.2.2 Dosy experiment results

Under the processing point of view, 2D dosy experiment is analyzed using the same module of TopSpin 4.1.1 used in the proper values of the constant T_1 experiment. The Stejskal-Tanner equation (eq. (2.5)) is used for the fit of the attenuation curves and the proper values of the constants are set automatically via the command setdiffparm. The procedure still consists in manually phasing and integrating the peaks, then the the integrals are exported and the software automatically compute the diffusion coefficient.

When performing the experiment relative to ^{1}H nucleus, the software gives the diffusion coefficient for each integrated peak, that is for each proton in the EMIm cation. Being diffusion strictly related to a translation, all the protons moves with the same D in the volume, so it has to be considered just a single coefficient for all the protons that is the averaged one. Indeed, even if D values are obtained for six protons, they are equal within the experimental error. This confirms the quality and the reliability of the measurement.

For what concerns fluorine and lithium, they show just a single peak, so no average is necessary.

Here all the diffusion coefficients extracted for all nuclei in the different samples

and temperatures are reported. The estimated error is of 1%. Looking at table

Table 3.12: *Diffusion coefficients measured for the different nuclei for the sample EMImTfO + LiTfO,estimated error of 1%*

$D\ [m^2/s]$	^1H	^{19}F	^7Li
298K	2.81E-11	1.52E-11	5.93E-12
288K	1.86E-11	9.75E-12	3.85E-12

Table 3.13: *Diffusion coefficients, EMImTfO, estimated error of 1%*

$D\ [m^2/s]$	^1H	^{19}F
298K	3.65E-11	2.37E-11
288K	2.78E-11	1.81E-11

3.12 and 3.13 separately, it' possible to notice that when decreasing the temperature from 298K to 288K the diffusion coefficient decreases. This behavior is related to the viscosity which increases lowering temperature and hindering the diffusion process.
The influence of temperature and viscosity on D is described by the equation (2.4) upholding the trend just explained.
Comparing now the samples, it seems that the presence of lithium salt generally works against the diffusion process since all the values related to ^{1}H and ^{19}F are bigger in EMImTfO than in EMImTfO + LiTfO.

3.3 2D Hoesy experiments

In this section all the processing steps related to the computation on the cross relaxation, σ, is reported both for ^{1}H - ^{19}F and ^{7}Li - ^{1}H Hoesy experiments, then the results are discussed.
As introduced in chapter 2, series of 2D Hoesy experiments have been recorded varying the mixing time, thus the results consist in a huge amount of spectra that have been processed and analyzed. Here the full processing procedure is reported in detail just for one series, that is a given nuclear pair for one sample at specific temperature. Before starting with the hoesy result I report the 1D the ^{1}H spectrum, figure 3.8, to understand at which frequency each proton (or group of protons) appears. It is mandatory to deeply understand the hoesy.
Considering the $[EMIm]^{+}$ cation, all the numbered protons must be identified on the ^{1}H spectrum.The spectral interpretation stands upon two main concepts: Chemical shift and Spin coupling.

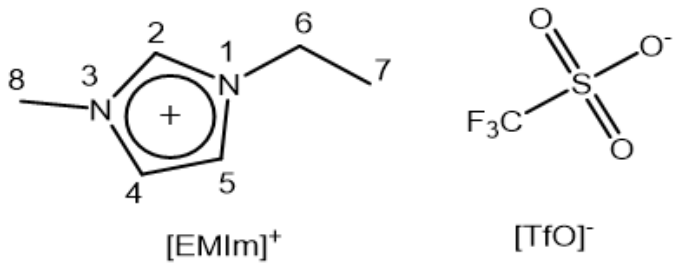

Figure 3.7: *Numbered structure of 1-ethyl-3- methylmidazolium trifluormethaneosulphonate*

- **Chemical shift:** nuclei, in this case ^{1}H, show a different resonance frequency depending on the atoms they are bonded to. If the bonding atom is attracting electrons, thus the nucleus is deshielded appearing at higher frequency. Conversely, if the nucleus is shielded, it appears at lower frequency. If some protons are bonded to the same atom seeing the same *panorama*, they are called *chemically equivalent* appearing as a single peak.

- **Spin coupling:** a single nucleus (or nuclei that are chemically equivalent) may feel the presence of others. When it occurs, the peak is split into n+1 lines (figure 3.9), where n is the number of equivalent partner nuclei the analyzed one interacts with. Generally speaking, a nucleus may feel the presence of partners across a distance of 3 bonds, even if there are some

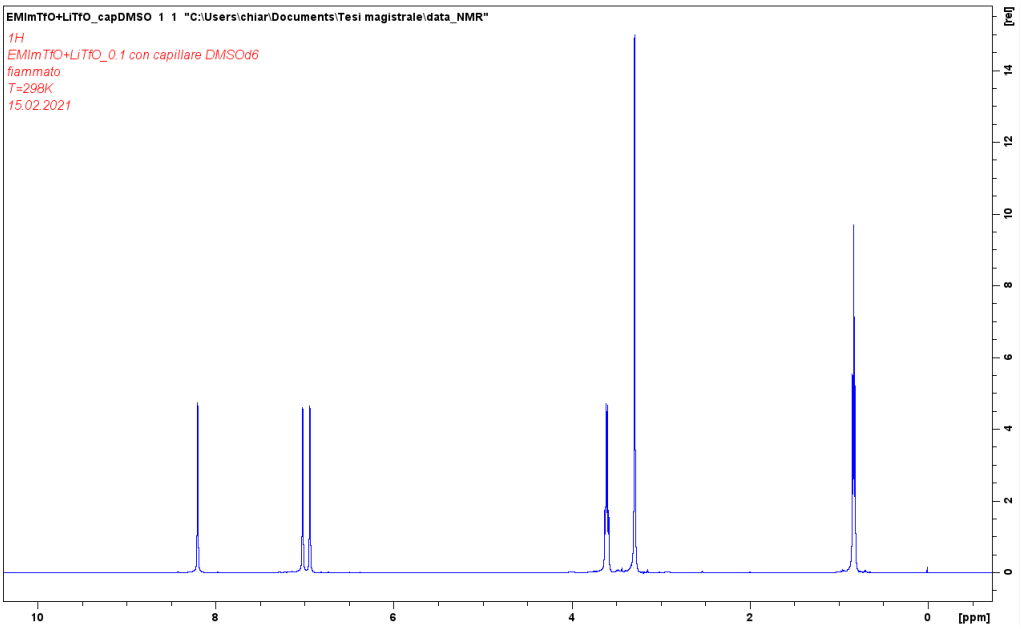

Figure 3.8: *1D spectrum ^1H 1-ethyl-3methylmidazolium trifluorosulphonate of the sample EMImTfO + LiTfO at 298K*

exceptions.

Considering both chemical shift and spin coupling it is possible to assign the peaks to the protons present on the $[EMIm]^+$ cation here named by their position as in figure 3.7.

Table 3.14: *Chemical shift of the protons in $[EMIm]^+$*

Chemical shift [ppm]	*Hi*	*multiplicity*
8.4	H2	singlet
7.2	H5	singlet
7.12	H4	singlet
3.76	H6	quartet
3.45	H8	triplet
0.99	H7	triplet

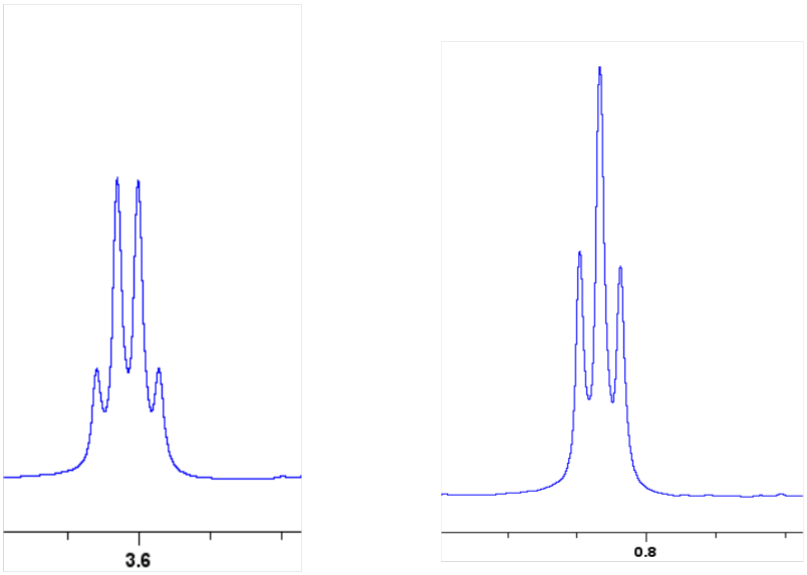

Figure 3.9: *Enlargements of 1D ^{1}H spectrum 1-ethyl-3-methylmidazolium trifluorosulphonate of EMImTfO + LiTfO at 298K: quartet corresponding to H6(left) and triplet corresponding to H7 (right)*

For sake of completeness here are also reported the 1D spectra of fluorine and lithium, but they do not require any particular interpretation since they both show a single peak. Just one lithium atom is present in EMImTfO+LiTfO sample only and 3 atom of fluorine that are chemically and magnetically equivalent.

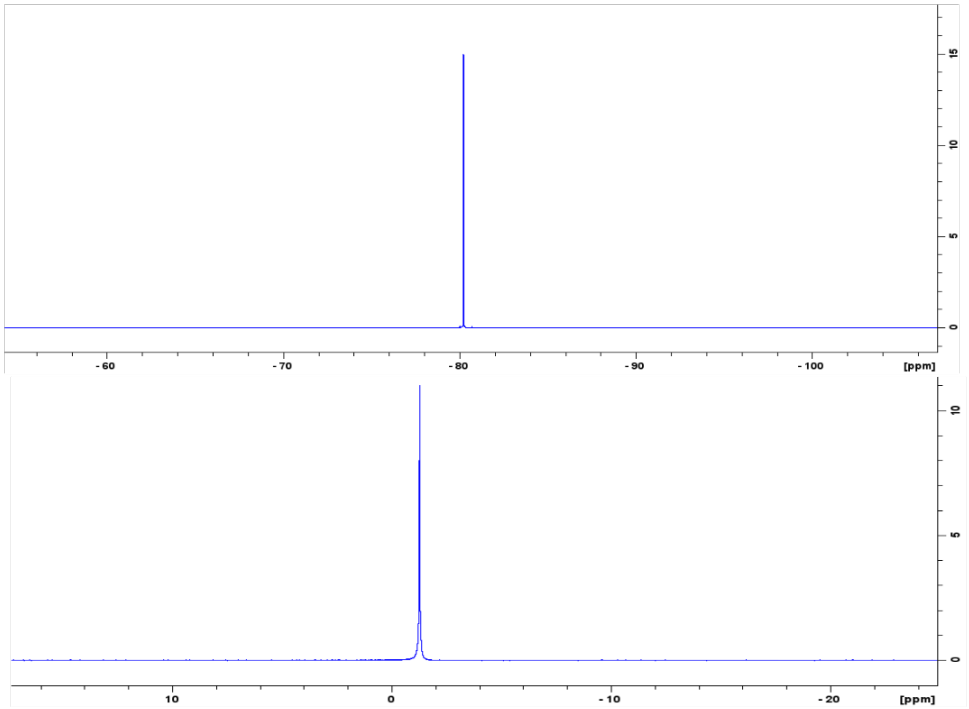

Figure 3.10: *1D ^{19}F (top) and ^{7}Li (bottom) spectra 1-ethyl-3-methylmidazolium trifluorosulphonate of EMImTfO + LiTfO at 298K*

3.3.1 2D ^{1}H - ^{19}F Hoesy

Acquisition and processing of 2D ^{1}H - ^{19}F spectra at variable mixing time

The ^{1}H - ^{19}F Hoesy e been performed on both samples at two different temperatures (298 K and 288 K).
The Fourier-transformed spectrum of a single ^{1}H - ^{19}F Hoesy experiment looks like the one in figure 3.11.
In such 2D correlation spectrum, we observe spots representing the interactions between protons and fluorine.
On the horizontal projection there is the ^{1}H spectrum just introduced and on the vertical dimension the ^{19}F internal projection that is a single peak, the spots in the middle of the map correspond to the interactions between Fluorine and each proton. Varying the mixing time the spots intensity varies too, an increase indicating qualitatively that the nuclei are closer.
At first sight it is not clear if mixing time really chances the intensity of spots from one experiment of the series to another thus the spectrum must be pro-

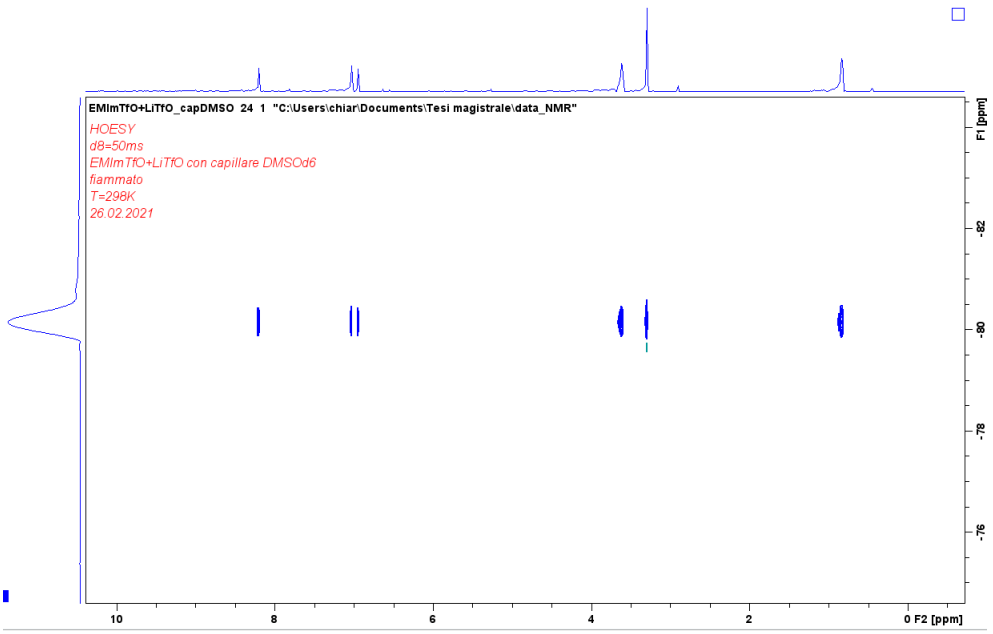

Figure 3.11: *2D ^{1}H - ^{19}F Hoesy, recored with a mixing of 0.05s for the sample EMImTfO + LiTfO at 298K*

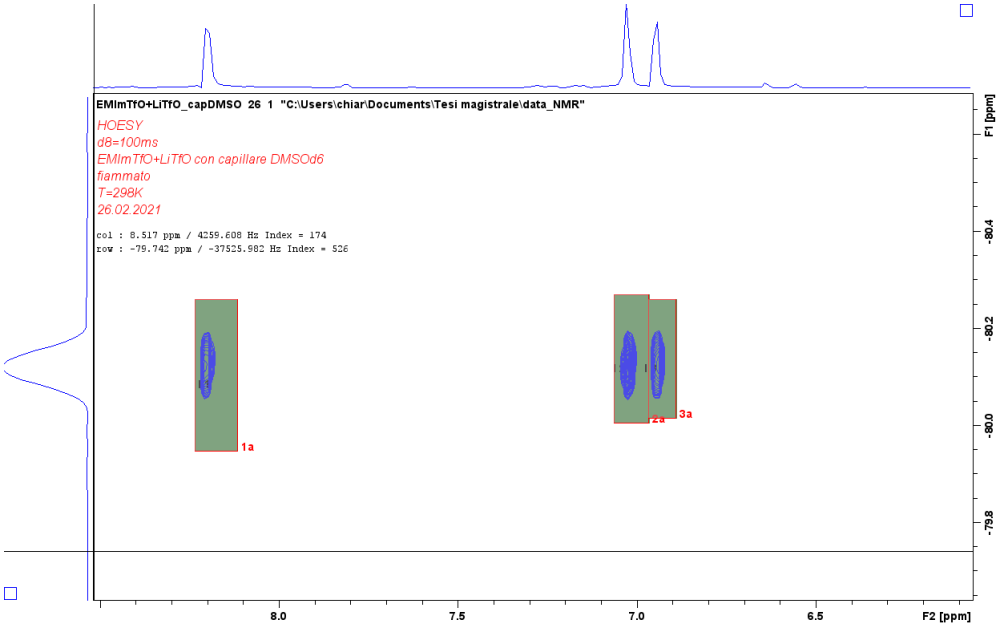

Figure 3.12: *^{1}H - ^{19}F Hoesy, mixing 0.1s, EMImTfO + LiTfO, 298K, imported integrals, detail*

cessed by integration taking out such intensities.

For sake of simplicity, in this work the full processing procedure is reported for only the ^{1}H - ^{19}F hoesy series on EMImTfO + LiTfO sample at 298K.
The integration has been manually performed for one experiment of the series by means of TopSpin 4.1.1, then integrals were saved and imported to the following experiments avoiding the manual procedure.
All in all there are 6 integrals per each experiment of the series related to the interactions of fluorine with protons staying in the position 2, 5, 4, 6, 8 and 7 of the $[EMIm]^{+}$ cation. The absolute integrals extracted for this series are reported in Table 3.15 for mixing time in range 20 ms - 4 s.

Table 3.15: *Absolute integral intensities extracted from the ^{1}H - ^{19}F of sample hosey EMImTfO + LiTfO at 298 K*

Mixing time [s]	*H2*	*H5*	*H4*	*H6*	*H8*	*H7*
0.02	2.72E10	2.41E10	1.97E10	5.61E10	1.04E11	6.76E10
0.05	2.66E10	2.88E10	1.52E10	4.45E10	1.00E11	5.18E10
0.1	7.82E10	8.23E10	7.48E10	1.87E11	2.35E11	2.27E11
0.12	8.70E10	9.83E1	8.26E10	2.17E11	2.68E11	2.61E11
0.15	1.12E11	1.20E11	1.02E11	2.60E11	3.10E11	3.11E11
0.2	1.37E11	1.44E11	1.33E11	3.22E11	3.83E11	3.94E11
0.25	1.63E11	1.69E11	1.60E11	3.76E11	4.45E1	4.64E11
0.3	1.87E11	1.91E11	1.84E11	4.22E11	4.97E11	5.22E11
0.35	2.09E11	2.09E11	2.07E11	4.61E11	5.46E11	6.02E11
0.4	2.25E11	2.28E11	2.25E11	4.94E11	5.81E11	6.20E11
0.45	2.42E11	2.42 E11	2.41E11	5.19E11	6.15E11	6.56E11
0.5	2.57E11	2.55E11	2.54E11	5.40E11	6.45E11	6.87E11
0.55	2.69E11	2.65E11	2.68E11	5.57E11	6.67E11	7.12E11
0.6	2.77E11	2.77E11	2.76E11	5.70E11	6.84E11	7.33E11
0.7	2.91E11	2.93E11	2.93E11	5.86E11	7.09E11	7.62E11
0.8	3.03E11	2.99E11	3.06E11	5.89e11	7.17E11	7.74E11
0.9	3.06E11	3.05E11	3.10E11	5.82E11	7.16E11	**7.75E11**
1	3.06E11	3.06E11	3.13E11	5.70E11	7.05E11	7.66E11
1.1	3.05E11	3.04E11	3.11E11	5.51E11	6.90E11	7.48E11
1.2	2.98E11	3.00E11	3.08E11	5.30E11	6.67E11	7.28E11
1.4	2.82E11	2.87E11	2.96E11	4.81E11	6.13E11	6.74E11
1.6	3.05E11	3.07E11	3.12E11	5.70E11	7.02E11	7.66E11
1.8	2.39E11	2.48E11	2.57E11	3.77E11	4.96E11	5.46E11
2	2.16E11	2.26E11	2.34E11	3.26E11	4.37E11	4.81E11
2.2	1.94E11	2.01E11	2.13E11	2.80E111	3.84E11	4.19E11
2.5	1.61E11	1.68E11	1.81E11	2.21E11	3.09E11	3.38E11
3	1.15E11	1.21E11	1.32E11	1.45E11	2.12E11	2.27E11
3.5	7.92E10	8.70E10	9.39E10	9.27E10	1.42E11	1.50E11
4	5.36E10	6.17E10	6.44E10	5.93E10	9.46E10	9.71E10

Plotting the data in table 3.15 the build up curves might be drawn and then fitted. As introduced in chapter 2, the data have been corrected by a factor that takes into account the number of nuclei contributing to the NOE signal (eq. (2.6) in section 2.2.3) and normalized by dividing all integrals by the highest value of all the series (value in bold in table 3.15) and again by ten. The resulting curves are reported in figure 3.13.

All the curves have the similar trend starting with a linear-like section, reaching then the maximum around a mixing time of 0.9 s and finally decreasing for

high values of τ. At first sight the shape looks good according to the results reported by [18] and [20], only the value at 1.6 s seems to be an outlier for all the protons thus it has been removed during the fit. Proton H7 is the one reaching the greatest intensity followed by H8 and H6 while H2, H4 and H5 fill the lower section and overlap themselves. The superimposition between H4 and H5 is quite intuitive because they stay on the ring close to each other (figure 3.7) seeing a similar panorama and showing very narrow difference in chemical shift (figure 3.8 and table 3.14) leading to an almost identical behavior in NOE experiments too.

Fitting of ^{1}H - ^{19}F build-up curves

All the curves have been fitted with all the equations presented in chapter 2 in order to compute the cross-relaxation, σ. For sake of simplicity here the fitting is reported just for one proton, H6, with all the equation, then all the computed σ are tabulated.
Figure 3.14 shows the build up curve of H6 fitted with the equation introduced in section 2.2.4. HOESY 1, HOESY 2 and HOESY 3 considering the relaxation rates either constants (labeled as "HOESY 1, 1 parameter", "HOESY 2, 1 parameter" and HOESY 3, 1 parameter" in figure 3.14) or parameters (the remaining curves in figure 3.14).
Starting which a visual interpretation aiming to evaluate which equation is suitable to fit the curve, it's clear that all fitting functions do not reproduce perfectly the curve when the relaxation rate is considered as a constant value (purple, red and pink lines) while all the others do (green, blue and light blue lines), the fitted curves are a bit "bent" when reaching the maximum and a bit shifted up in their terminal part .
Of course a visual inspection is not enough to judge the goodness of the fitting and its reliability, but it is necessary to analyze the data outcoming from the fitting performed using the Origin software and here reported in table 3.16 for proton H6 only.
Table 3.16 lists the experimental relaxation rates of H6 and fluorine as well as values coming out of the fitting process and the differences between experimental and fitted values.

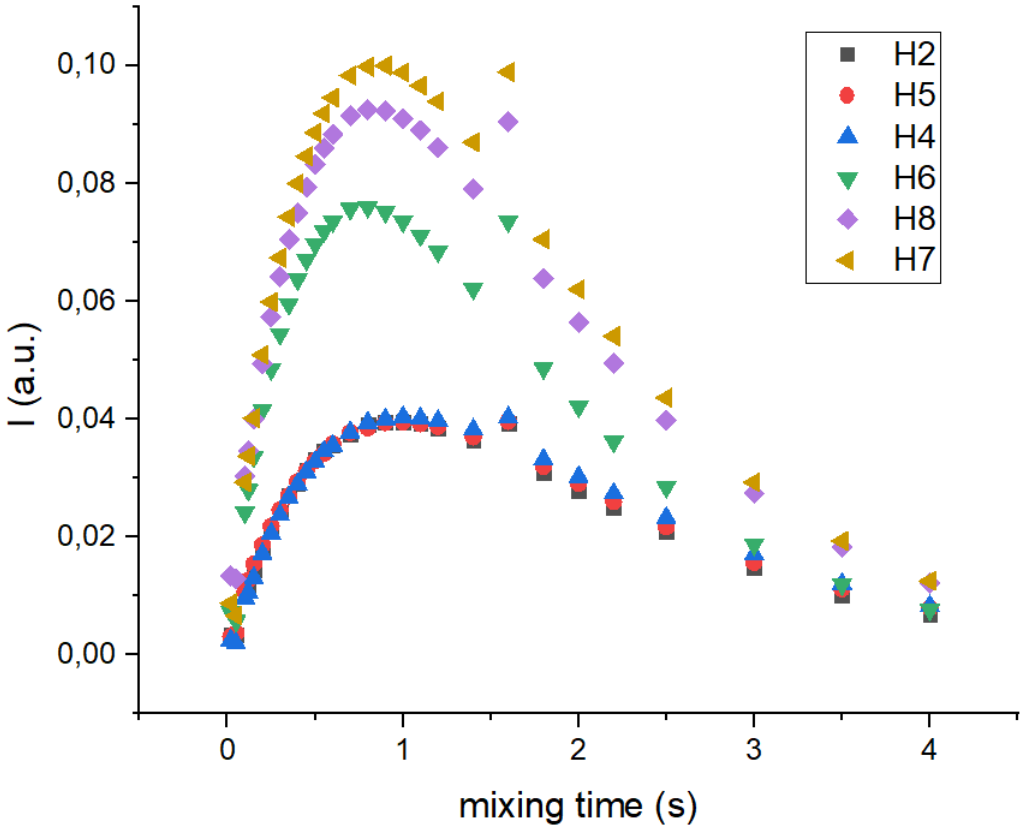

Figure 3.13: *Build up curves, hoesy ^{1}H - ^{19}F, EMImTfO + LiTfO, 298K*

A detail discussion of the different fits of figure 3.14 is reported in the following.

- **HOESY 1, 1 parameter:** in this case the cross relaxation is the only parameter to be fitted while the relaxation rate is derived from T_1. HOESY 1, is the first Solomon equation (2.7) that includes the average of the relaxation rate of each proton and fluorine. It seems a reasonable approximation reported also in [22] and [21] and [20], but the fitting does not reproduce properly the build up curve. That seems to be caused by the relaxation rate considered a constant value.

- **HOESY 1, 2 parameters:** it has been already claimed as the best fitting solution since it well reproduced the curve and it converges. Comparing data in table 3.16, the cross relaxations outcoming from 1 or 2 parametrized fitting are not completely different but not similar enough

to be considered both reliable, thus only HOESY1, 2 parameters has been chosen.

- **HOESY 2, 1 parameter:** HOESY 2, equation 2.8 and 2.9, overcomes the approximation of an averaged relaxation rate but considers separately the relaxation rates of protons and Fluorine as constants coming from T_1 as in [22] and [21]. In principle, this approach should be more precise. The result is basically the same of HOESY 1, 1 parameter (figure 3.14, purple and red lines) being these fitted curved almost superimposed, thus neither of them is able to properly fit the curve.

- **HOESY 2, 3 parameters:** in this case the relaxation of rates of of fluorine and protons are considered fitt-able values in analogy with HOESY 1, 2 parameters. Looking at table 3.16, it can be seen that, despite the acceptable R-squared values, HOESY 2, 3 parameters, is unable to converge due to overparametrization of the model, thus it is not a reliable option for the computation of the cross relaxation, even if it weel reproduces the build-up curve (blue line in figure 3.14).

- **HOESY 3, 1 parameter:** Equation (2.10), proposed in [20], takes into account also the diffusive motion of the molecule in the volume of the sample that might influence the cross relaxation. As in previous cases when the fitting have been performed considering only one parameter, it does not properly reproduce the the build up curve (figure 3.14, pink line). The pink line shows some differences with respect the purple and red ones, it is a bit shifted down. As stated in [20], neglecting the diffusion block in equation (2.10) may introduce a considerable error when you are interested in absolute σ, but in this work the discussion will be carried on the relative cross relaxations so the assumption of negligible diffusion is reasonable.

- **HOESY 3, 3 parameters:** In this case the fitting presented more or less the same issue of HOESY 2, 3. Indeed, even if this fitting function seems to be suitable since the fitting converges and well reproduces the curves, focusing on table 3.17 it is clear that this equation is not reliable too because the calculated errors of R_I and R_S are too big.

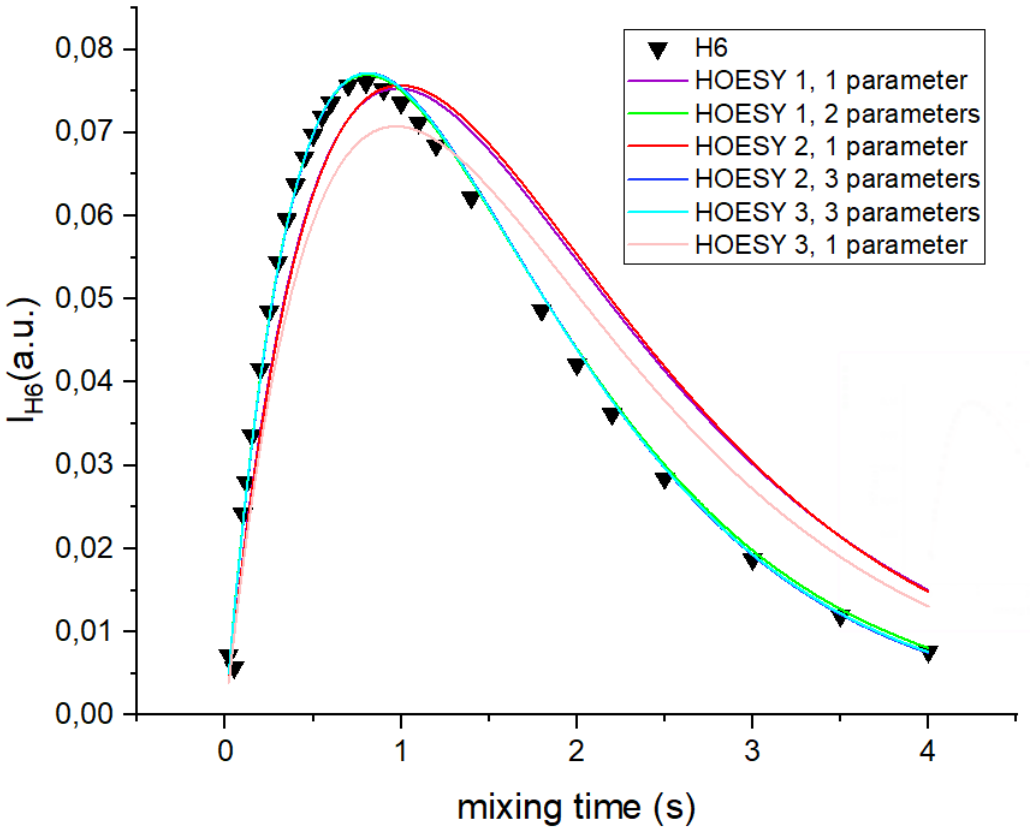

Figure 3.14: *Build up curve with relative fitting obtained for the H6 signal of ^{1}H - ^{19}F hoesy spectra for the sample EMImTfO + LiTfO at 298K*

Table 3.16: *Fitting outputs obtained for H6 of the sample EMImTfO + LiTfO at 298K*

$H6$	$\sigma\ [s^{-1}]$	$R-squared$	$converged?$	$well-fitted?$
HOESY1,1 par.	0.21053±0.00559	0.89018	yes	no
HOESY1,2 par.	0.26259±0.00619	0.97866	yes	yes
HOESY2,1 par.	0.10325±0.00289	0.88583	yes	no
HOESY2,3 par.	0.12885±0.00302	0.97871	no	no
HOESY3,1 par.	0.10556±5.04E-5	0.90725	yes	no
HOESY3,3 par.	0.13794±3.01E-5	0.99998	yes	yes
Linear(0-0.3s)	0.181331±0.01467	0.96221	yes	quite good

As anticipated in section 2.2.3, a linear fitting has also been performed considering the initial section of the curve only from 20 ms to 300 ms , as represented in figure 3.15. The corresponding σ are tabulated in the last row of table 3.16. The linear fitting of the first part of the curves converges and behaves suffi-

Table 3.17: *Experimental and fitted relaxation rates for the pair H6-F used in the fitting procedure of the build-up curve of H6 obtained from 2D ^{1}H - ^{19}F hoesy of sample EMImTfO + LiTfO at 298K (The * means that the experimental error are only estimated because the Origin software wasunable to compute it)*

$H6$	Exp	$HOESY1, 2par.$	$HOESY2, 3par.$	$HOESY3, 3par.$
Ravg	1.03	1.2598±0.024		
R_I	1.07		1.2320±0.02*	1.2416±185
R_S	1.00		1.2320±0.02*	1.2416±185
$\Delta Ravg$		0.2244		
ΔRh			0.1652	0.1749
ΔRf			0.2279	0.2376

ciently well even if not perfectly. Anyway, considering only the beginning of the curves is a strong assumption that may lead to approximated results.

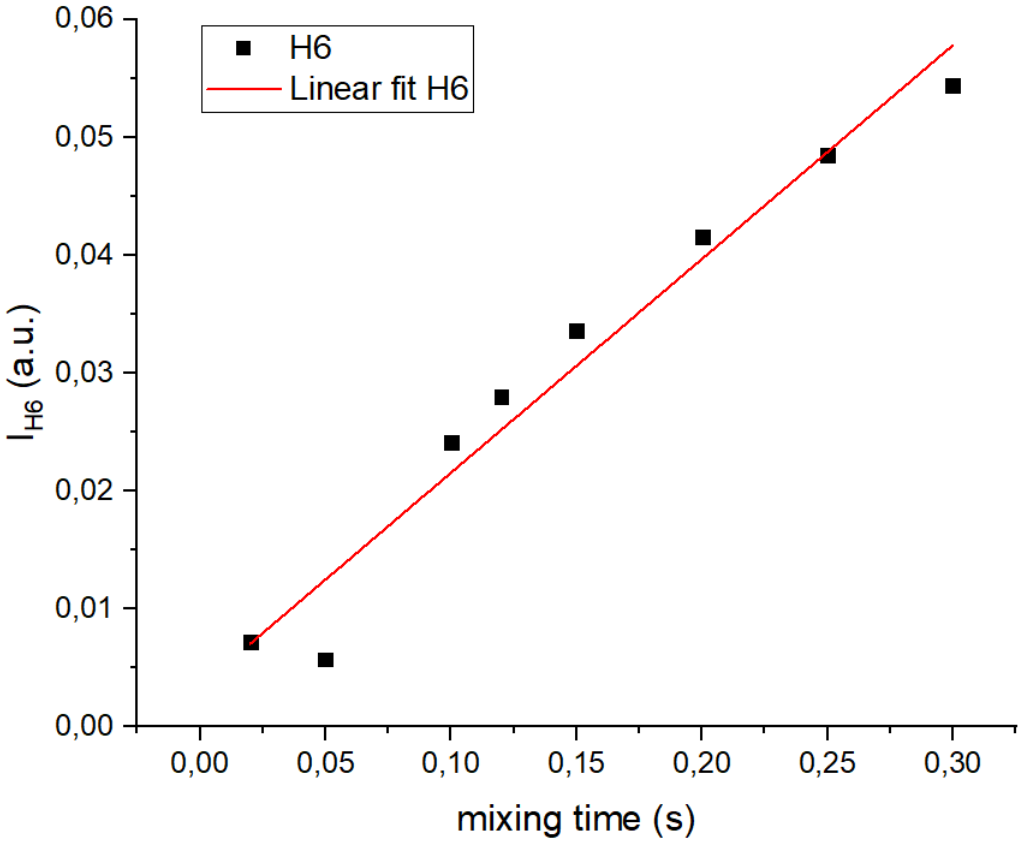

Figure 3.15: *Initial part of the H6 build up curve with relative linear fitting (0.02-0.3 s) obtained from ^{1}H - ^{19}F hoesy of the sample EMImTfO + LiTfO at 298K*

In view of this, HOESY 1, 2 parameters (considering σ and R both fit-able) is the best option for the computation of the cross relaxation, thus it will be the one selected in all the experiments presented from now on.
The bad performances of HOESY 1, 1 par. (fixing the relaxation rate as calculated from T_1) might be related to the inherent error of the inversion recovery experiment, in particular its processing that generates an experimental error that propagates leading to an incorrect value for the relaxation rate. This systematic error may be overcome considering the relaxation rate as a parameter. This turns out to be reasonable since the difference between computed and fitted values are not so huge (table 3.17). Hence, HOESY 1, 2 parameters has been chosen to fit the build up curves of all the other experiments.
Figure 3.16 reportes the ^{1}H - ^{19}F build up curves for the series EMImTfO + LiTfO at 298K with the final fitting with HOESY1,2 par. The corresponding cross relaxations computed for all protons are listed in table 3.18. The fit using HOESY 1, 2 par. converges and well reproduces the curves for all the protons in all 2D ^{1}H - ^{19}F hoesy experiments presented in this section as in figures 3.17, 3.18, 3.19 and tables 3.19, 3.20, 3.21. Each table reports the fitted values of σ and Ravg with their associated error, the R-squared parameter which evaluates the quality of the fitting and the difference, ΔRavg, between the Ravg computed from experimental values of T_1 and the fitted ones.
HOESY 1,2 par. generally leads to a high quality fitted curves, as R-squared values confirm. R-squared values (tables from 3.18 to 3.21) are all close enough to 1 indicating the goodness of the fit, even if in table 3.20, related to EMImTfO sample at 288 K, they are a bit lower than the others due to some outliers. Anyway the fitting is considered reliable.

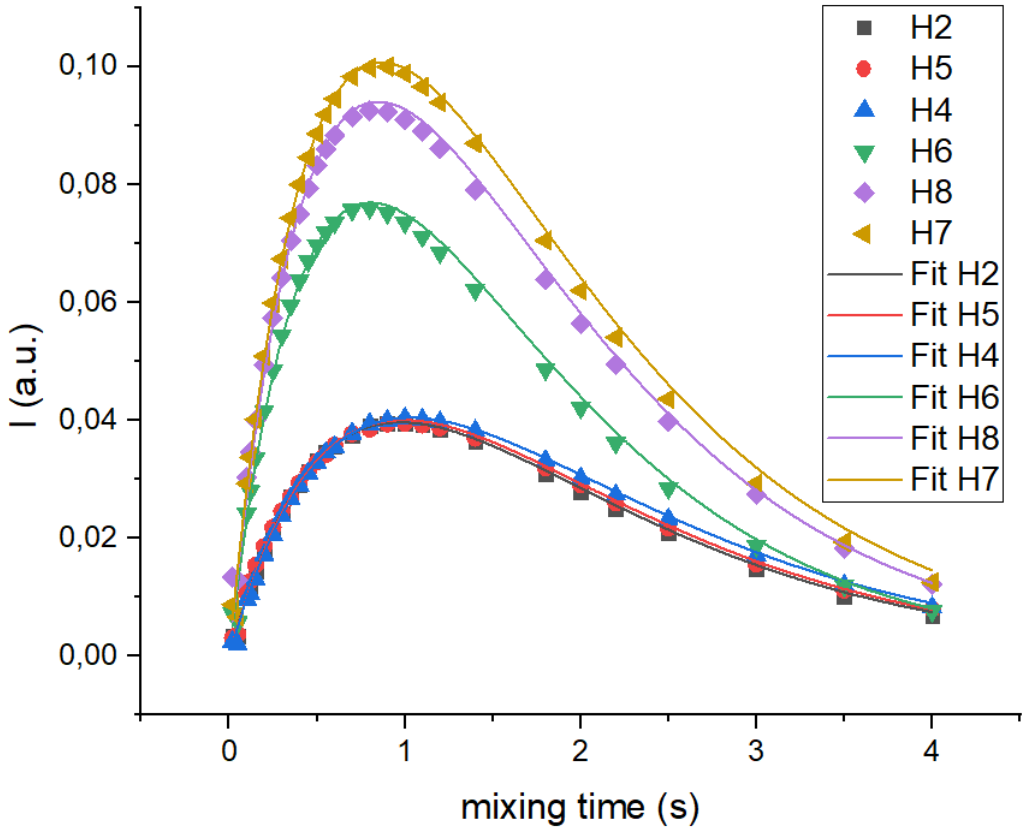

Figure 3.16: *Build up curves with relative final fitting, obtained from ^{1}H - ^{19}F hoesy for all protons of the sample EMImTfO + LiTfO at 298K*

Table 3.18: *Fitting outputs obtained from ^{1}H - ^{19}F hoesy for all protons of the sample EMImTfO + LiTfO, 298K*

	σ $[s^{-1}]$	$Ravg$	$R-squared$	ΔRavg
H2	0.112±0.002	1.028±0.012	0.992	0.219
H5	0.110±0.001	1.012±0.011	0.992	0.201
H4	0.107±0.001	0.972±0.010	0.993	0.189
H6	0.263±0.006	1.260±0.024	0.979	0.224
H8	0.305±0.006	1.205±0.020	0.981	0.219
H7	0.320±0.007	1.183±0.020	0.983	0.218

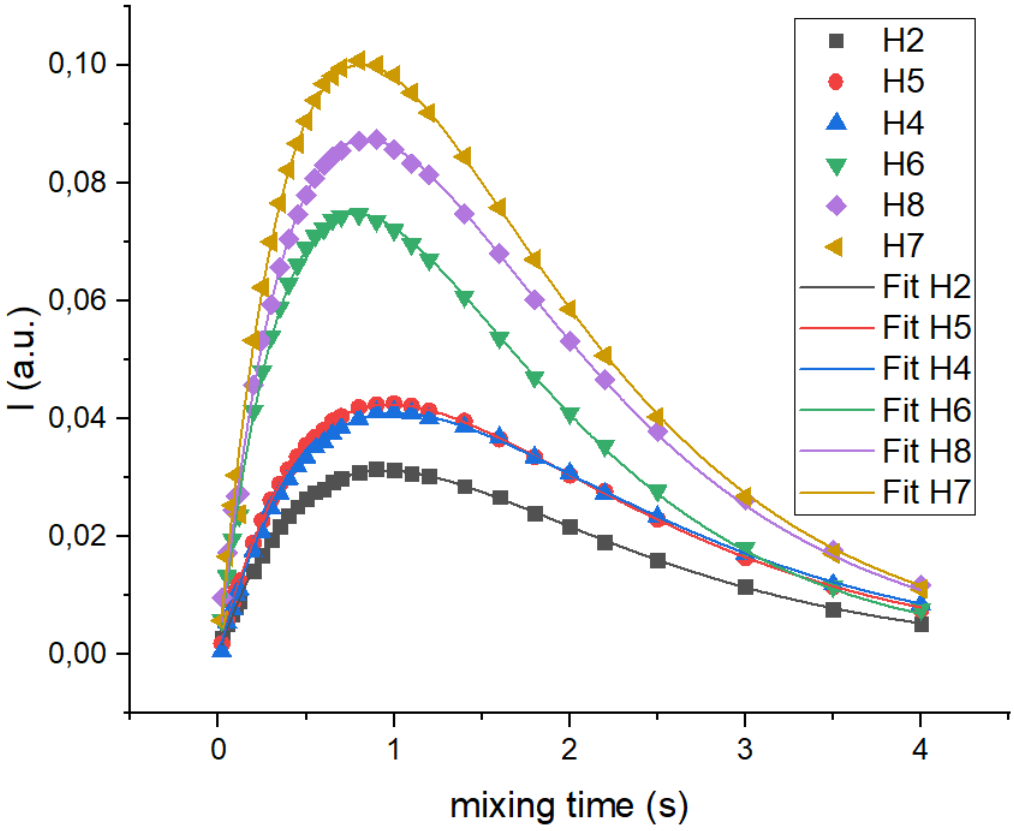

Figure 3.17: *Build up curves with relative final fitting, obtained from ^{1}H - ^{19}F hoesy for all protons of the sample EMImTfO + LiTfO at 288K*

Table 3.19: *Fitting outputs obtained from ^{1}H - ^{19}F hoesy for all protons of the sample EMImTfO + LiTfO at 288K*

	σ [s^{-1}]	*Ravg*	$R-squared$	ΔRavg
H2	0.090±4.62E-4	1.057±0.004	0.999	0.078
H5	0.119±2.53E-4	1.030±0.002	0.9998	0.127
H4	0.110±5.71E-4	0.990±0.004	0.999	0.064
H6	0.263±0.00140	1.300±0.006	0.999	0.187
H8	0.286±0.00238	1.214±0.008	0.997	0.164
H7	0.339±0.00368	1.259±0.011	0.996	0.153

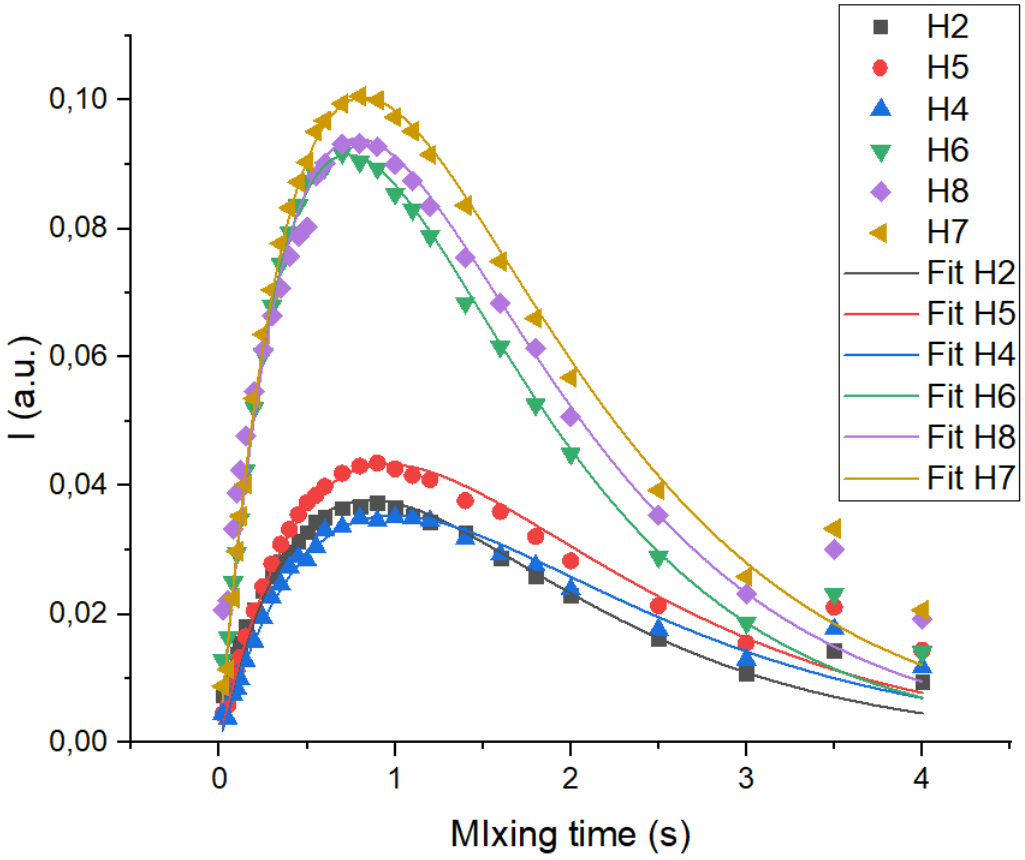

Figure 3.18: *Build up curves with relative final fitting, obtained from ^{1}H - ^{19}F hoesy for all protons of the sample EMImTfO at 298K*

Table 3.20: *Fitting outputs obtained from ^{1}H - ^{19}F hoesy for all protons of the sample EMImTfO, 298K*

	σ $[s^{-1}]$	*Ravg*	$R-squared$	ΔRavg
H2	0.120±0.004	1.172±0.031	0.949	0.353
H5	0.123±0.004	1.048±0.026	0.971	0.294
H4	0.097±0.003	1.011±0.025	0.962	0.262
H6	0.343±0.006	1.393±0.019	0.989	0.342
H8	0.329±0.002	1.301±0.036	0.945	0.263
H7	0.337±0.006	1.251±0.020	0.986	0.311

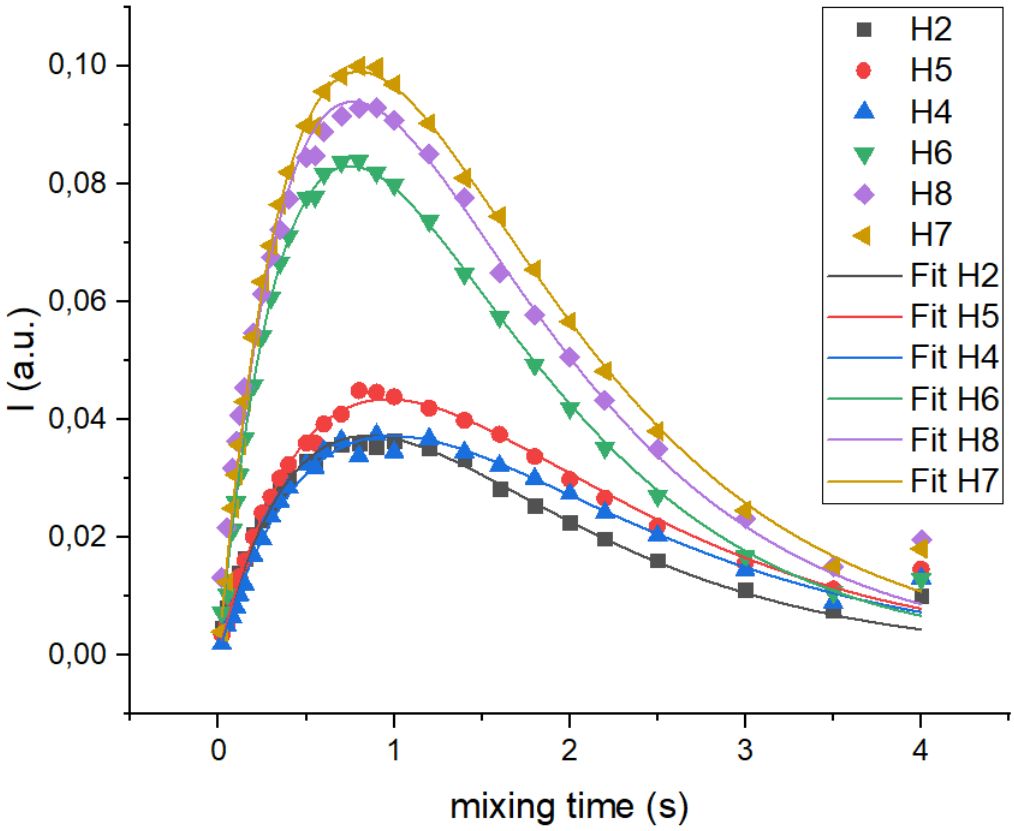

Figure 3.19: *Build up curves with relative final fitting, obtained from ^{1}H - ^{19}F hoesy for all protons of the sample EMImTfO at 288K*

Table 3.21: *Fitting outputs obtained from ^{1}H - ^{19}F hoesy for all protons of the sample EMImTfO, 288K*

	σ $[s^{-1}]$	$Ravg$	$R-squared$	ΔRavg
H2	0.119±0.003	1.180±0.021	0.976	0.353
H5	0.119±0.003	1.027±0.021	0.972	0.294
H4	0.102±0.002	1.012±0.018	0.981	0.262
H6	0.343±0.003	1.358±0.011	0.996	0.342
H8	0.337±0.008	1.331±0.024	0.977	0.263
H7	0.341±0.004	1.282±0.010	0.996	0.311

^{1}H - ^{19}F cross relaxation

In this section the cross relaxation values are discussed comparing them at different temperatures and passing from one sample to the other one.
Actually, the comparison among cross relaxations is not really meaningful and reliable when considering the absolute values, but it becomes a very powerful tool when dealing with relative values and giving the information about the disposition of fluorine (lithium when dealing with ^{7}Li - ^{1}H hoesy) on the $[EMIm]^{+}$ cation.
Table 3.22 reports the normalized σ for all the protons when different fitting are performed in order to underline that, even if the HOESY 1, 2 parameter has been selected as the best option to fit the curves, also the other fitting functions lead to comparable, reasonable and reliable results when considering relative relaxation rates. The data here reported for the fitting comparison are for only the EMImTfO + LiTfO at 298 K. HOESY 2, 3 par. and HOESY 3,3 par. are neglected as the fit either does not converge or give too high errors, respectively.

Table 3.22: *Relative cross relaxation, obtained from the fit with different user-defined functions of the build-up curves derived from ^{1}H - ^{19}F hoesy for the sample EMImTfO + LiTfO at 298 K*

σ *norm*	$H2$	$H5$	$H4$	$H6$	$H8$	$H7$
HOESY1 1 par.	0.336 ±0.009	0.346 ±0.009	0.332 ±0.009	0.823 ±0.012	0.956 ±0.013	1.00 ±0.013
HOESY1 2 par.	0.346 ±0.008	0.344 ±0.008	0.333 ±0.008	0.817 ±0.032	0.953 ±0.029	1.00 ±0.013
Linear fitting	0.347 ±0.021	0.357 ±0.022	0.359 ±0.022	0.803 ±0.032	0.856 ±0.029	1.00 ±0.034
HOESY2 1 par.	0.397 ±0.003	0.316 ±0.004	0.319 ±0.004	0.772 ±0.006	0.933 ±0.006	1.00 ±0.006
HOESY3 1 par.	0.291 ±3.54E-4	0.316 ±1.35E-4	0.319 ±0.002	0.760 ±1.47E-4	0.945 ±0.003	1.00 ±1.93E-4

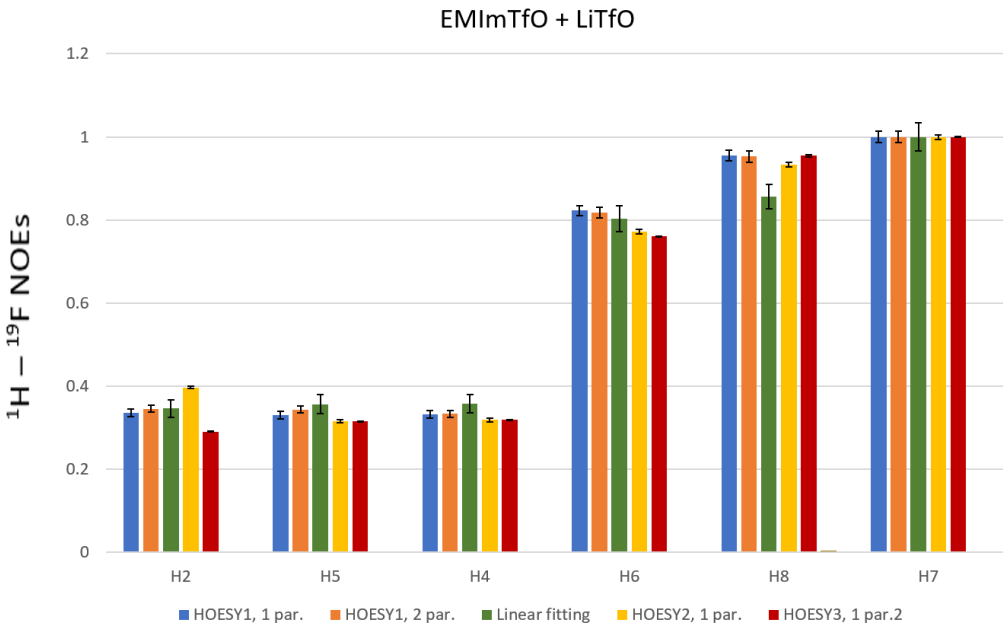

Figure 3.20: *Comparison of normalized cross relaxations,obtained from the fit with different user-defined functions of the build-up curves derived from ^1H - ^{19}F hoesy, EMImTfO + LiTfO, 298K*

Figure 3.20 visually describes the data in table 3.22 highlighting that the relative cross relaxations computed with different converging fitting are comparable. As shown in the histogram, proton H7 shows the maximum σ whatever fitting is performed. In light of that, H7 will have a unitary relative σ for all the fitting proposed, while all the other protons assume lower relative cross relaxation.

The histogram stresses out that also HOESY 1, 1 parameter, HOESY 2, 1 parameter and HOESY 3, 1 parameter proposed in previous studies [21], [22] and [20] leads to reliable cross relaxation, but in this work the HOESY 1, 2 parameters has been preferred since it better reproduces the build up curves.

All the normalized σ computed with HOESY 1, 2 parameters are reported in Tables 3.23 and 3.24 for sample EMImTfO + LiTfO and EMImTfO, respectively. A deeper discussion of the results in terms of (micro)structural organization will be given in section 3.4

Table 3.23: *Relative cross relaxation,obtained from the fit with HOESY 1, 2 par of the build-up curves derived from ^{1}H - ^{19}F hoesy of the sample EMImTfO + LiTfO*

σ *norm*	$298K$	$288K$
H2	0.346±0.008	0.265±0.004
H5	0.344±0.008	0.350±0.004
H4	0.333±0.008	0.325±0.004
H6	0.817±0.032	0.776±0.005
H8	0.953±0.029	0.844±0.006
H7	1.00±0.013	1.00±0.007

Table 3.24: *Relative cross relaxation, ^{1}H - ^{19}F hoesy, for the sample EMImTfO*

σ *norm*	$298K$	$288K$
H2	0.350±0.010	0.350±0.006
H5	0.359±0.009	0.350±0.007
H4	0.283±0.009	0.300±0.006
H6	1.00±0.012	0.8916±0.007
H8	0.959±0.017	0.990±0.011
H7	0.983±0.012	1.00±0.007

3.3.2 2D ^{7}Li - ^{1}H Hoesy

Acquisition and processing of 2D ^{7}Li - ^{1}H spectra at variable mixing time and fitting of the derived build-up curves

The analysis and processing of ^{7}Li - ^{1}H Hoesy follows the same pathway of the ^{1}H - ^{19}F Hoesy consisting in the integration of the correlation peaks appearing on the raw spectra, the plot of such data to draw the build up curve and finally the fit of such curves.
Figure 3.21 shows as an example the 2D ^{7}Li - ^{1}H hoesy spectrum acquired at 298 K on the sample EMImTfO + LiTfO with a mixing time of 1.2 s. Unlike

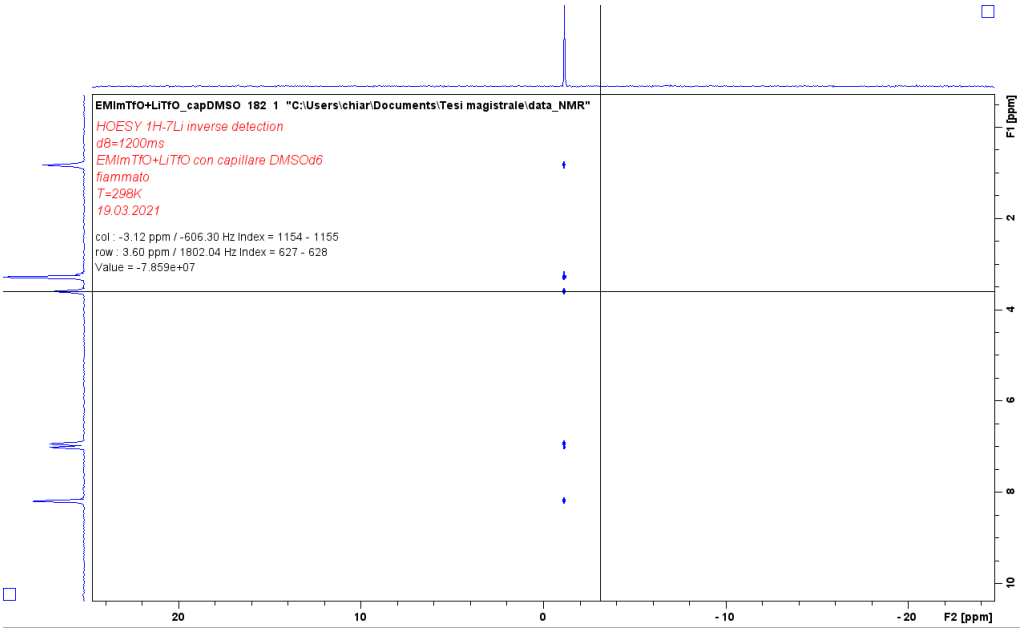

Figure 3.21: *^{7}Li - ^{1}H Hoesy, mixing 1.2 s, EMImTfO + LiTfO, 298K*

the 2D ^{1}H - ^{19}F hoesy, in the ^{7}Li - ^{1}H hoesy spectra the lithium projection appears in the horizontal dimension, while the proton spectrum is reported as the vertical projection. The reason is that these experiments were performed following an inverse pulse sequence.
The absolute integrals extracted for this eries are reported in table 3.25, for mixing times in the range 50 ms - 6 s. For what concerns the fitting, all the trials performed with the already introduced equations have lead to the same conclusion of ^{1}H - ^{19}F hoesy, thus the fitting function HOESY1, 2 parameters was selected as the best one also in this case.

Table 3.25: *Integral intensities ^{7}Li - ^{1}H hosey for the sample EMImTfO + LiTfO at 298 K*

Mixing time [s]	*H2*	*H5*	*H4*	*H6*	*H8*	*H7*
0.05	2.85E09	1.42E09	1.88E09	2.83E09	7.80E09	4.11E09
0.12	1.07E10	5.94E09	6.86E09	9.68E09	2.00E10	1.09E10
0.15	1.23E10	6.71E09	8.70E09	1.20E10	2.40E10	1.25E10
0.2	1.41E10	9.46E09	9.10E09	1.73E10	3.04E10	1.34E10
0.25	1.72E10	9.11E10	1.18E10	1.93E10	3.50E10	1.90E10
0.3	1.93E10	1.44E10	1.29E10	1.99E10	3.89E10	1.88E10
0.35	2.26E10	1.24E10	1.58E10	2.18E10	4.49E10	2.21E10
0.4	2.33E10	1.49E10	1.67E10	2.47E10	4.78E10	2.54E10
0.45	2.60E10	1.42E10	1.87E10	2.55E10	5.02E10	2.73E10
0.5	2.82E10	1.71E10	1.79E10	2.93E10	5.46E10	2.85E10
0.6	3.03E10	2.14E10	2.22E10	2.94E10	6.00E10	3.10E10
0.7	3.24E10	2.04E10	2.28E10	3.44E10	5.96E10	3.14E10
0.9	3.48E10	2.33E10	2.28E10	3.56E10	6.19E10	3.62E10
1.2	3.49E10	2.60E10	2.61E10	3.83E10	**6.60E10**	3.86E10
1.5	3.47E10	2.42E10	2.42E10	3.60E10	6.14E10	3.39E10
1.8	3.12E10	1.70E10	2.67E10	2.41E10	5.35E10	3.22E10
2	3.21E10	2.30E10	2.38E10	2.86E10	5.37E10	3.12E10
2.5	2.52E10	2.04E10	1.89E10	2.44E10	4.56E10	2.29E10
3	2.11E10	1.76E10	1.81E10	1.54E10	3.70E10	1.89E10
5	9.01E09	8.25E09	5.57E09	9.18E09	1.36E10	5.73E09
6	3.88E09	4.50E09	3.41E09	4.86E09	7.86E09	1.00E08

The build up curves of ^{7}Li - ^{1}H hosey with relative fitting and associated tables are reported in the following (figure 3.22, 3.23, 3.24 and tables 3.26, 3.27, 3.28). As for ^{1}H - ^{19}F hosey, the curves are drawn plotting data that have been already corrected and normalized according to the procedure described in chapter 2.

Table 3.26: *Fitting outputsobtained from ^{7}Li - ^{1}H hoesy for all protons of the sample EMImTfO + LiTfO at 298K*

	σ [s^{-1}]	*Ravg*	$R - squared$	ΔRavg
H2	0.126±0.002	0.845±0.013	0.981	0.051
H5	0.075±0.004	0.733±0.031	0.928	0.184
H4	0.084±0.002	0.777±0.017	0.980	0.190
H6	0.137±0.005	0.929±0.031	0.949	0.215
H8	0.257±0.005	0.941±0.017	0.983	0.097
H7	0.134±0.003	0.893±0.015	0.989	0.153

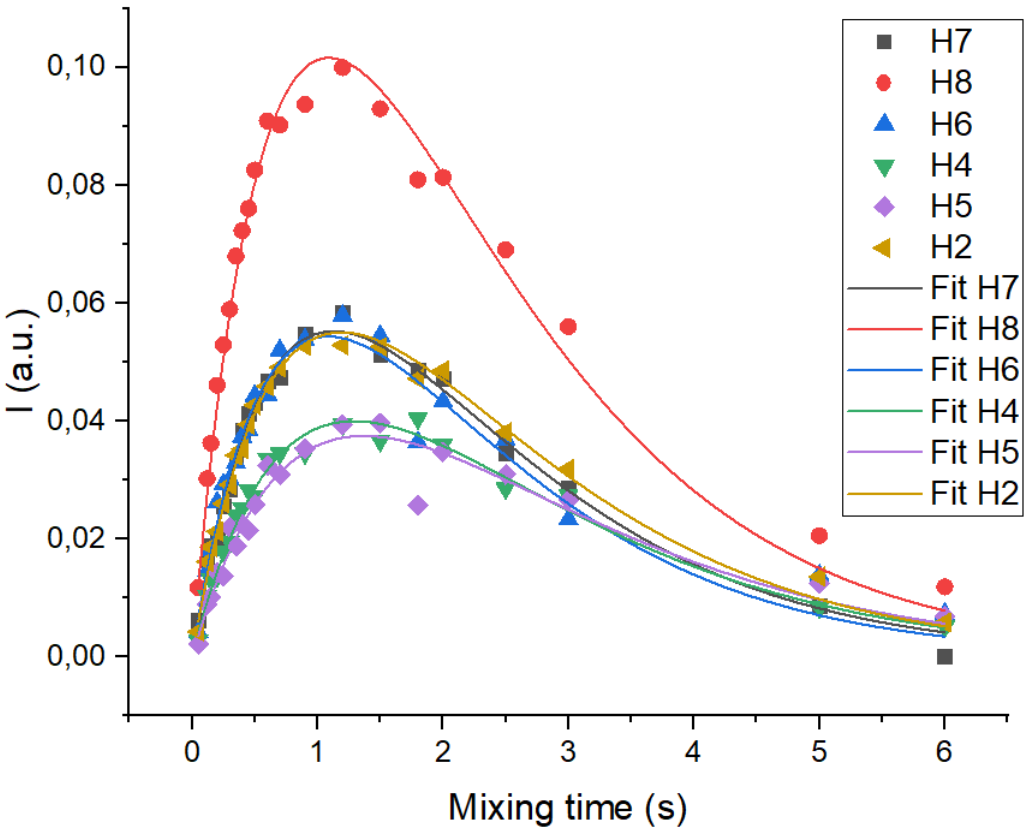

Figure 3.22: *Build up curves with relative final fitting obtained ^{7}Li - ^{1}H hoesy for all protons the sample EMImTfO + LiTfO at 298K*

Table 3.27: *Fitting outputs obtained from ^{7}Li - ^{1}H hoesy for all protons of the sample EMImTfO + LiTfO at 288K*

	σ $[s^{-1}]$	$Ravg$	$R-squared$	ΔRavg
H2	0.134±0.008	0.824±0.046	0.908	0.093
H5	0.091±0.008	0.719±0.066	0.798	0.141
H4	0.096±0.008	0.784±0.066	0.840	0.141
H6	0.144±0.012	0.862±0.071	0.826	0.125
H8	0.252±0.014	0.905±0.05	0.901	0.188
H7	0.138±0.013	0.834±0.077	0.822	0.103

Compared to the ^{1}H - ^{19}F ones, the ^{7}Li - ^{1}H build-up curves obtained at the same temperature are more irregular even if the trend found in previous sections and studies [18], [20] is more or less maintained. In particular the curves in figure 3.23 obtained at the lowest (288 K) appears very scattered with respect the other graphs presented until now and the fitting lines are not passing

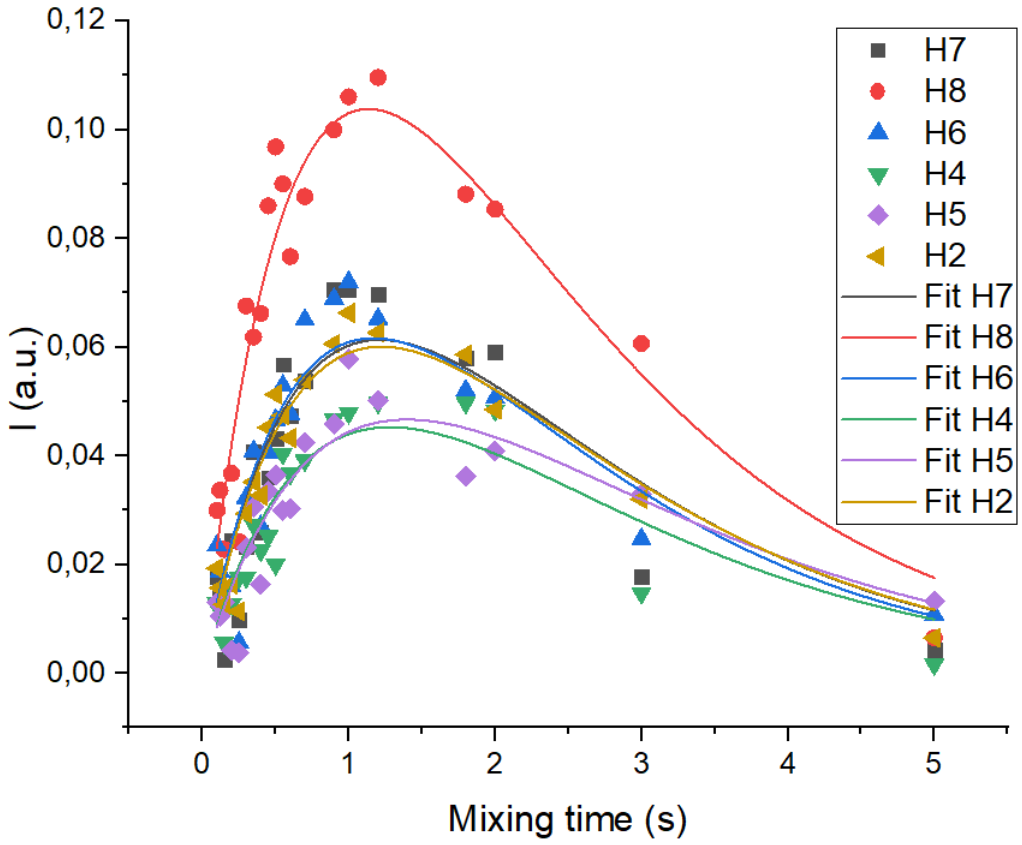

Figure 3.23: *Build up curves with relative final fitting obtained from ^{7}Li - ^{1}H hoesy for all protons of the sample EMImTfO + LiTfO at 288K*

through or closer enough to the majority of points causing low R-squared index (table 3.27). Despite the bad quality of the fitting, the data coming out from it seems to be consistent and comparable with the ones of the other series thus they have been considered reliable. To increase the reliability of the lithium - proton structural data, an additional series of 2D ^{7}Li - ^{1}H hoesy experiments has been run at a higher temperature, 318 K (Figure 3.24, table 3.28). At the same temperature, points are indeed less scattered.
Considering now the relative position of the curves, it's clear that H8 proton reaches the greatest values at all temperatures being the others much more lower in the graph. Except of H8, all the other curves occupy a quite narrow section of the plot, H2, H6 and H7 are almost overlapping one another at 298 K and 288 K and a bit less at 318 K. H4 and H5 overlap themselves following the same behavior of the just mentioned protons. All in all H8 is the only proton that

breaks off showing sensibly higher values.

Table 3.28: *Fitting outputs, all protons, ^{7}Li - ^{1}H hoesy for the sample EMImTfO + LiTfO at 318K*

	σ $[s^{-1}]$	*Ravg*	$R - squared$	ΔRavg
H2	0.163±0.010	0.980±0.052	0.927	0.047
H5	0.101±0.006	0.941±0.052	0.914	0.104
H4	0.099±0.007	0.919±0.060	0.901	0.170
H6	0.144±0.008	1.107±0.051	0.940	0.295
H8	0.312±0.014	1.145±0.044	0.958	0.329
H7	0.157±0.008	1.005±0.046	0.949	0.174

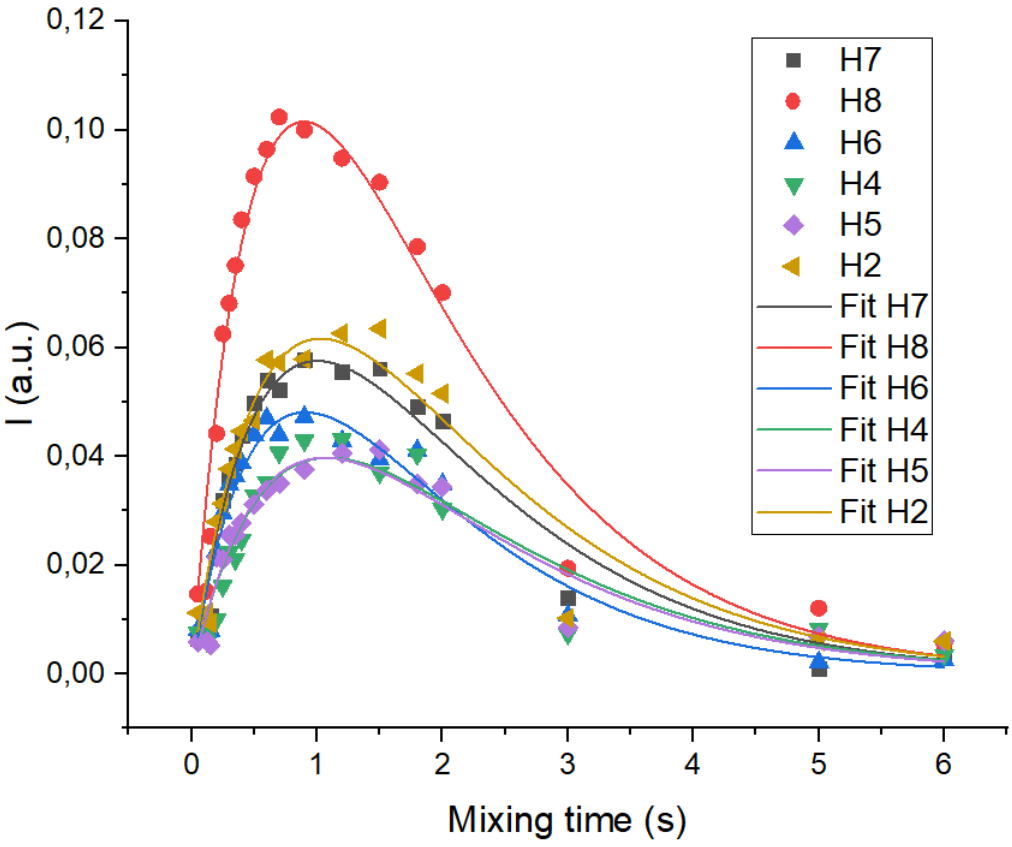

Figure 3.24: *Build up curves with relative final fitting, ^{7}Li - ^{1}H hoesy for the sample EMImTfO + LiTfO at 318K*

^{7}Li - ^{1}H Relative cross relaxation

As already stated when dealing with ^{1}H - ^{19}F hoesy, also in this case it is more meaningful and reliable paying attention to the relative cross relaxations than on the absolute ones. The normalization have been done dividing each cross relaxation of a single series by the greatest one of such series. The normalized values are reported in Tables 3.29 and will be discussed in section 3.4. Analyzing the table 3.29 we can denote that the experimental errors are generally a bit greater than in table 3.27 and 3.28. The bigger uncertainties are coming out from a less precise fitting and showing lower R-squared values than their analogous in ^{1}H - ^{19}F hoesy series and the normalization propagates such errors. Nevertheless, we are still dealing with manageable experimental errors not compromising the reliability of the ^{7}Li - ^{1}H hoesy.

Table 3.29: *Normalized cross relaxation, obtained from the fit with HOESY 1, 2 par. of the build-up curves derived from ^{7}Li - ^{1}H hoesy for the sample EMImTfO + LiTfO*

σ *norm*	$298K$	$288K$	$318K$
H2	0.491±0.008	0.532±0.022	0.524±0.024
H5	0.291±0.012	0.361±0.022	0.325±0.020
H4	0.329±0.008	0.382±0.022	0.318±0.021
H6	0.533±0.011	0.570±0.026	0.463±0.022
H8	1.00±0.011	1.00±0.028	1.00±0.028
H7	0.521±0.008	0.549±0.027	0.502±0.022

3.4 Result interpretation

NOE experiments are performed in order to point out the interaction between protons placed on $[EMIm]^+$ cation and fluorine of the anion or lithium.
Being the just mentioned interaction quite specific, the goal of the analysis carried out is to exactly understand with which position they are strongly interacting.
Figures 3.25, 3.26, 3.27 and 3.28 summarize the relative ^{1}H-^{19}F cross relaxation values listed in Tables 3.27 and 3.28, whereas the relative ^{7}Li-^{1}H cross relaxations are sketched in Figures 3.29, 3.30 and 3.31. For sake of simplicity the positions of the protons have been reported in figure 3.25 only.

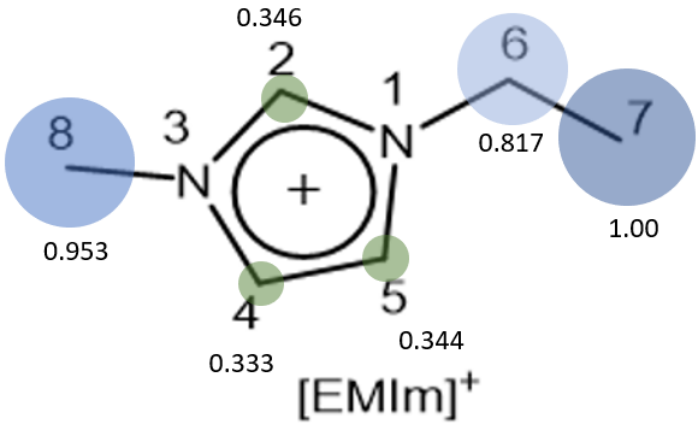

Figure 3.25: *Normalized cross relaxations on $[EMIm]^+$ cation, ^1H - ^{19}F hoesy, EMImTfO + LiTfO, 298K*

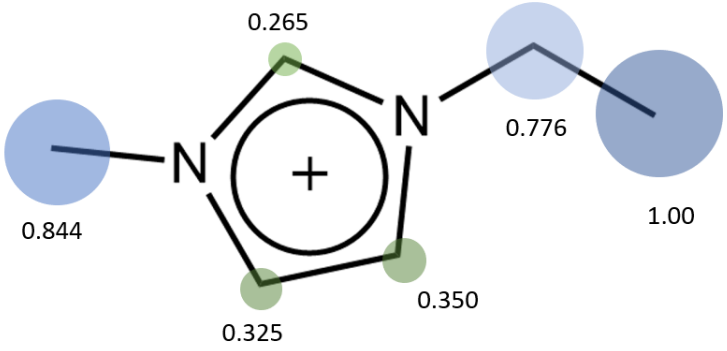

Figure 3.26: *Normalized cross relaxations on $[EMIm]^+$ cation, ^1H - ^{19}F hoesy for the sample EMImTfO + LiTfO at 288K*

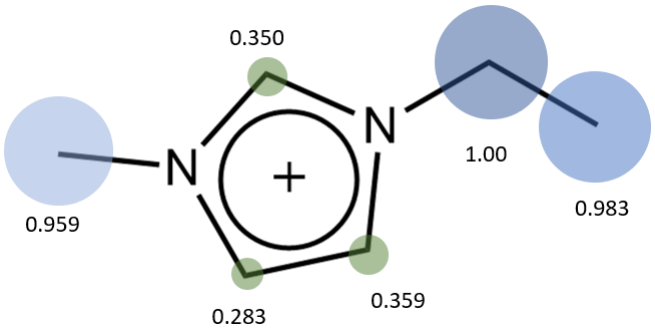

Figure 3.27: *Normalized cross relaxations on [EMIm]$^+$ cation, ^1H - ^{19}F hoesy, EMImTfO, 298K*

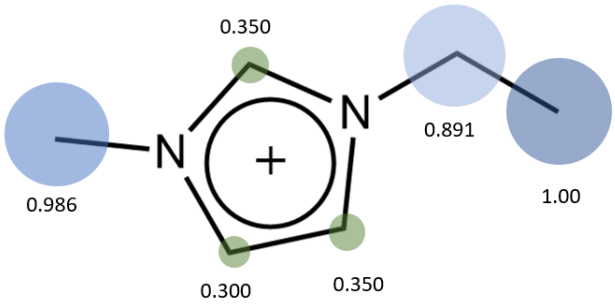

Figure 3.28: *Normalized cross relaxations on [EMIm]$^+$ cation, ^1H - ^{19}F hoesy, EMImTfO, 288K*

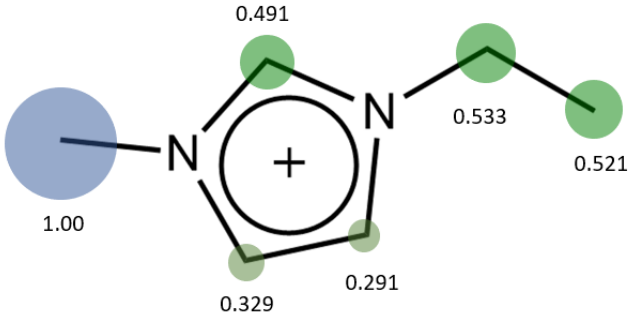

Figure 3.29: *Normalized cross relaxations on [EMIm]$^+$ cation, ^7Li - ^1H hoesy, EMImTfO, 298K*

Figures 3.25 and 3.26 graphically represent the data in table 3.23. The relative proportions among protons are almost retained changing the temperature from figure 3.25 to figure 3.26 meaning that the highest cross relaxations are found on the alkyl chains while on the aromatic ring they are considerably lower. H5 and H4 show as expected a similar behavior also when dealing with relative

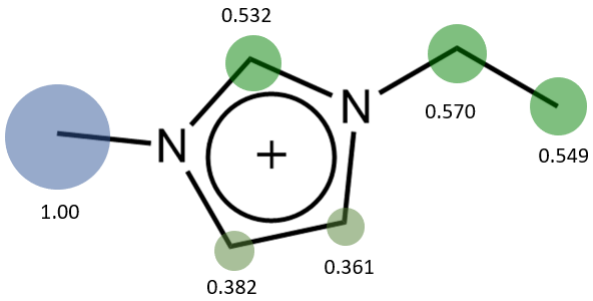

Figure 3.30: *Normalized cross relaxations on [EMIm]$^+$ cation, ^{7}Li - ^{1}H hoesy, EMImTfO, 288K*

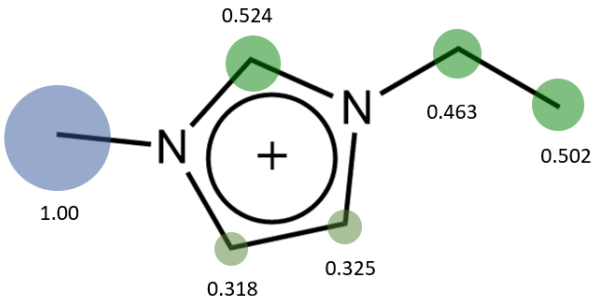

Figure 3.31: *Normalized cross relaxations on [EMIm]$^+$ cation, ^{7}Li - ^{1}H hoesy, EMImTfO, 318K*

σ. Figures 3.27 and 3.28 show the situation for the neat sample at the two temperatures. At 298 K the highest cross relaxation is formally placed on proton H6 while at 288 K it is still on proton H7 as in EMImTfO + LiTfO. However, the difference in intensity between H7 and H6 is very narrow making this change not relevant. Hence, the general trend confirms what stated form the blended sample being the interactions much more intense on the alkyl chains than on the ring. Indeed, no critical points have jumped out comparing the two samples thus indicating that the presence of the LiTfO salt does not affect the general trend implying greatest cross relaxations on the alkyl chain.
Focusing now on the relative ^{7}Li-^{1}H cross relaxation values reported in figure 3.29, 3.30 and 3.31, they enlighten a clear and global trend common to all temperatures: the highest relative cross relaxation value is found for H8 proton, with values in all the other positions consistently lower. Protons H2, H6 and H7 show relative cross relaxations around 0.5, while H5 and H4 show values around 0.3. These features are observed at all the investigated temperatures.

A naif interpretation of the observed ^{1}H-^{19}F and ^{7}Li-^{1}H cross-relaxation values in terms of interaction strength is tempting but, as described in the introduction, not fully reliable. In the following, the observed values are discussed in the light of the different interpretations of the intermolecular NOE proposed until now:

- **Short-range behavior:** According to the first intermolecular NOE interpretation proposed by [16] and [15] the interactions detected during an intermolecular NOE experiment indicate the presence of spins across a distance lower then $1/\vec{r}^{\,6}$ from the investigated isotope, as in intramolecular NOE.
  This statement means that intermolecular NOE has a short-range behavior including only the interactions relative to the first shell of spins surrounding an isotope, thus the relative cross relaxations computed from HOESY show the closest interactions between protons and fluorine or lithium.
  Under the prospective of short-range behavior the graphs reported in figure from 3.25 to 3.31 point out where the closest and strongest interactions are: fluorine mainly interacts with the alkyl chains, especially with H7 while lithium is located preferentially close to H8 since all the other cross relaxations are considerably lower.

- **Long-range behavior:** In 2013 the authors of ref. [17] propose a long-range behavior of NOE in ionic liquids stating that the interactions detected include not only the spins belonging to the closest shell, but also spins staying far away from the investigated isotope across a distance that may reach $1/\vec{r}$.
  Under this point of view the relative cross relaxation reported in graph from 3.25 to 3.31 are not really describing the first solvation shell, rather they are the sum of the short-range and long-range phenomena describing the solvation environment beyond the first solvation shell.
  All in all this interpretation does not allow stating where fluorine or lithium mainly interact with the $[EMIm]^{+}$ cation.
  Indeed, this new theory proposed the co-existence of long and short range interactions and the supremacy of one of the two effect should be related to the resonance frequencies of the selected isotopes.

- **Short-range vs long-range depending on the selected isotope:** The interpretation of intermolecular NOE proposed by [13] demonstrates that short-range and long-range behavior are both possible depending on the isotopes selected. If the isotopes have similar gyromagnetic ratios generating a narrow difference in their resonance frequency, long-range phenomena occurs next to the short range ones while when a considerable difference between isotopes' resonance frequency exists only short-range interactions are detected by the NOE. Having ^{1}H and ^{19} F similar gyromagnetic ratios, γ_{H}=4257.75 s^{-1} G^{-1} and γ_{F}= 4004.71 s^{-1} G^{-1}, the NOEs involving such isotopes show up a long-range behavior, thus the cross relaxations reported in graph from 3.25 to 3.28 are not actually indicating the strongest interactions occurring among the first neighbours, but the sum of both long-range and short-range phenomena. Conversely, ^{7}Li and ^{1}H show considerably different gyromagentic ratio being γ_{Li}=1654.6s^{-1} G^{-1}, thus the cross relaxation in figure from 3.29 to 3.31 are really indicating the strongest interaction that are mainly on H8 proton meaning that lithium preferentially interacts with $[EMIm]^{+}$ in position 8.
  The project I carried out during this thesis work intended to demonstrate the validity of the latter interpretation of the intermolecular NOE, that is the isotope-dependency of the short-range and long-range contribution. This was done in collaboration with colleagues from the University of Wien, who performed a massive work using molecular dynamics (MD) simulations on the same systems.
  The data collected and analyzed in this thesis work match nicely with the simulations performed by our colleagues in Wien thus proving the short-range vs short-range behavior theory dependence on the isotopes selection as proposed in 2013 [17].
  Figure 3.32 reports the comparison between simulations and experimental data which shows an excellent agreement. In ^{1}H - ^{19}F on the neat sample all the simulated values are identical or very similar to the experimental ones except for H6 which is 0.64 in the simulations while experimentally is 0.90.
  In ^{1}H - ^{19}F on the blended sample the results match almost perfectly in all the positions while in ^{7}Li - ^{1}H hoesy there are some small differences on the ring in position 4 and on the chain in position 7, but they are not

significant since the simulations confirm that highest cross relaxation is on proton H8.

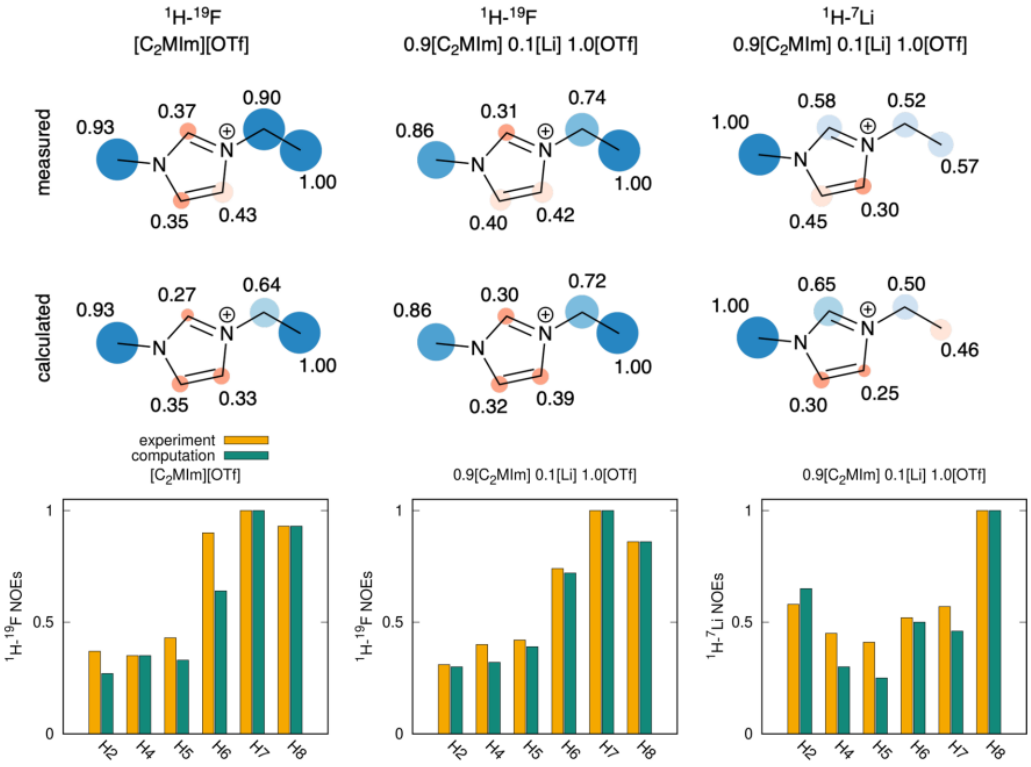

Figure 3.32: *Simulated and experimental data comparison:^{1}H - ^{19}F and ^{7}Li-^{1}H on EMImTfO + LiTfO sample at 298 K, ^{1}H - ^{19}F on EMImTfO sample at 298 K [13]*

3.5 1D Hoesy experiments

1D hoesy experiments have been carried out on the EMIm-TfO + LiTfO sample at 298 K only and, as introduced in chapter 2, they have to be intended as trials in order to verify whether they are a reliable tool for the measurement of the cross relaxation.
2D hoesy experiments are the traditional method to pursue such goal, but they require quite long time. For instance in our case experiment lasted 2 or 4 hours, thus more then two days were necessary to complete a series. Conversely, 1D are much faster taking from 2 to 10 minutes per experiment thus, if they were reliable, the long acquisition time of traditional hoesy would be overcome.
In this section the results related to the 1D hoesy are reported for ^{1}H - ^{19}F and ^{7}Li - ^{1}H and considering also selective and non selective sequences.

3.5.1 1D ^{1}H - ^{19}F Hoesy

Acquisition and processing of 1D ^{1}H - ^{19}F spectra and fitting of the derived build-up curves

1D ^{1}H - ^{19}F 1D Hoesy have been carried out considering both the selective and non selective sequences. They should theoretically lead to the same result, but were tested anyway to evaluate the effect on the overall quality of the spectra, in particular signal-to-noise and artefacts. Following the analysis done on ^{1}H - ^{19}F hoesy, the fitting was directly performed with the fitting function HOESY 1, 2 parameters.
The raw 1D hoesy spectra made by peaks like the in in figure 3.33. The processing procedure for this kind of experiments follow the same pathway proposed in previous case consisting in phasing the spectrum, integrating the peaks and exporting such integrals in order to draw the build up curves.
Unfortunately, not all the spectra of the series are perfectly similar to the figure 3.33, but some of them cannot be correctly phased neither automatically nor manually. In these non phasable spectra some peaks seem to be in anti-phase and such behavior has been found at very low and very high mixing times, as shown in figure 3.34 for mixing time of 50 ms.
Note that no considerable differences have been noticed in this respect using the selective or non selective pulses on the heteronucleus.
An anti-phase behavior and non selective sequences, may intuitively lead to incorrect or even negative integrals, but I made anyway an attempt to integrate

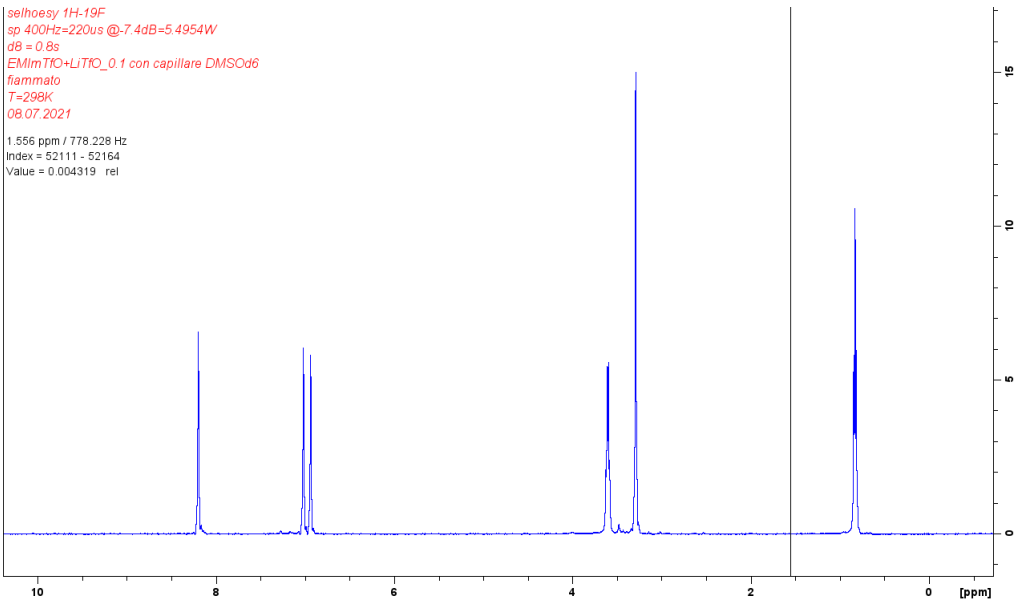

Figure 3.33: *1D ^{1}H - ^{19}F 1D Hoesy spectrum rune using a selective pulse on fluorine and a mixing time of 0.8 s for the sample EMImTfO + LiTfO at 298K*

the spectra.

As in 2D hoesy, the data have been normalized and corrected as described in chapter 2 thus here the fitted build up curves and the corresponding cross relaxations are directly reported (Figures 3.35 and 3.36 and Tables 3.30 and 3.31).

Starting from a visual analysis of the curves, they seem pretty good and this is a quite surprising result considering the odd shape of the signals at certain mixing times. Somehow the anti-phased peak are not influencing the shape of the build up curves that seem almost perfect.

Considering the mutual positions of the curves, there are no significant variations with respect the corresponding 2D hoesy being H7 the proton showing the higher values while H2, H4 and H5 located the lower part of the graph.

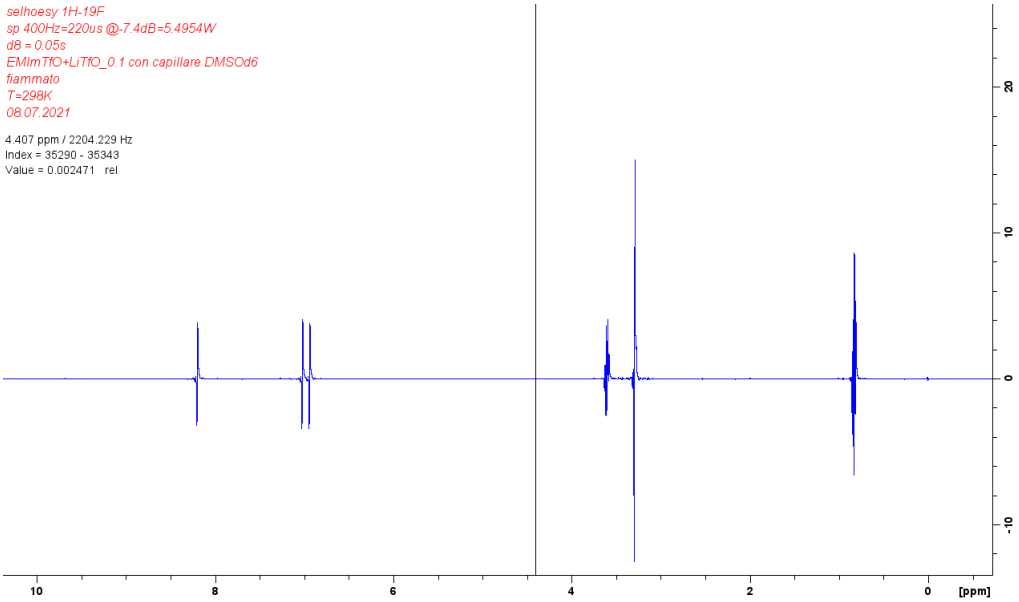

Figure 3.34: *1D ^{1}H - ^{19}F 1D Hoesy spectrum run using a selective pulse on fluorine and a mixing time of 0.05 s for EMImTfO + LiTfO at 298K*

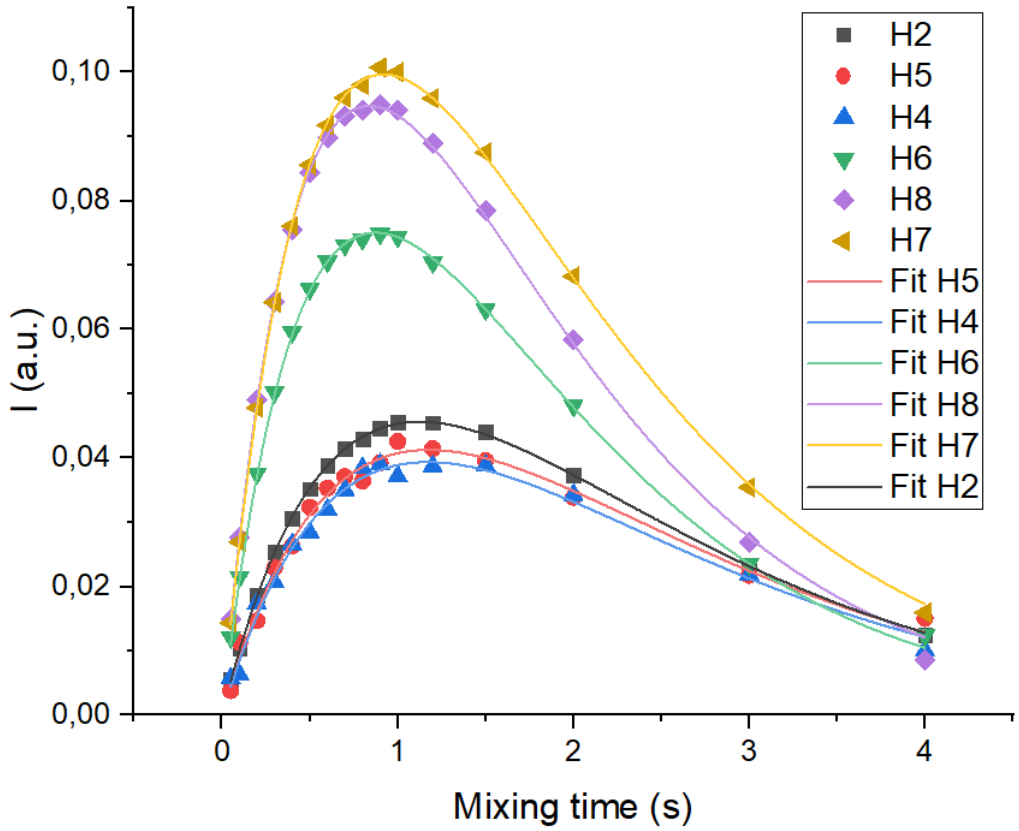

Figure 3.35: *Build up curves with relative final fitting obtained for all protons from 1D ^{1}H - ^{19}F hoesy, using non-selective sequence on fluorine for the sample EMImTfO + LiTfO at 298K*

Table 3.30: *Fitting outputs obtained for all protons from 1D ^{1}H - ^{19}F hoesy, using non-selective sequence on fluorine for the sample EMImTfO + LiTfO at 298K*

	σ $[s^{-1}]$	*Ravg*	$R-squared$	ΔRavg
H2	0.110±0.004	0.893±0.003	0.9997	0.083
H5	0.095±0.002	0.853±0.018	0.987	0.063
H4	0.091±0.002	0.856±0.018	0.987	0.074
H6	0.235±0.001	1.160±0.007	0.999	0.125
H8	0.310±0.003	1.219±0.009	0.999	0.232
H7	0.298±0.001	1.115±0.004	0.9996	0.034

Looking at figure 3.35 and 3.36 with their relative tables (3.30 and 3.31) it is possible to note the goodness of the fitting performed with HOESY 1, 2 parameters being the R-squared values so close to one, higher than 0.99 for the selective sequence and higher than 0.98 for the non selective one. Moreover, the

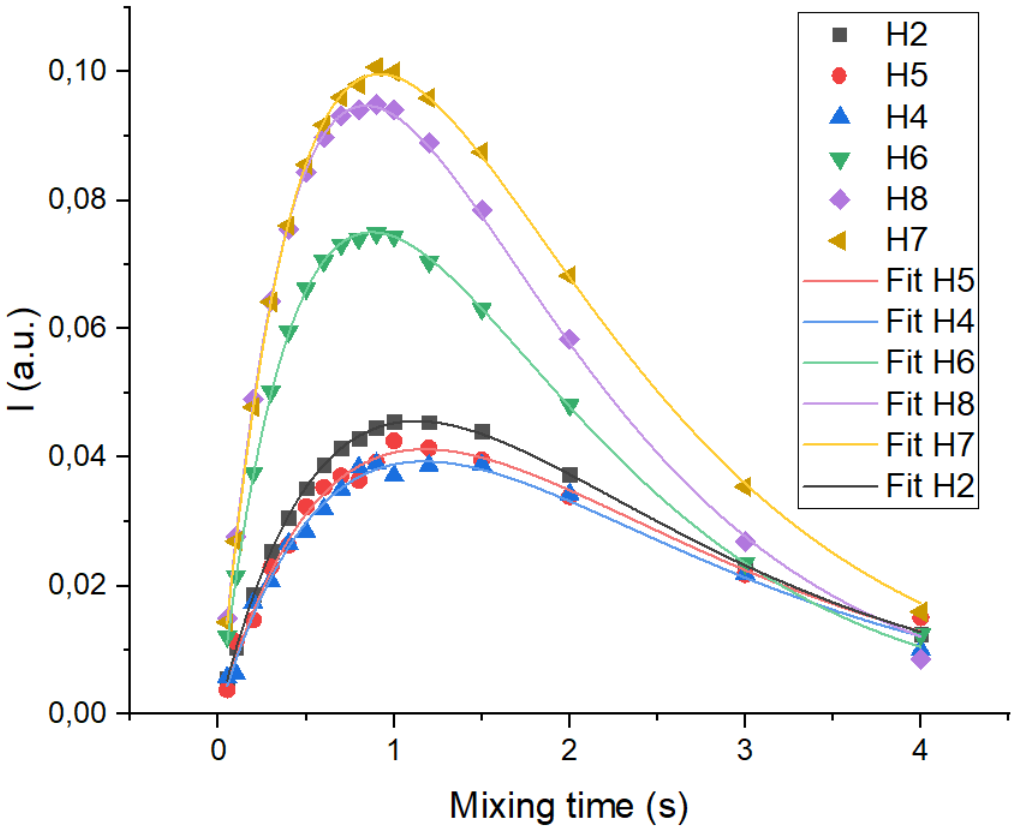

Figure 3.36: *Build up curves with relative final fitting obtained from 1D ^{1}H - ^{19}F hoesy, using selective sequence on fluorine for the sample EMImTfO + LiTfO at 298K*

Table 3.31: *Fitting outputs obtained for all protons from 1D ^{1}H - ^{19}F hoesy, using selective sequence on fluorine for the sample EMImTfO + LiTfO at 298K*

	σ $[s^{-1}]$	$Ravg$	$R-squared$	ΔRavg
H2	0.112±0.0004	0.899±0.003	0.9996	0.090
H5	0.097±0.001	0.856±0.009	0.997	0.066
H4	0.089±0.001	0.858±0.011	0.995	0.075
H6	0.246±0.002	1.166±0.006	0.999	0.130
H8	0.307±0.003	1.247±0.011	0.998	0.261
H7	0.300±0.002	1.121±0.005	0.999	0.034

ΔRavg computed is very low meaning that the Ravg computed starting from T_1 and the one coming out from the fitting are very close. Thus it seems worth trying to fit the curves with all the equations proposed considering Ravg, or R_I and R_S, constant values.

This analysis have been done considering proton H2, which shows very small

ΔRavg and H6 which shows slightly higher ΔRavg . As in figure 3.37 and 3.38,

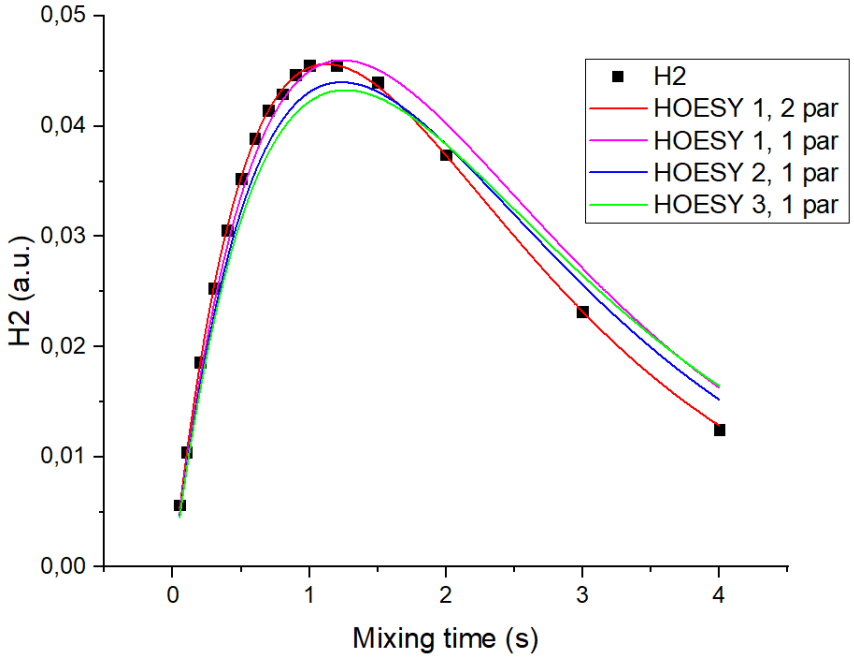

Figure 3.37: *Build up curves,fitted using different functions, relative to the H2 signal of 1D ^{1}H - ^{19}F hoesy for the sample EMImTfO + LiTfO at 298K*

the three trial fits (purple, blue and green lines) using the relaxation rate as constant parameter are not satisfactory since they still do not well reproduce the curve, even though the different between computed and fitted values is very narrow. Hence, HOESY 1, 2 parameters (red line) is still considered the best option.

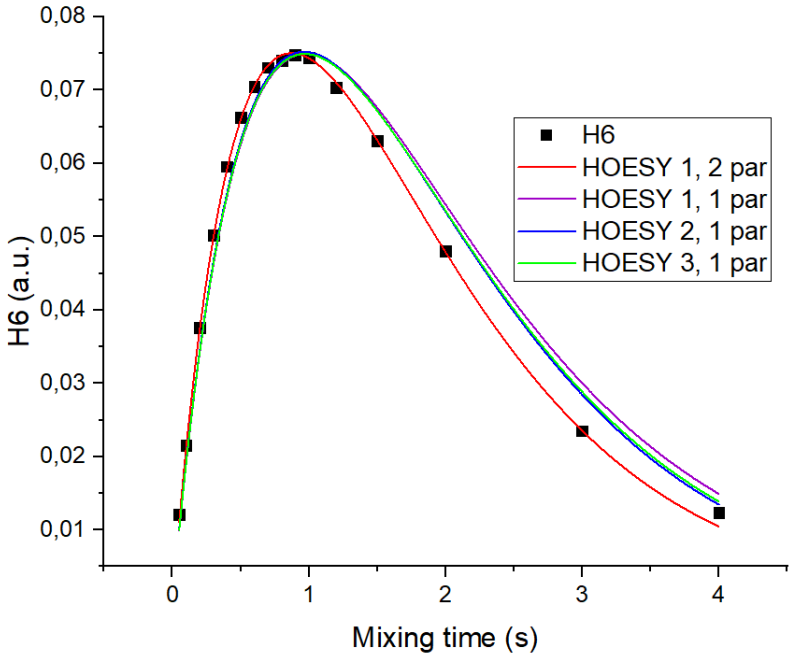

Figure 3.38: *build up curves,fitted using different functions, relative to the H6 signal of 1D ^{1}H - ^{19}F 1D hoesy for the sample EMImTfO + LiTfO at 298K*

^{1}H - ^{19}F cross relaxation 1D hoesy and their interpretation

As for the 2D Hoesy, the real discussion and comparison must be carried out on the relative cross relaxation considering both the data acquired with the selective and non selective sequence. The normalized relative cross relaxation values extracted from the analysis of 1D ^{1}H - ^{19}F 1D hoesy are listed in Table 3.32 and summarized in figures 3.39 and 3.40.
The temperature is not specified in the tables because all the ^{1}H - ^{19}F 1D hoesy are performed at 298 K.

Table 3.32: *Normalized relative cross relaxation, obtained from the fit with HOESY 1, 2 par. of the build-up curves derived from 1D ^{7}Li - ^{1}H hoesy for the sample EMImTfO + LiTfO*

σ norm	*non selective*	*selective*
H2	0.356±0.003	0.384±0.004
H5	0.308±0.005	0.315±0.004
H4	0.295±0.005	0.289±0.004
H6	0.757±0.004	0.802±0.005
H8	1.00±0.005	1.00±0.006
H7	0.961±0.004	0.977±0.005

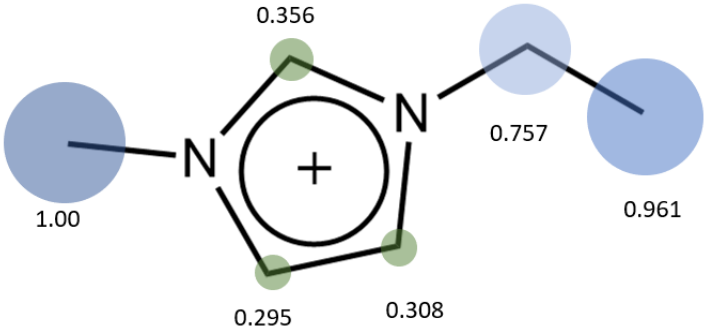

Figure 3.39: *Normalized cross relaxations on $[EMIm]^{+}$ cation, ^{1}H - ^{19}F 1D hoesy, non selective sequence, EMImTfO + LiTfO, 298K*

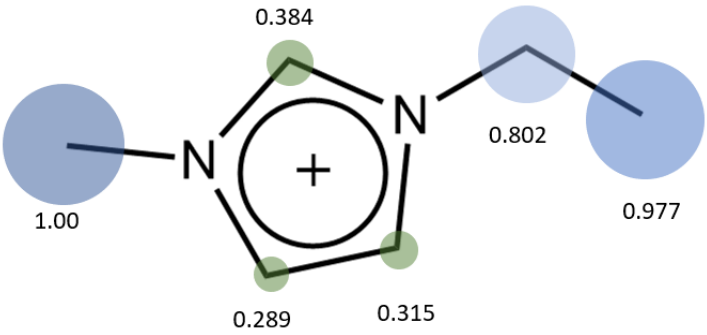

Figure 3.40: *Normalized cross relaxations on $[EMIm]^{+}$ cation, ^{1}H - ^{19}F 1D hoesy, selective sequence, EMImTfO + LiTfO, 298K*

As anticipated, the two sequences lead to very similar results: the highest values is on H8 but H7 reaches almost the same in both cases, then there is H6 which is around 0.8 and all the other protons belonging to there ring show a relative cross relaxation around 0.3-0.35.
Looking deeply into figure 3.39 and 3.40 it is possible to notice that when deal-

ing with selective sequence the values are slightly higher, except for H4, but the difference is so narrow that can be classified as irrelevant.
The real remarkable result is the higher relative cross relaxations on the alkyl chains, but according to the latest interpretation of NOE [13], already introduced in section 3.5, ^{1}H and ^{19}F NOE contain a significant long- range contribution thus the computed cross relaxation values describe the scenario of the solvation shell beyond the first one.

Magnitude processing

For sake of completeness, the signals in the 1D ^{1}H - ^{19}F hoesy spectra have also been processed in magnitude mode aiming to test whether this processing mode can overcome the odd shape of the peaks. Using the magnitude mode during the integration step in TopSpin, the absolute values of the peak are considered, thus no negative integrals are possible.
Figure 3.41 shows the build up curve obtained plotting the absolute integrals processed with magnitude mode. Looking at the curves, the trends are basically respecting what stated when speaking about the raw spectra of ^{1}H - ^{19}F 1D hoesy: itis possible to recognize a sort of well-shaped section at medium mixing times corresponding to the phased spectra while at low and high mixing time there are scattered points.
All in all the magnitude mode is not a good option for this kind of experiment because it does not solve the issues related to the anti-phased peaks, but it seems to enhance it because following the traditional procedure the curves of 1D ^{1}H - ^{19}F hoesy are somehow much better.

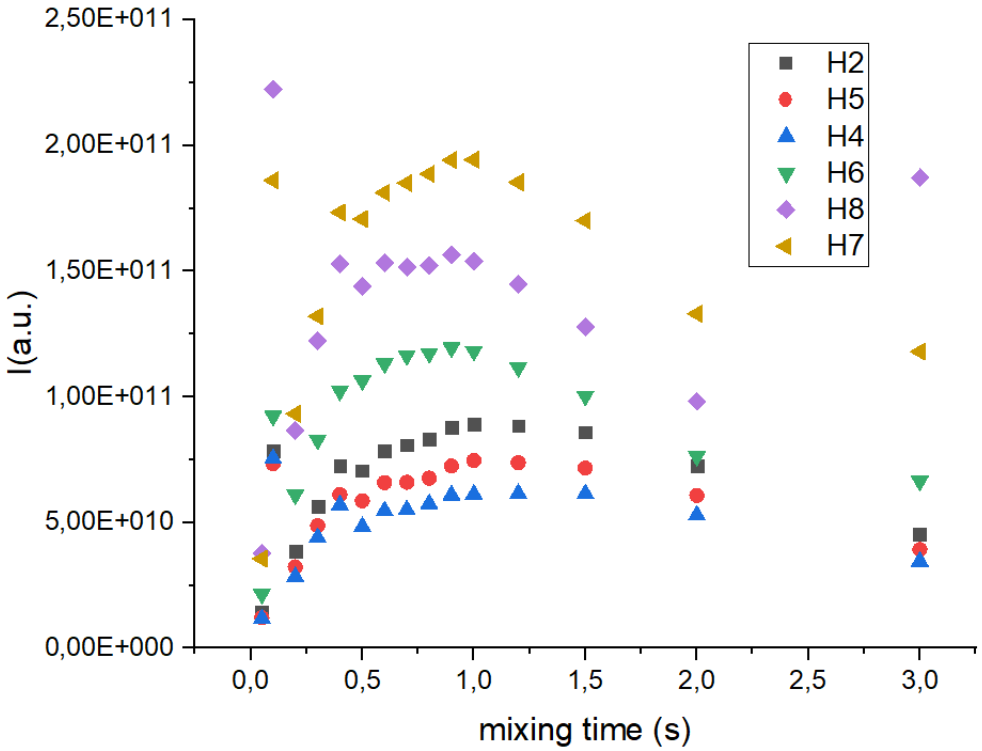

Figure 3.41: *Build up curves, obtained from 1D ^{1}H - ^{19}F hoesy using the magnitude mode to process the signals, for the sample EMImTfO + LiTfO at 298K*

Comparative results interpretation of 1D and 2D ^{1}H - ^{19}F hoesy

The 1D hoesy have been performed as trials experiments aiming to verify whether they are reliable tool for the measurement of the cross relaxation as the 2D hoesy are. Figures 3.42 and 3.43 show the comparison of the cross relaxation for the EMImTfO + LiTfO sample at 298 K both for 2D hoesy and 1D hoesy with non selective sequence.

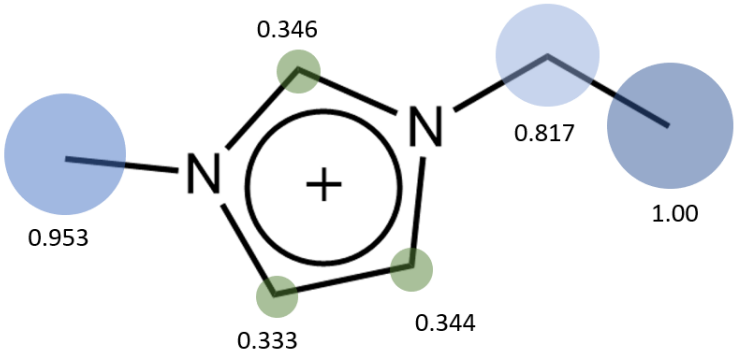

Figure 3.42: *Normalized cross relaxations on [EMIm]$^+$ cation, obtained from 2D ^1H - ^{19}F hoesy, EMImTfO + LiTfO at 298K*

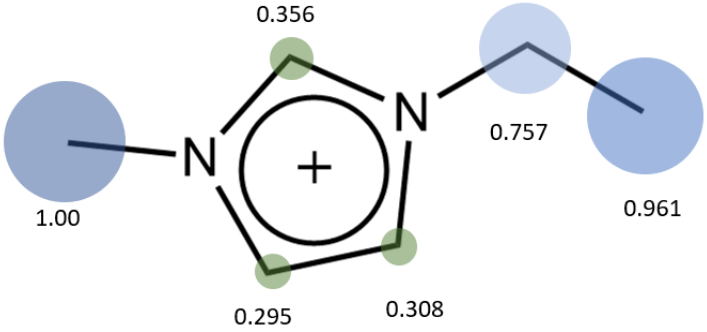

Figure 3.43: *Normalized cross relaxations on [EMIm]$^+$ cation, obtained from 1D ^1H - ^{19}F hoesy, using non selective sequence, for the sample EMImTfO + LiTfO at 298K*

Figures 3.42 and 3.43, even if not identical, are very similar and underline the results already described for ^{1}H - ^{19}F hoesy: the higher relative cross relaxation is observed on the alkyl chains. H7 and H8 show the biggest values equal or very close to 1, H6 has a considerable cross relaxations around 0.8 while 0.3 on the ring.

3.5.2 1D ^{7}Li - ^{1}H Hoesy

1D hoesy experiments have been performed also for the^{7}Li - ^{1}H on the blended sample, but at 288 K. In this case the spectra acquired show a pretty bad quality and the anti-phased peaks issue is enhanced with respect to 1D ^{1}H - ^{19}F hoesy because it affects each spectrum whatever mixing time is considered.
In figures 3.44 and 3.45 there are some examples of the spectra recorded. As

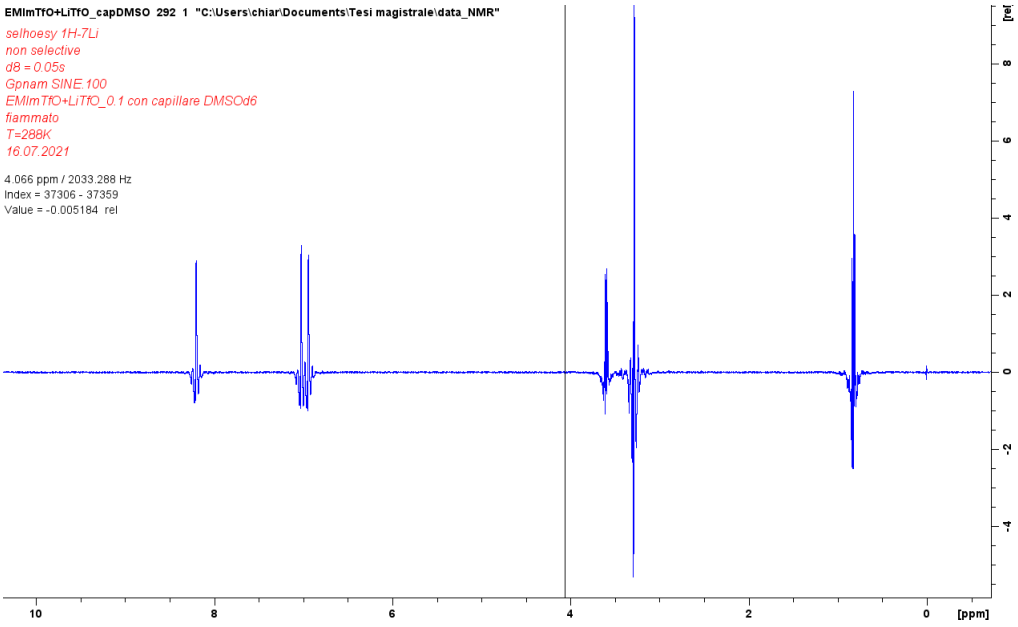

Figure 3.44: *1D ^{7}Li - ^{1}H Hoesy spectrum, run with a mixing of 0.05 for the sample EMImTfO + LiTfO at 288K*

in 1D ^{1}H - ^{19}F hoesy, the peaks have been integrated even though the spectra are completely not phase-able, that led to negative integrals, thus the build up curve cannot be drawn.
In order to overcome this issue, it was tried to process them in magnitude mode. Following this new pathway a sort of build up curve might be drawn, figure 3.46, but it's clearly not fitt-able from whatever of the equation mentioned until now. Since it was not possible to draw any significant curve, the analysis on 1D ^{7}Li - ^{1}H hoesy has been stopped here. No cross relaxation have been computed.

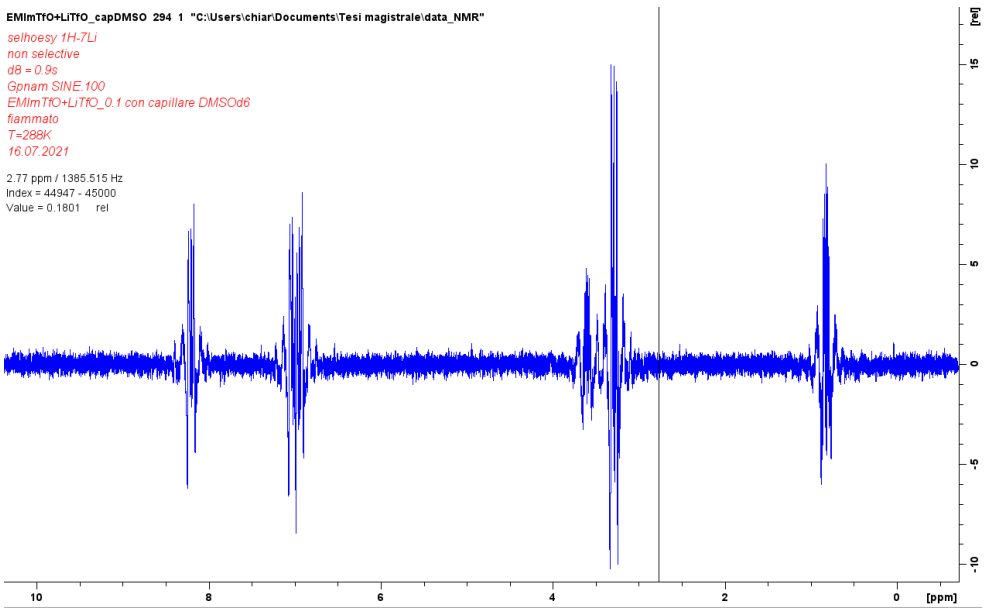

Figure 3.45: *1D ^{7}Li - ^{1}H Hoesy spectrum,run with a mixing time of 0.9s for the sample EMImTfO + LiTfO at 288K*

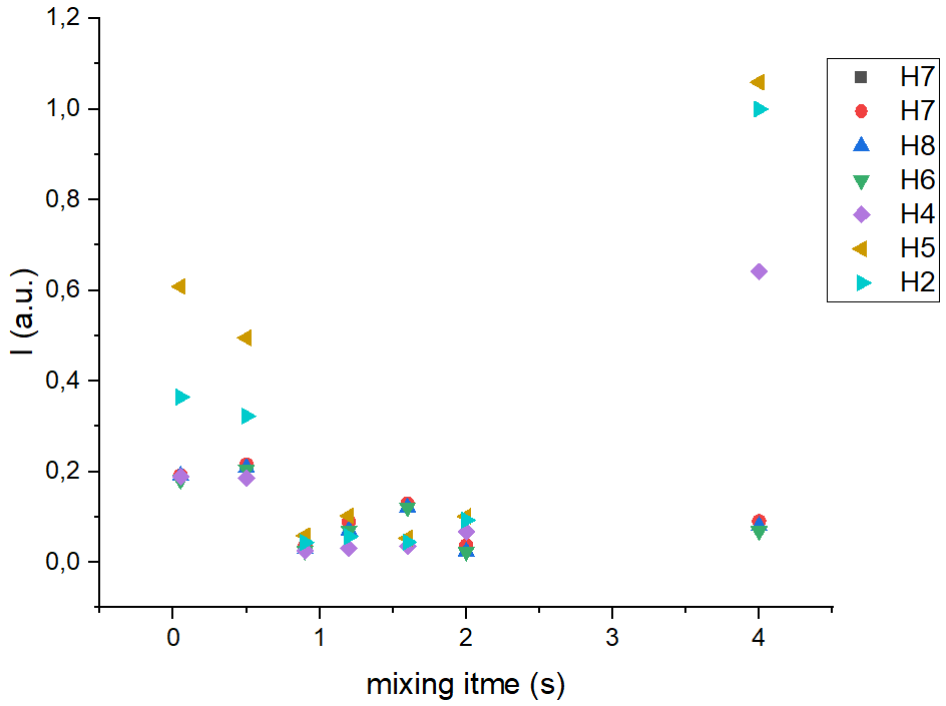

Figure 3.46: *Trial build up curves,obtained from the integration in magnitude mode of the signals of ^{7}Li - ^{1}H hoesy for the sample EMImTfO + LiTfO at 288K*

3.5.3 Considerations on 1D hoesy experiments

In conclusion 1D hoesy experiments seem to lead to a reliable result for ^{1}H - ^{19}F only, while they do not work at all when dealing with lithium.
The reliability of 1D experiments, even if restricted to certain application, gives the opportunity to overcome long-lasting drawback of the traditional hoesy, but the issues of anti-phased peaks jumped out both for 1D ^{1}H - ^{19}F and ^{7}Li - ^{1}H 1D hoesy must be further investigated.
It is still unknown what causes the odd phase of the peaks and why it affects only at low and high mixing time for the ^{1}H - ^{19}F, however the deriving build up curves are almost perfect without outlier or any scattering phenomenon.
For what concerns the ^{7}Li - ^{1}H, the anti-phased peak issues is extremely enhanced becoming unmanageable so that the build up curve cannot be drawn.
To exclude that the anti-phased peaks are due to the sample itself it would be appropriated to test other samples.

Chapter 4

Conclusions and perspective

2D hoesy experiments are the standard methodology for the analysis of the nanostructural organization in ionic liquids. Such method well worked giving very good results because they match with the simulations done by our colleagues in Wien, as stated in the study [13], allowing us to obtain the complementary pictures of the closest neighbours via ^{1}H-^{7}Li NOE and the solvation beyond the first shell via ^{1}H-^{19}F NOE. The novelty and the validity of the results rely upon the tunability of the length-scale for observable interactions: in the angstrom distance range for the short-range contacts and in nanometers range for the long-range contacts. The latter are thus directly compared to the structural features derived from the X-ray and neutron scattering experiments. Here I report only the comparison graphs taken from this study. The extremely

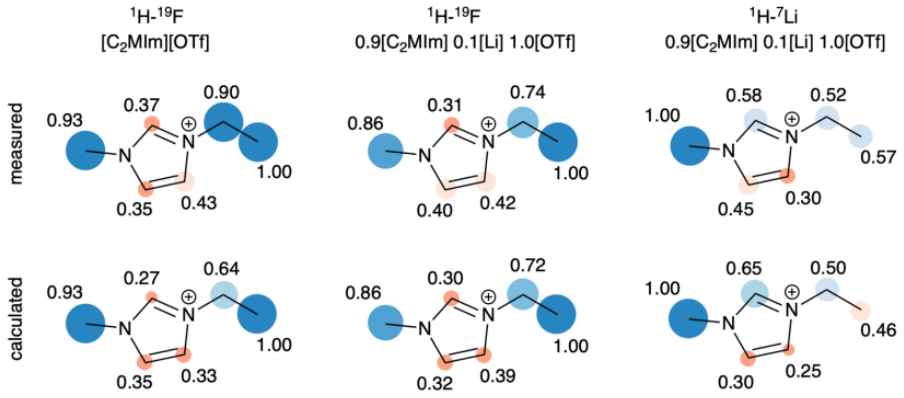

Figure 4.1: *Simulated and experimental data comparison:^{1}H - ^{19}F and ^{7}Li-^{1}H on EMImTfO + LiTfO sample at 298 K, ^{1}H - ^{19}F on EMImTfO sample at 298 K, [13]*

high match of simulations and experimental data is very meaningful since it

proves the theory proposed in 2013 by [17] paving the way to a new chapter in the interpretations of the NOE on ionic liquids and a new use of NMR complementary to X-ray/neutron scattering.
Despite being a remarkable result, some critical issues have arisen following this methodology regarding, in particular, the normalization of data and the fitting of the build up curves.
Normalization was roughly made dividing each integral intensity of a series by the highest value of such series and then by ten, as explained in chapter 2, otherwise the proposed equations would not be able to fit the curves. Although not elegant, this procedure is reliable, but it would be better to follow a more rigorous one.
For what concerns the fitting, it has been already stressed that the only one equations converging and well reproducing the curve is the Salomon equation, called in this work HOESY 1, and strictly when the averaged relaxation rate is considered a fit-able parameter. It is still unknown why a quantity that can be computed and treated as a constant must be fitted: the reasons probably lies in the experimental error coming from the T_1 analysis.
This problem did not prevent the measurement of the cross relaxation since it has been overcome as already explained, but it would be nice to actually understand, if possible, where this issue comes from and and thus, if solved, having more well behaving equations to fit the build up curves.

The 1D hoesy have been performed to verify whether they are a reliable tool for the measurement of the cross relaxations and hence overcome the disadvantage of the long duration of the traditional methodology, since they are much faster. 1D hoesy have been performed both on ^{1}H - ^{19}F and ^{7}Li - ^{1}H showing two different behaviors: ^{1}H - ^{19}F hoesy seem to be a reliable tool leading to results similar to the 2D hoesy, but when dealing with 1D^{7}Li - ^{1}H do not work at all. Even though 1D ^{1}H - ^{19}F hoesy well behave, some critical points have been underlined especially regarding the anti-phased peaks present in the spectra and the fitting.
The anti-phased peaks surprisingly do not generated any negative integral and do not affect the build up curve, which appears almost perfect. Also the cross relaxations computed following this procedure are comparable and very similar to the ones coming from 2D experiments.
Despite the anti-phased peaks seem to not affect the analysis, it is necessary

to understand why they are generated and how to avoid them because, even if this phenomenon is negligible in 1D ^{1}H - ^{19}F, it makes the ^{7}Li - ^{1}H 1D hoesy completely unmanageable.
The good results obtained with 1D ^{1}H - ^{19}F is surprising and unexpected, but it is necessary to investigate also why it this issue is automatically solved without any intervention.
These anti-phased peaks might be related to the sample itself, or lock inference thus further experiments on different samples and maybe selecting also different isotopes should be performed.
For what concerns the fitting 1D hoesy experiments show the same critical points of the traditional ones.

All in all the traditional hoesy experiments work very well since their results match with the simulations performed by our colleagues and thus demonstrate the 2013 theory proposed by [17].
1D hoesy can be considered a reliable tool for the computation of cross relaxations only under some circumstances like ^{1}H - ^{19}F, anyway it seems worth investigating further this technique as a faster methodology than the traditional one.

Appendix A

Publication on *The Journal of Physical Chemistry Letters*

As part of a wider project in collaboration with my supervisor, my co-supervisors and our colleagues of University of Vienna and Harvard medical school, this work has been published on the The Journal of Physical Chemistry Letters on September 2021 gaining also the cover of this scientific magazine.
Using both intermolecular NOE and molecular dynamics here is proved how the short-range or long-range behavior depends on the isotopes selected.

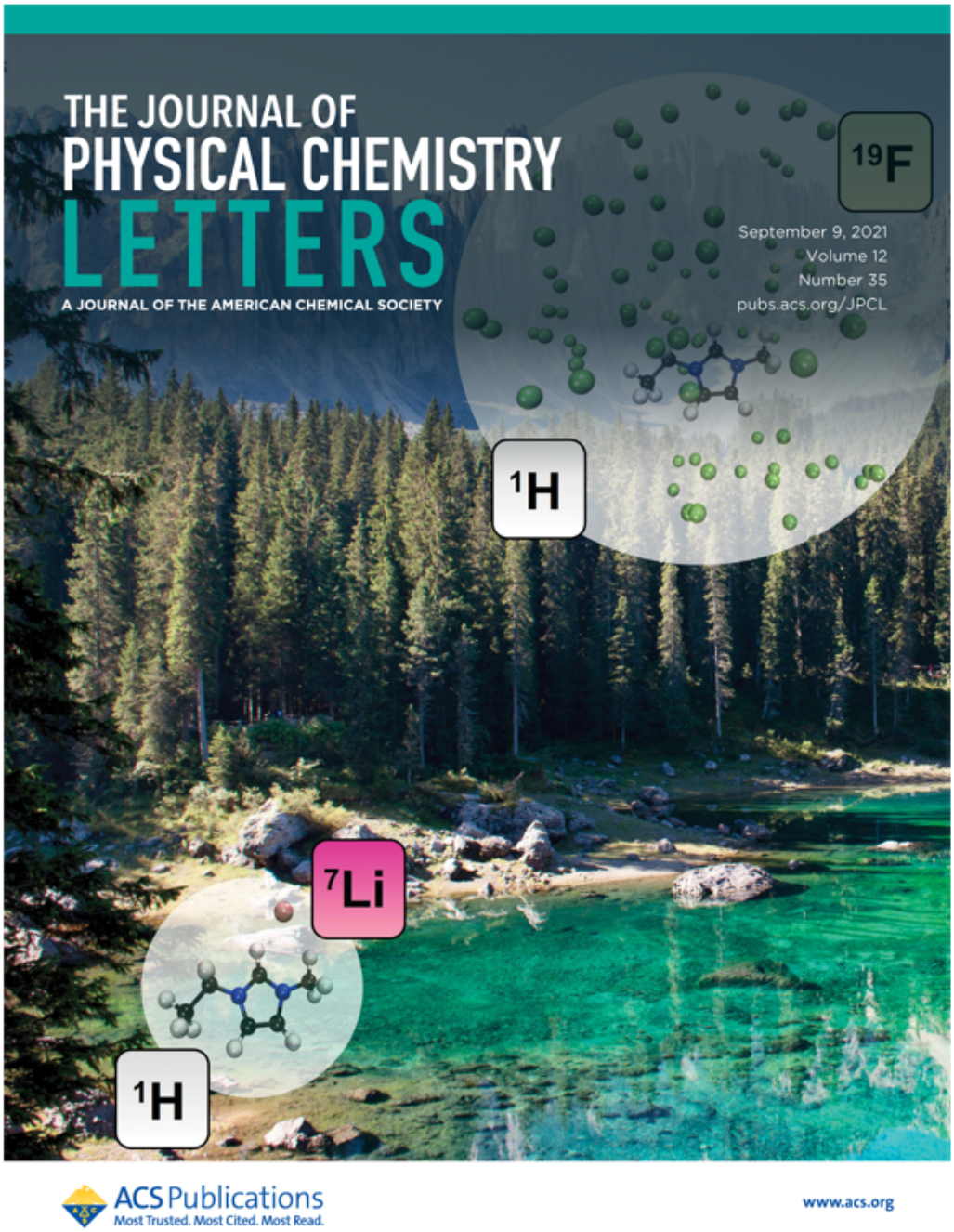

Figure A.1: *Cover of The Journal of Physical Chemistry Letters, September 2021*

THE JOURNAL OF PHYSICAL CHEMISTRY LETTERS
A JOURNAL OF THE AMERICAN CHEMICAL SOCIETY

pubs.acs.org/JPCL

Letter

The Intermolecular NOE Depends on Isotope Selection: Short Range vs Long Range Behavior

Philipp Honegger,[⊥] Maria Enrica Di Pietro,[⊥] Franca Castiglione,* Chiara Vaccarini, Alea Quant, Othmar Steinhauser, Christian Schröder,* and Andrea Mele

Cite This: *J. Phys. Chem. Lett.* 2021, 12, 8658−8663

Read Online

ACCESS | Metrics & More | Article Recommendations | Supporting Information

ABSTRACT: The nuclear Overhauser effect (NOE) is a powerful tool in molecular structure elucidation, combining the subtle chemical shift of NMR and three-dimensional information independent of chemical connectivity. Its usage for intermolecular studies, however, is fundamentally limited by an unspecific long-ranged interaction behavior. This joint experimental and computational work shows that proper selection of interacting isotopes can overcome these limitations: Isotopes with strongly differing gyromagnetic ratios give rise to short-ranged intermolecular NOEs. In this light, existing NOE experiments need to be re-evaluated and future ones can be designed accordingly. Thus, a new chapter on intermolecular structure elucidation is opened.

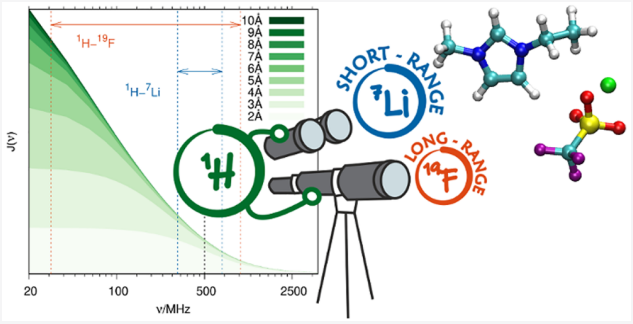

Ionic liquids (ILs) continuously attract interest in their applications and the still open issues on their fundamental knowledge.[1] One of their most fascinating aspects is the so-called "nanostructural organization" of polar and apolar domains,[2,3] whose formation, nevertheless, does not lead to phase inhomogeneities or phase separation. Such a paradigmatic feature points out that for ILs and more generally for "soft matter", the nanoscopic size of the intermolecular structures cannot be observed optically. Instead, they need to be probed by electromagnetic radiation providing indirect information on molecular structure and processes. Since the interpretation of such spectral features is often nontrivial and may lead to contradicting viewpoints, it can be augmented by molecular dynamics (MD) simulations which serve as a mathematical microscope into the atomistic world.[4−6]

The tremendous synergy of spectroscopic methods and MD simulations is the charming toolkit for understanding interactions in liquid media leading to a particular structure and corresponding physicochemical properties. In 1995, the pioneering NMR paper by Osteryoung[7] first showed the potential of the nuclear Overhauser effect (NOE) as a detection tool of intermolecular contacts in liquids that opens the route to NOE-based investigations on the local structure of ILs.[8] The unique role of NOE in the large repertoire of NMR techniques is related to the fact that NOE depends on spatial dipolar interactions of nuclei rather than chemical connectivity via chemical bonds. Consequently, NOE is a powerful tool to characterize the structure, interaction, and dynamics in liquids.[9,10] On the level of molecular processes, the temporal evolution (randomization rate) of the NOE is described by the time correlation function (TCF)

$$G(t) = \left\langle \frac{1}{r(0)^3}\frac{1}{r(t)^3}\left(\frac{3}{2}\cos^2(\theta(t)) - \frac{1}{2}\right)\right\rangle \quad (1)$$

with $\vec{r}(t)$ as the vector connecting the two interacting nuclei I and S at time t, and $\theta(t)$ is the angle swept by this vector during timespan t. In the frequency domain, this corresponds to the spectral density function (SDF)

$$J(\nu) = \mathrm{Re}\left[\int_0^\infty e^{-i2\pi\nu t} G(t)\, dt\right] = \int_0^\infty \cos(-2\pi\nu t) G(t)\, dt \quad (2)$$

with Re extracting the real part of the Fourier transformation. Cross-relaxation rates are then calculated using Larmor frequencies $\nu_I = \gamma_I\, \nu$ and $\nu_S = \gamma_S\, \nu$:

$$\sigma_L(\nu) = 0.6J(\nu_I + \nu_S) - 0.1J(|\nu_I - \nu_S|) \quad (3)$$

The intramolecular NOE has become a standard technique in molecular structure elucidation. The distance of the interacting nuclei $\vec{r}$ is constant except for molecular vibrations and segmental motion and depends only on molecular rotation. This yields a strict $1/r^6$ distance dependence that ensures that a meaningful NOE can only occur up to 4−5 Å.[11] This well-known distance dependence mediated by dipole-coupling can

Received: July 13, 2021
Accepted: August 16, 2021

https://doi.org/10.1021/acs.jpclett.1c02253
J. Phys. Chem. Lett. 2021, 12, 8658−8663

be understood from eq 1. The situation changes for intermolecular NOEs, where the interacting spins are not located on the same molecule:[12]

- A reference spin interacts with *many* surrounding spins. Instead of one internuclear distance, there is a distribution of distances, known as the radial distribution function (RDF). We are primarily interested in the contact shell surrounding a reference molecule. The molecules beyond form the bulk (Figure S1). The number of partner spins increases by an order of r^2 with increasing distance.
- The greater the distance between two interacting spins, the more time the spin-joining vector needs to randomize its length and orientation. The randomization time also increases by order of r^2 (Figure S2).
- Summing up over all spherical distance shells r adds an order of r.

Thus, in the extreme case, using model theory, Halle predicted a long-ranged intermolecular NOE decaying by an order of $1/r$.[12] MD simulations expanding on those models showed a somewhat more beneficial but still long-ranged behavior between $1/r$ and $1/r^3$.[13] Structural short-ranged information is present in intermolecular NOEs too but buried by unspecific magnetization transfers between the reference molecule and a multitude of distant bulk molecules.[14]

The lower the frequency of the spectral density function $J(\nu)$, the more long-ranged the NOE becomes. As pointed out by Weingärtner and co-workers in their seminal paper, the interaction range depends on the spectrometer frequency.[15]

The approach proposed by Castiglione et al. in ref 16 and treated in this work seeks to select general cases in which the short-distance based interpretation on NOE still holds but, at the same time, does not contradict the general theory of intermolecular cross-relaxation. The cross-relaxation rate σ_L is a linear combination of the high-frequency part $J(\nu_I + \nu_S)$ and the low-frequency part $J(|\nu_I - \nu_S|)$ of the SDF. Indeed, the long-ranged contributions of $J(\nu \to 0)$ can be made negligible by selecting isotopes maximizing the frequency difference $|\nu_I - \nu_S| = |(\gamma_I - \gamma_S)\cdot\nu|$.

In this instance, we propose that the heteronuclear NOE of ^{1}H (γ_H = 42.577 MHz T^{-1}) and ^{7}Li (γ_{Li} = 16.546 MHz T^{-1}) is of a shorter range than the one between ^{1}H and ^{19}F (γ_F = 40.078 MHz T^{-1}). This theory was tested by O'Dell and co-workers using a combination of MD simulations and quantitative HOESY analysis.[17,18] The elegant (yet not straightforward) fit of suitably normalized HOESY build-up curves with a modified expression including both the longitudinal relaxation times and diffusion coefficients allows for the precise calculation of absolute intermolecular cross-relaxation rates and their comparative use between different ionic liquids, concentrations, or temperatures.[19,20]

The following calculations are based on a 500 MHz ^{1}H NMR spectrometer (cf. eq 3):

- In the homonuclear extreme case, $J(2\nu)$ and $J(0)$ contribute, e.g., 2ν = 1000 MHz for ^{1}H. The high-frequency part is short-ranged but the low-frequency part is long-ranged, as can be seen in the top panel of Figure 1, rendering the ^{1}H−^{1}H NOEs long-ranged.
- The same is true for ^{1}H−^{19}F NOEs. The gyromagnetic ratios are similar ($\nu_I + \nu_S$ = 970 MHz and $|\nu_I - \nu_S|$ = 30 MHz) resulting in similar problems as the homonuclear case.

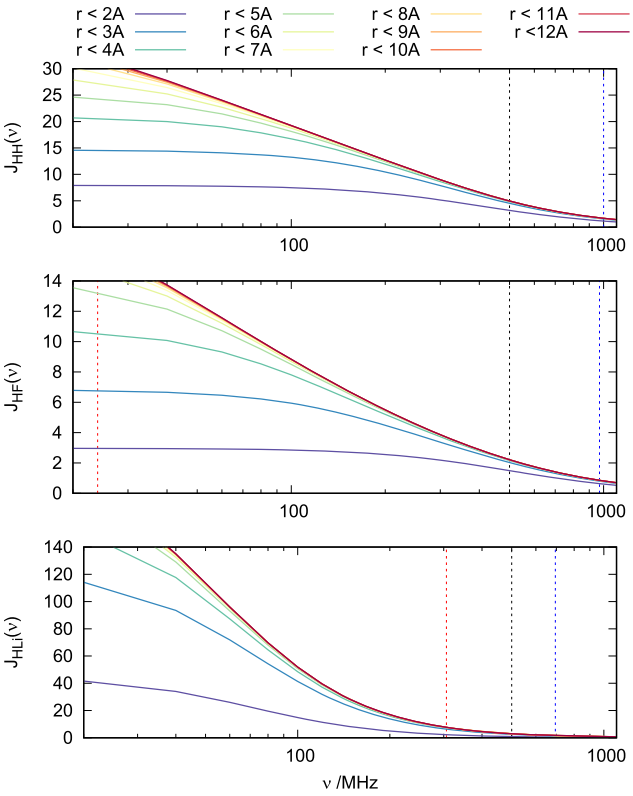

Figure 1. SDF $J(\nu)$ of the H8−H8 (top), H8−F (middle), and H8−Li (bottom) spin pairs, resolved into cumulative contributions. The lower the frequency, the more long-ranged the $J(\nu)$ becomes. Explicitly marked frequencies are the following: spectrometer (black), high-frequency contribution $J(\nu_I + \nu_S)$ (blue), low-frequency contribution $J(\nu_I - \nu_S)$ (red, beyond range for ^{1}H−^{1}H)

- For ^{1}H−^{7}Li NMR, the gyromagnetic ratios differ significantly; hence both terms at $\nu_I + \nu_S$ = 694 MHz and $|\nu_I - \nu_S|$ = 306 MHz draw from a similar part of the SDF and avoid the low-frequency part, prospecting a more beneficial short-ranged behavior.

The less similar the gyromagnetic ratios, the higher is the low-frequency $|\nu_I - \nu_S|$, avoiding the long-ranged low-frequency SDF limit $J(\nu \to 0)$.

In this proof-of-concept study, we perform semiquantitative experimental NOE measurements of the ionic liquid/salt solution 0.9 1-ethyl-3-methylimidazolium [C_2MIm]·0.1 Li·1.0 triflate [OTf] (Scheme 1). The simple fit of the HOESY build-up curves with the fundamental expression derived by Solomon equations[11,21] gives relative cross-relaxation rates, with no need for elaborate normalization or fitting procedures. Still, we demonstrate that these relative values do reflect the heteronuclear proximity when interpreted bearing in mind the isotope dependency of short- and long-range contributions. This joint theoretical and experimental validation represents

Scheme 1. Chemical Structure of the IL/Salt Mixture

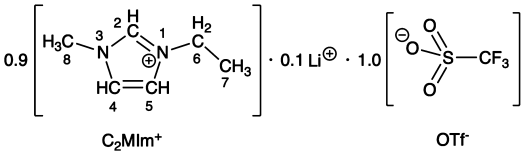

https://doi.org/10.1021/acs.jpclett.1c02253
J. Phys. Chem. Lett. 2021, 12, 8658−8663

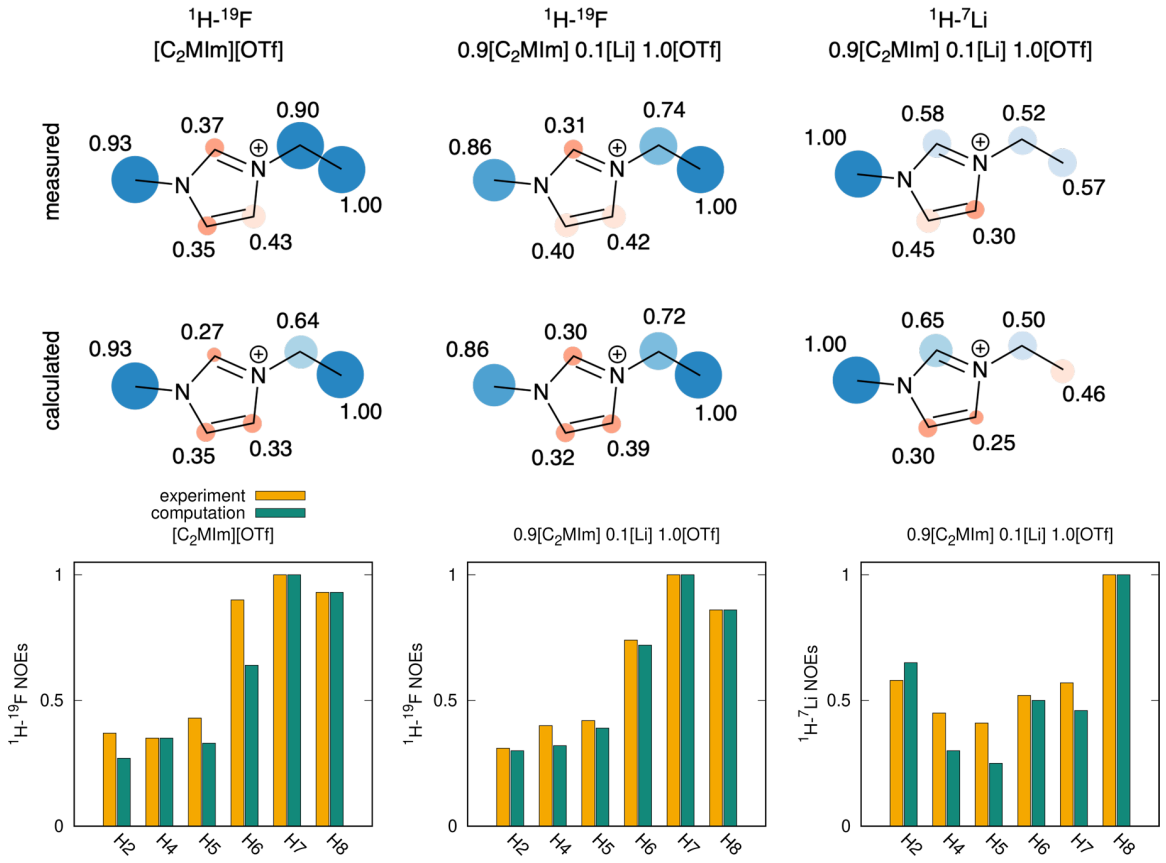

Figure 2. Top: Experimental (upper row) and computational (bottom row) C_2MIm^+-F and C_2MIm^+-Li NOEs for the neat IL [C_2MIm][OTf] and its mixture with [Li][OTf], normalized to the most intense NOE signal per molecule. Experimental parameters: T = 298 K, mixing times were 900 ms (C_2MIm^+-F) and 1200 ms (C_2MIm^+-Li). Bottom: Comparison of experimental and simulated NOEs.

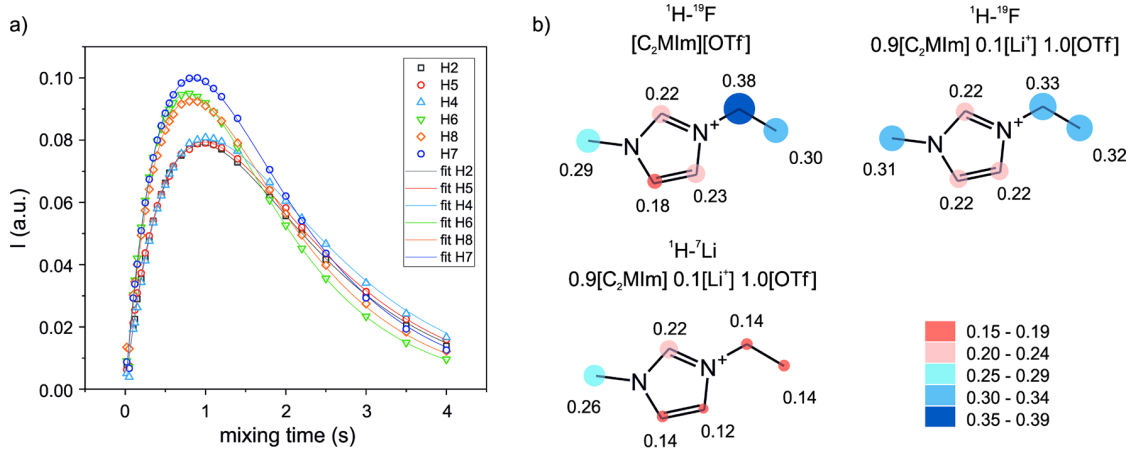

Figure 3. (a) ^{1}H–^{19}F HOESY build-up curves for the mixture 0.9[C_2MIm]·0.1 Li·1.0[OTf] and corresponding fit using eq 4. (b) Cross relaxations obtained from the fit with eq 4 of the corrected and normalized ^{1}H–^{19}F and ^{1}H–^{7}Li NOEs observed for the neat IL and its mixture with [Li][OTf].

then a first step for some "nuts and bolts" guidelines for the interpretation of intemolecular NOEs for non-NMR-specialists; thus it is of broad interest for the wider chemist community.

Our interpretations of the experimental NOEs are supported by an MD simulation. In contrast to preceding works, we modeled the molecules as both fully atomistic and polarizable. Nonpolarizable ILs exhibit exaggerated directed electrostatic interactions. In actuality, electronic charge distributions are flexible upon molecular contact, and thus ILs are less viscous,[22] necessitating polarizable force fields to allow for realistic pair diffusion dynamics important to the NOE. Furthermore, we calculate the NOE directly from the trajectory instead of using models such as hard-sphere free diffusion,[23] spin eccentricity,[24] or the monoexponential Bloembergen–Purcell–Pound equation,[25] thus avoiding their intrinsic model assumptions. The TCF $G(t)$ is obtained from nuclear positions in the trajectory and transformed into the SDF $J(\nu)$, necessitating a trajectory

https://doi.org/10.1021/acs.jpclett.1c02253
J. Phys. Chem. Lett. 2021, 12, 8658–8663

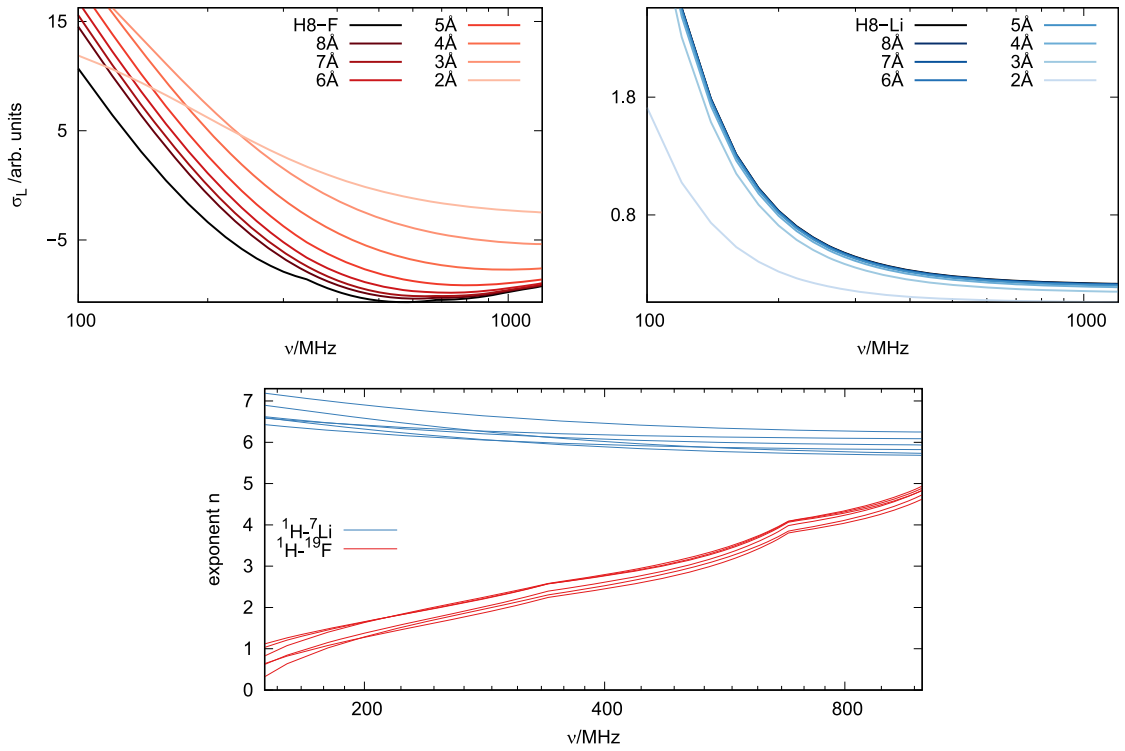

Figure 4. Cumulative contributions of shell-resolved cross-relaxation rates $\sigma_L(r,\nu)$ of the H8−F spin pairs (left) and the H8−Li spin pairs (right). σ_L converges faster for ^{1}H−^{7}Li spin pairs than ^{1}H−^{19}F spin pairs. Bottom: Interaction range of the H−F spin pairs (red) and the H−Li spin pairs (blue), represented by the exponent of the decay law $1/r^n$.

length of at least $(100\ \text{MHz})^{-1}$ = 10 ns (see Supporting Information for details).

We found cross-peaks of all C_2MIm^+ protons interacting with the CF_3 group of OTf^- (Figure S3a) and Li^+ (Figure S3b). The individual signal intensities are proportional to the magnitude of the given cross-relaxation and hint about the intensity of the mutual interaction. Figure 2 (top row) presents the NOEs of the neat IL [C_2MIm][OTf] and solution 0.9[C_2MIm]·0.1Li·1.0[OTf]. Some considerations can be drawn about the trends in experimental NOE values:

- The short-ranged ^{1}H−^{7}Li HOESY reflects specific Li-cation interactions. Li preferentially interacts with N−CH_3 (H8) and roughly equivalently with all other proton sites. The alkyl chain of imidazolium-based ILs is known to form hydrophobic domains, excluding charged functional groups.[13,26] This can be seen in the ^{1}H−^{7}Li RDFs of the MD simulation as well (Figure S1): The H8−Li atom pair forms a higher peak at a short distance (≈3−4 Å) than either H6−Li and H7−Li.
- ^{1}H−^{19}F HOESY contains considerable contributions from the bulk. The most intense correlations of the anion are with the alkyl protons. Yet this behavior is neither chemically intuitive nor justified by the RDFs (Figure S1). The H−F NOEs are contaminated with unspecific long-ranged contributions and thus arbitrarily unreliable. In this respect, we observe that there is no considerable variation between the neat and Li-loaded samples.

For a semiquantitative analysis of HOESY cross-peaks, integrated volumes were corrected by a factor $N_I\ N_S/(N_I + N_S)$, with N_I the number of ^{1}H and N_S the number of ^{19}F or ^{7}Li nuclei contributing to the observed NOE signal.[16,27−32] The corresponding corrected and normalized NOE build-up curves obtained from 29 ^{1}H−^{19}F and 23 ^{1}H−^{7}Li spectra, at increasing mixing time, are displayed in Figures 3a and S4. As expected, from 20 ms to 700−900 ms, a linear increase is observed in ^{1}H−^{19}F build-up curves, then a maximum is reached, and an exponential decay is observed afterward. Similar behavior is seen in ^{1}H−^{7}Li HOESY, with the maximum shifted to 1.2 s.

All curves were fitted using an exponential function derived from the fundamental Solomon equations,[11,21] using R (total longitudinal relaxation rate constant) and σ_{IS} as fit-able parameters:

$$\text{NOE} = \frac{1}{2}\exp[-(R - \sigma_{IS})\tau](1 - \exp[-2\sigma_{IS}\tau]) \quad (4)$$

Figure 3b displays the cross relaxations σ_{IS} obtained by fitting. Findings are in agreement with NOEs for both ^{1}H−^{19}F and ^{1}H−^{7}Li interactions. As a result of the correction, the difference in intensity between the interactions at the different sites is reduced. For instance, looking at the ^{1}H−^{19}F cross relaxations, those with the alkyl protons are still dominating, but the differences with the imidazolium protons are less significant. Similarly, the ^{1}H−^{7}Li cross-relaxation at N−CH_3 site has the highest value but less marked difference to the other protons.

The computational ^{1}H−^{19}F and ^{1}H−^{7}Li NOEs are shown Figure 2 (second row). We find a reasonably good match between experimental and simulated NOEs (Figure 2, bottom). The most significant observed difference is in the ^{1}H−^{7}Li NOE of the imidazolium H4 and H5 protons in the mixture and the ^{1}H−^{19}F NOE of the CH_2 protons in the neat IL. Since the overall trend of NOEs is faithfully reproduced,

https://doi.org/10.1021/acs.jpclett.1c02253
J. Phys. Chem. Lett. 2021, 12, 8658−8663

these four diverging values out of 33 spin pairs are not systematic and are likely local artifacts. The polarizabilities used in this work are more or less a function of the hybridization and the number of attached protons but take less into account the immediate chemical environment. Nevertheless, the emerging induced dipoles of these carbons based on these polarizabilities react individually to their local environment. Of course, an exact quantum-mechanical determination of the polarizabilities is also possible[33,34] and leads to slight variations in the respective carbon polarizabilities and hence slightly different induced dipoles, but using new polarizabilities would require a complete reparametrization of the polarizable force field. The one applied in this work, however, has already proven to reproduce experimental NMR results.[35]

The reasonable agreement with the experimental values validates the accuracy of the MD simulation; thus the computational NOE calculations can be used to decompose observable sum spectra into different components. We dissect $\sigma_L(\nu)$ into contributions from spin pairs at different distances,

$$\sigma_L(\nu) = \sum_{r=0}^{r_{max}} \sigma_L(r, \nu) \quad (5)$$

Figures 4 (top) and S5 display the convergence to the experimentally observable $\sigma_L(\nu)$.

The $^1H-^{19}F$ contributions converge at larger distances than $^1H-^7Li$ contributions, meaning the latter are barely affected by spin interactions with the bulk. In addition, the frequency dependence of the $^1H-^{19}F$ spin pairs is more pronounced: The spacing between the curve bundles varies from wide (low ν, long-ranged) to small (high ν, short-ranged). In order to quantify the changed range dependence, we fitted the spatially resolved $\sigma_L(r,\nu)$ to a $1/r^n$ law, shown in Figure 4(bottom). The H−Li spin pairs show a relatively consistent short-ranged $1/r^6$ distance dependence. The range of H−F spin-pairs is long and additionally depends on the spectrometer frequency.

In summary, this contribution follows up the 2013 milestone paper by Gabl, Steinhauser, and Weingärtner, who introduced the fundamental concept that the structural information from intermolecular NOE is severely affected by the Larmor frequency of the interacting nuclei: "frequency does matter",[15] strongly discouraging the usage of intermolecular NOEs for structure determination in the chemist's community. Their work studied a $^1H-^{19}F$ NOE.

Here we demonstrate how gyromagnetic ratios of interacting nuclei determine the intermolecular NOE range. The larger their difference, the larger the Larmor frequency difference $|\nu_I - \nu_S|$ becomes, avoiding the long-ranged low-frequency limit. We studied the IL electrolyte 0.9[C_2MIm]·0.1 Li·1.0[OTf] as a prototypical example with at least two remarkable outcomes:

- The good agreement between HOESY measurements and calculations validates the correctness of the computational results.
- Computational signal decomposition confirms that the $^1H-^{19}F$ signal contains significant interactions with the bulk. In contrast, the $^1H-^7Li$ signal converges at small distances and is thus specific.

Our work provides experimentalists with a clear-cut interpretation tool for the structural use of intermolecular NOE: Proper selection of isotopes with differing gyromagnetic ratios overcomes the fundamental long-ranged limitation of intermolecular NOEs and provides intermolecular structural information.

Finally, the long-range interpretation of intermolecular NOEs should not prevent chemists from measuring them, as their interpretation adds value to other structural methods for assessing mesoscopic order, such as WAXS, SAXS, or SANS. As previously shown by some of us, the joint use of NOEs, scattering techniques, and MD simulations is a powerful investigating tool for nanostructured liquids.[36]

■ ASSOCIATED CONTENT

Supporting Information

The Supporting Information is available free of charge at https://pubs.acs.org/doi/10.1021/acs.jpclett.1c02253.

Theory and experimental and computational methods in detail (PDF)

■ AUTHOR INFORMATION

Corresponding Authors

Franca Castiglione − *Department of Chemistry, Materials and Chemical Engineering "G. Natta", Politecnico di Milano, 20133 Milano, Italy;* orcid.org/0000-0003-2413-8808; Email: franca.castiglione@polimi.it

Christian Schröder − *Department of Computational Biological Chemistry, University of Vienna, 1090 Vienna, Austria;* orcid.org/0000-0002-2167-5096; Email: christian.schroeder@univie.ac.at

Authors

Philipp Honegger − *Department of Systems Biology, Harvard Medical School, Boston, Massachusetts 02115, United States; Department of Computational Biological Chemistry, University of Vienna, 1090 Vienna, Austria;* orcid.org/0000-0001-8225-671X

Maria Enrica Di Pietro − *Department of Chemistry, Materials and Chemical Engineering "G. Natta", Politecnico di Milano, 20133 Milano, Italy;* orcid.org/0000-0002-2370-1948

Chiara Vaccarini − *Department of Chemistry, Materials and Chemical Engineering "G. Natta", Politecnico di Milano, 20133 Milano, Italy*

Alea Quant − *Department of Computational Biological Chemistry, University of Vienna, 1090 Vienna, Austria*

Othmar Steinhauser − *Department of Computational Biological Chemistry, University of Vienna, 1090 Vienna, Austria;* orcid.org/0000-0003-0839-6460

Andrea Mele − *Department of Chemistry, Materials and Chemical Engineering "G. Natta", Politecnico di Milano, 20133 Milano, Italy; CNR-SCITEC Istituto di Scienze e Tecnologie Chimiche, 20133 Milano, Italy;* orcid.org/0000-0002-0351-0538

Complete contact information is available at: https://pubs.acs.org/10.1021/acs.jpclett.1c02253

Author Contributions

⊥P.H. and M.E.D.P. contributed equally.

Notes

The authors declare no competing financial interest.

■ ACKNOWLEDGMENTS

M.E.D.P. thanks Politecnico di Milano for her postdoctoral fellowship in the framework of the "MSCA EF Master Class 2018" funding program.

REFERENCES

(1) Welton, T. Ionic liquids: a brief history. *Biophys. Rev.* **2018**, *10*, 691−706.
(2) Canongia Lopes, J. N. A.; Pádua, A. A. H. Nanostructural Organization in Ionic Liquids. *J. Phys. Chem. B* **2006**, *110*, 3330−3335.
(3) Triolo, A.; Russina, O.; Bleif, H.-J.; Di Cola, E. Nanoscale Segregation in Room Temperature Ionic Liquids. *J. Phys. Chem. B* **2007**, *111*, 4641−4644.
(4) Judeinstein, P.; Zeghal, M.; Constantin, D.; Iojoiu, C.; Coasne, B. Interplay of Structure and Dynamics in Lithium/Ionic Liquid Electrolytes: Experiment and Molecular Simulation. *J. Phys. Chem. B* **2021**, *125*, 1618−1631.
(5) Berrod, Q.; Ferdeghini, F.; Judeinstein, P.; Genevaz, N.; Ramos, R.; Fournier, A.; Dijon, J.; Ollivier, J.; Rols, S.; Yu, D.; et al. Enhanced ionic liquid mobility induced by confinement in 1D CNT membranes. *Nanoscale* **2016**, *8*, 7845−7848.
(6) Castiglione, F.; Saielli, G.; Mauri, M.; Simonutti, R.; Mele, A. Xenon Dynamics in Ionic Liquids: A Combined NMR and MD Simulation Study. *J. Phys. Chem. B* **2020**, *124*, 6617−6627.
(7) Mantz, R. A.; Trulove, P. C.; Carlin, R. T.; Osteryoung, R. A. ROESY NMR of Basic Ambient-Temperature Chloroaluminate Ionic Liquids. *Inorg. Chem.* **1995**, *34*, 3846−3847.
(8) Mele, A.; Tran, C. D.; De Paoli Lacerda, S. H. The Structure of a Room-Temperature Ionic Liquid with and without Trace Amounts of Water: The Role of C-H···O and C-H···F Interactions in 1-n-Butyl-3-Methylimidazolium Tetrafluoroborate. *Angew. Chem., Int. Ed.* **2003**, *42*, 4364−4366.
(9) Zhu, H.; O'Dell, L. A. Nuclear magnetic resonance characterisation of ionic liquids and organic ionic plastic crystals: common approaches and recent advances. *Chem. Commun.* **2021**, *57*, 5609.
(10) Damodaran, K. Recent NMR Studies of Ionic Liquids. *Annu. Rep. NMR Spectrosc.* **2016**, *88*, 215−244.
(11) Neuhaus, D.; Williamson, M. P. *The Nuclear Overhauser Effect in Structural and Conformational Analysis*; Wiley-VCH: Weinheim, Germany, 2000.
(12) Halle, B. Cross-relaxation between macromolecular and solvent spins: The role of long-range dipole couplings. *J. Chem. Phys.* **2003**, *119*, 12372.
(13) Braun, D.; Steinhauser, O. The intermolecular NOE is strongly influenced by dynamics. *Phys. Chem. Chem. Phys.* **2015**, *17*, 8509−8517.
(14) Frezzato, D.; Rastrelli, F.; Bagno, A. Nuclear Spin Relaxation Driven by Intermolecular Dipolar Interactions: The Role of Solute-Solvent Pair Correlations in the Modeling of Spectral Density Functions. *J. Phys. Chem. B* **2006**, *110*, 5676−5689.
(15) Gabl, S.; Steinhauser, O.; Weingärtner, H. From Short-Range to Long-Range Intermolecular NOEs in Ionic Liquids: Frequency Does Matter. *Angew. Chem., Int. Ed.* **2013**, *52*, 9242−9246.
(16) Castiglione, F.; Appetecchi, G. B.; Passerini, S.; Panzeri, W.; Indelicato, S.; Mele, A. Multiple points of view of heteronuclear NOE: Long range vs short range contacts in pyrrolidinium based ionic liquids in the presence of Li salts. *J. Mol. Liq.* **2015**, *210*, 215−222.
(17) Martin, P.-A.; Chen, F.; Forsyth, M.; Deschamps, M.; O'Dell, L. A. Correlating Intermolecular Cross-Relaxation Rates with Distances and Coordination Numbers in Ionic Liquids. *J. Phys. Chem. Lett.* **2018**, *9*, 7072−7078.
(18) Gyabeng, D.; Qiao, L.; Zhang, H.; Oteo, U.; Armand, M.; Forsyth, M.; Chen, F.; O'Dell, L. A. Anion-cation interactions in novel ionic liquids based on an asymmetric sulfonamide anion observed by NMR and MD simulations. *J. Mol. Liq.* **2021**, *327*, 114879.
(19) Martin, P.-A.; Salager, E.; Forsyth, M.; O'Dell, L. A.; Deschamps, M. On the measurement of intermolecular heteronuclear cross relaxation rates in ionic liquids. *Phys. Chem. Chem. Phys.* **2018**, *20*, 13357.
(20) Gyabeng, D.; Martin, P.-A.; Pal, U.; Deschamps, M.; Forsyth, M.; O'Dell, L. A. Investigating Intermolecular Interactions in a DME-Based Hybrid Ionic Liquid Electrolyte by HOESY NMR. *Front. Chem.* **2019**, *7*, 4.
(21) Solomon, I. Relaxation Processes in a System of Two Spins. *Phys. Rev.* **1955**, *99*, 559.
(22) Schröder, C. Comparing reduced partial charge models with polarizable simulations of ionic liquids. *Phys. Chem. Chem. Phys.* **2012**, *14*, 3089−3102.
(23) Hwang, L.-P.; Freed, J. H. Dynamic effects of pair correlation functions on spin relaxation by translational diffusion in liquids. *J. Chem. Phys.* **1975**, *63*, 4017−4025.
(24) Ayant, Y.; Belorizky, E.; Fries, P.; Rosset, J. Intermolecular contribution to dipole-dipole relaxation rates of small molecules. *J. Phys. (Paris)* **1977**, *38*, 325−337.
(25) Bloembergen, N.; Purcell, E. M.; Pound, R. V. Relaxation effects in nuclear magnetic resonance absorption. *Phys. Rev.* **1948**, *73*, 679.
(26) Hayes, R.; Warr, G. G.; Atkin, R. Structure and Nanostructure in Ionic Liquids. *Chem. Rev.* **2015**, *115*, 6357.
(27) Hou, S.-S.; Tzeng, J.-K.; Chuang, M.-H. Intermolecular association and supramolecular structures of PNVF-LiPFN and PVP-LiPFN complexes in the aqueous phase. *Soft Matter* **2010**, *6*, 409−415.
(28) Khatun, S.; Castner, E. W., Jr Ionic liquid-solute interactions studied by 2D NOE NMR spectroscopy. *J. Phys. Chem. B* **2015**, *119*, 9225−9235.
(29) Castiglione, F.; Moreno, M.; Raos, G.; Famulari, A.; Mele, A.; Appetecchi, G. B.; Passerini, S. Structural organization and transport properties of novel pyrrolidinium-based ionic liquids with perfluoroalkyl sulfonylimide anions. *J. Phys. Chem. B* **2009**, *113*, 10750−10759.
(30) Lee, H. Y.; Shirota, H.; Castner, E. W., Jr Differences in ion interactions for isoelectronic ionic liquid homologs. J. Phys. *J. Phys. Chem. Lett.* **2013**, *4*, 1477−1483.
(31) Zuccaccia, C.; Bellachioma, G.; Cardaci, G.; Macchioni, A. Solution structure investigation of Ru (II) complex ion pairs: Quantitative NOE measurements and determination of average interionic distances. *J. Am. Chem. Soc.* **2001**, *123*, 11020−11028.
(32) Di Pietro, M. E.; Castiglione, F.; Mele, A. Anions as Dynamic Probes for Ionic Liquid Mixtures. *J. Phys. Chem. B* **2020**, *124*, 2879−2891.
(33) Heid, E.; Szabadi, A.; Schröder, C. Quantum mechanical determination of atomic polarizabilities of ionic liquids. *Phys. Chem. Chem. Phys.* **2018**, *20*, 10992−10996.
(34) Bedrov, D.; Piquemal, J.-P.; Borodin, O.; MacKerell, A.; Roux, B.; Schröder, C. Molecular Dynamics Simulations of Ionic Liquids and Electrolytes Using Polarizable Force Fields. *Chem. Rev.* **2019**, *119*, 7940−7995.
(35) Honegger, P.; Overbeck, V.; Strate, A.; Appelhagen, A.; Sappl, M.; Heid, E.; Schröder, C.; Ludwig, R.; Steinhauser, O. Understanding the Nature of Nuclear Magnetic Resonance Relaxation by Means of Fast-Field-Cycling Relaxometry and Molecular Dynamics Simulations−The Validity of Relaxation Models. *J. Phys. Chem. Lett.* **2020**, *11*, 2165.
(36) Lo Celso, F.; Yoshida, Y.; Castiglione, F.; Ferro, M.; Mele, A.; Jafta, C.; Triolo, A.; Russina, O. Direct experimental observation of mesoscopic fluorous domains in fluorinated room temperature ionic liquids. *Phys. Chem. Chem. Phys.* **2017**, *19*, 13101−13110.

https://doi.org/10.1021/acs.jpclett.1c02253
J. Phys. Chem. Lett. 2021, 12, 8658−8663

Bibliography

[1] Thomas Welton. Room-Temperature Ionic Liquids. Solvents for Synthesis and Catalysis. *Chemical Reviews*, 99(8):2071–2083, 1999.

[2] Shiguo Zhang, Jiaheng Zhang, Yan Zhang, and Youquan Deng. Nanoconfined Ionic Liquids. *Chemical Reviews*, 117(10):6755–6833, 2017.

[3] Tom Welton. Ionic liquids: a brief history. *Biophysical Reviews*, 10(3):691–706, 2018.

[4] Yong Lei Wang, Bin Li, Sten Sarman, Francesca Mocci, Zhong Yuan Lu, Jiayin Yuan, Aatto Laaksonen, and Michael D. Fayer. Microstructural and Dynamical Heterogeneities in Ionic Liquids. *Chemical Reviews*, 120(13):5798–5877, 2020.

[5] Maria Enrica Di Pietro, Franca Castiglione, and Andrea Mele. Anions as Dynamic Probes for Ionic Liquid Mixtures. *Journal of Physical Chemistry B*, 124(14):2879–2891, 2020.

[6] Jason P. Hallett and Tom Welton. Room-temperature ionic liquids: Solvents for synthesis and catalysis. 2. *Chemical Reviews*, 111(5):3508–3576, 2011.

[7] Thomas Jennifer L., Anthony Wasserscheid,Peter Welton. Physicochemical properties of ILs, in Ionic Liquids in Synthesis. *Wiley-VCH*, 2002.

[8] Riccardo Bini, Olga Bortolini, Cinzia Chiappe, Daniela Pieraccini, and Tiziana Siciliano. Development of cation/anion "interaction" scales for ionic liquids through ESI-MS measurements. *Journal of Physical Chemistry B*, 111(3):598–604, 2007.

[9] José N. A. Canongia Lopes and Agilio A. H. Padua. Nanostructural Organization in Ionic Liquids. *J. Phys. Chem. B*, 110:3330–3335, 2006.

[10] Alessandro Triolo, Olga Russina, Hans-Jurgen Bleif, and Emanuela Di Cola. Nanoscale segregation in room temperature ionic liquids. *The journal of physical chemistry. B*, 111(18):4641–4644, may 2007.

[11] Michael Neuhaus, David; Williamson. The nuclear Overhauser effect in structural and conformational analysis. chapter 1-2, pages 3–39. VCH publishers, 1989.

[12] Timothy D W Claridge. *High-Resolution NMR Technique in Organic Chemistry*. Elsevier, second edi edition, 2009.

[13] Philipp Honegger, Maria Enrica Di Pietro, Franca Castiglione, Chiara Vaccarini, Alea Quant, Othmar Steinhauser, Christian Schröder, and Andrea Mele. The Intermolecular NOE Depends on Isotope Selection: Short Range vs Long Range Behavior. *The Journal of Physical Chemistry Letters*, pages 8658–8663, 2021.

[14] Robert A. Mantz, Paul C. Trulove, Richard T. Carlin, and Robert A. Osteryoung. ROESY NMR of basic ambient-temperature chloroaluminate ionic liquids. *Inorganic Chemistry*, 34(14):3846–3847, 1995.

[15] Andrea Mele, Chieu D. Tran, and Silvia H. De Paoli Lacerda. The structure of a room-temperature ionic liquid with and without trace amounts of water: The role of C-HO and C-HF interactions in 1-n-butyl-3-methylimidazolium tetrafluoroborate. *Angewandte Chemie - International Edition*, 42(36):4364–4366, 2003.

[16] Andrea Mele, Greta Romanò, Matteo Giannone, Enzio Ragg, Giovanni Fronza, Guido Raos, and Valentina Marcon. The local structure of ionic liquids: Cation-cation NOE interactions and internuclear distances in neat [BMIM][BF4] and [BDMIM]-[BF 4]. *Angewandte Chemie - International Edition*, 45(7):1123–1126, 2006.

[17] Sonja Gabl, Othmar Steinhauser, and Hermann Weingärtner. From short-range to long-range intermolecular NOEs in ionic liquids: Frequency does matter. *Angewandte Chemie - International Edition*, 52(35):9242–9246, 2013.

[18] Franca Castiglione, Giovanni Battista Appetecchi, Stefano Passerini, Walter Panzeri, Serena Indelicato, and Andrea Mele. Multiple points of view

of heteronuclear NOE: Long range vs short range contacts in pyrrolidinium based ionic liquids in the presence of Li salts. *Journal of Molecular Liquids*, 210:215–222, 2015.

[19] W.A. Henderson [Q. Zhou, P.D. Boyle, L. Malpezzi, A. Mele, J.-H. Shin, S. Passerini. Phase behavior of ionic liquid–LiX mixtures: pyrrolidinium cations and TFSI anions—linking structure to transport properties. *Chem. Mater. 23*, 2011.

[20] Pierre Alexandre Martin, Elodie Salager, Maria Forsyth, Luke A. O'Dell, and Michaël Deschamps. On the measurement of intermolecular heteronuclear cross relaxation rates in ionic liquids. *Physical Chemistry Chemical Physics*, 20(19):13357–13364, 2018.

[21] Yves Lingscheid, Sven Arenz, and Ralf Giernoth. Heteronuclear NOE spectroscopy of ionic liquids. *ChemPhysChem*, 13(1):261–266, 2012.

[22] Yves Lingscheid, Mathias Paul, Andreas Bröhl, Jörg Martin Neudörfl, and Ralf Giernoth. Determination of inter-ionic and intra-ionic interactions in a monofluorinated imidazolium ionic liquid by a combination of X-ray crystallography and NOE NMR spectroscopy. *Magnetic Resonance in Chemistry*, 56(2):80–85, 2018.